



HAL
open science

Serpentinization of New Caledonia peridotites: from depth to (sub-)surface

Marc Ulrich, Manuel Muñoz, Philippe Boulvais, Michel Cathelineau,
Dominique Cluzel, Stéphane Guillot, Christian Picard

► To cite this version:

Marc Ulrich, Manuel Muñoz, Philippe Boulvais, Michel Cathelineau, Dominique Cluzel, et al.. Serpentinization of New Caledonia peridotites: from depth to (sub-)surface. *Contributions to Mineralogy and Petrology*, 2020, 175 (9), pp.91. 10.1007/s00410-020-01713-0 . hal-03510813

HAL Id: hal-03510813

<https://cnrs.hal.science/hal-03510813>

Submitted on 30 Jan 2022

HAL is a multi-disciplinary open access archive for the deposit and dissemination of scientific research documents, whether they are published or not. The documents may come from teaching and research institutions in France or abroad, or from public or private research centers.

L'archive ouverte pluridisciplinaire **HAL**, est destinée au dépôt et à la diffusion de documents scientifiques de niveau recherche, publiés ou non, émanant des établissements d'enseignement et de recherche français ou étrangers, des laboratoires publics ou privés.



HAL
open science

Serpentinization of New Caledonia peridotites: from depth to (sub-)surface

Marc Ulrich, Manuel Munoz, Philippe Boulvais, Michel Cathelineau, Dominique Cluzel, Stephane Guillot, Christian Picard

► To cite this version:

Marc Ulrich, Manuel Munoz, Philippe Boulvais, Michel Cathelineau, Dominique Cluzel, et al.. Serpentinization of New Caledonia peridotites: from depth to (sub-)surface. Contributions to Mineralogy and Petrology, Springer Verlag, 2020, 75 (9), pp.91. 10.1007/s00410-020-01713-0 . insu-02890835

HAL Id: insu-02890835

<https://hal-insu.archives-ouvertes.fr/insu-02890835>

Submitted on 7 Jul 2020

HAL is a multi-disciplinary open access archive for the deposit and dissemination of scientific research documents, whether they are published or not. The documents may come from teaching and research institutions in France or abroad, or from public or private research centers.

L'archive ouverte pluridisciplinaire **HAL**, est destinée au dépôt et à la diffusion de documents scientifiques de niveau recherche, publiés ou non, émanant des établissements d'enseignement et de recherche français ou étrangers, des laboratoires publics ou privés.

[Click here to view linked References](#)

Serpentinization of New Caledonia peridotites: from depth to (sub-)surface

Marc ULRICH¹, Manuel MUÑOZ², Philippe BOULVAIS³, Michel CATHELIN⁴,
Dominique CLUZEL⁵, Stéphane GUILLOT⁶, Christian PICARD⁷.

¹ Université de Strasbourg, CNRS, IPGS UMR 7516, F-67000 Strasbourg

² Géosciences Montpellier, Univ. Montpellier, CNRS, Montpellier, France

³ Géosciences Rennes-UMR 6118, University Rennes, CNRS, F-35000 Rennes, France

⁴ Georessources CNRS UMR 7566, Vandoeuvre-lès-Nancy, France

⁵ ISEA, Université de la Nouvelle-Calédonie, BP R4, 98851 Nouméa Cedex, New Caledonia

⁶ Univ. Grenoble Alpes, Univ. Savoie Mont Blanc, CNRS, IRD, IFSTTAR, ISTerre, 38000
Grenoble, France

⁷ Laboratoire Chrono-environnement CNRS UMR 6249 Besançon, France

*Keywords: Serpentinization, New Caledonia ophiolite, subduction, obduction, serpentine
geochemistry, meteoric fluid circulation.*

31
32
33
34
35
36
37
38
39
40
41
42
43
44
45
46
47
48
49
50
51
52
53
54
55
56
57
58
59
60
61
62
63
64
65

ABSTRACT

Serpentinization processes occur at geological settings notably during oceanic subduction and obduction, where mantle rocks interact with water. Different types of serpentine minerals form according to temperature and pressure conditions, and potentially chemical exchanges. Therefore, the characterization of serpentine minerals, and the possible occurrence of multiple serpentine generations in mantle rocks provide essential constraints on the conditions of fluid-rock interactions in the mantle. The serpentinite sole of the Peridotite Nappe of New Caledonia (Southwest Pacific) is the result of several superimposed serpentinisation events. The latter were discriminated using mineralogical and geochemical approaches and modeling.

Lizardite represents more than 80% of the entire serpentine content of the ophiolite. It is crosscut by several veins of other serpentine species in the serpentinite sole. The relative chronology appears as follows: lizardite 1 → lizardite 2 → antigorite → chrysotile → polygonal serpentine. The transition from primary/magmatic minerals to lizardite 1 is almost isochemical. Then, the development of lizardite 2 yields an enrichment in fluid-mobile elements such as Cs, Rb, Ba, U and light rare-earth elements and an apparent increase of the Fe^{3+}/Fe_T ratio. The modeling of $\delta^{18}O$ values (1.9‰ to 13.9‰) and δD values (88‰ to 106‰) of all serpentine species through Monte-Carlo simulations show that New Caledonia serpentines were mainly formed in equilibrium with fluids released by the dehydration of altered oceanic crust (AOC) during subduction between 250°C and 350°C. AOC-derived fluids are not the unique source of fluids since a low temperature (100-150°C) meteoric component is also predicted by the models. Thus, serpentine acts as a tape-recorder of fluid-rock interactions into the mantle from depth to (sub-)surface.

INTRODUCTION

Serpentinization is a hydrothermal alteration process that leads to upper mantle hydration. Serpentine minerals are ubiquitous in ultramafic rocks from various geological settings and their crucial role in tectonic and chemical processes has been widely documented over the past two decades: In divergent environments, which include ultraslow and slow-spreading centers and mantle-exhuming passive margins, serpentine occurs mainly along fractures and detachment faults, weakening the upper mantle, promoting strain localization and resulting in the exhumation of serpentinized peridotites at the seafloor (Andréani et al. 2014; 2007; Cannat et al. 1995; Chenin et al. 2017; Delacour et al. 2008; Gillard et al. 2019; Guillot et al. 2015; Mével 2003; Picazo et al. 2012). Such tectonic processes involve significant mass transfer between the mantle and oceanic reservoirs (Alt and Shanks III 2003; Iyer et al. 2008; Kodolanyi et al. 2012; Pinto et al. 2016; Rouméjon et al. 2015; Schwarzenbach et al. 2015). Also, the rheology of serpentinized rocks strongly influences deformation and seismicity in the forearc and controls geodynamics of the subduction zone

66 (Hyndman and Peacock 2003; Peacock and Hyndman 1999; Stern 2002). Here again, serpentine is
67 assumed to be one of the most efficient ways to recycle water and fluid-mobile elements (FME) into
68 the deeper mantle (Debret et al. 2013; Deschamps et al. 2012; 2011; Klein et al. 2017; Poli and
69 Schmidt 2002; Rüpke et al. 2004; Savov et al. 2005; Scambelluri et al. 2004). Thus, the uppermost
70 part of the oceanic lithosphere is hydrothermally altered before entering subduction zones. Then, the
71 dehydration of the subducting slab favors the formation of forearc serpentine, which hosts a large
72 amount of water (up to ~13 wt.%). The circulation of such an amount of aqueous fluids may, in turn,
73 transport fluid-mobile elements (FME) deep into the mantle down to ~150 km (Ulmer and
74 Trommsdorff 1995; Wunder et al. 2001). At temperature above ~650°C, serpentine is no longer stable
75 and aqueous fluids are liberated by serpentine breakdown, triggering mantle wedge melting that gives
76 rise to arc volcanism (Hattori and Guillot 2003; Iwamori 1998; Reynard 2013; Schmidt and Poli 1998;
77 Ulmer and Trommsdorff 1995; 1999). Therefore, studying serpentinite is fundamental in the aim of
78 addressing questions about plate tectonics and global geochemical cycles.

79 When convergence results in the closure of ocean basins, slices of the forearc mantle may be
80 obducted. Serpentinite then acts as a lubricant, facilitating the ophiolite emplacement and subsequent
81 exhumation of the high pressure rocks (Agard et al. 2016; Guillot et al. 2009; 2000; Schwartz et al.
82 2001). However, the conditions of fluid-rock interactions and serpentine formation, as well as the
83 nature and source of serpentinizing fluids, are mostly unconstrained.

84 In New Caledonia (NC), large ultramafic massifs form an extensive and well-exposed ophiolite
85 obducted during the Late Eocene, termed Peridotite Nappe (Figure 1; Avias 1967). Peridotites
86 recorded various degrees of serpentinization, and the base of the Peridotite Nappe is made of a thick
87 serpentinite sole characterized by multiple generations of serpentine veins, the origin of which
88 remains unclear (Frost et al. 2013; Gautier et al. 2016; Mothersole et al. 2017; Quesnel et al. 2016b;
89 Ulrich et al. 2014). In this paper, the source and nature of the fluids involved in the serpentinization
90 are therefore unraveled thanks to new petrological, mineralogical and geochemical data as well as
91 geochemical modeling.

92 93 **GEOLOGICAL SETTINGS**

94 New Caledonia is an island of the SW Pacific, ~1300 km to the east of Australia, which forms
95 the northernmost part of the Norfolk Ridge, an elongated slice of thinned and largely submarine
96 continental crust, rifted from the Gondwana margin during the Late Cretaceous. The Peridotite
97 Nappe tectonically overlies a patchwork of pre-Oligocene terranes and covers at present about one-
98 third of the island. The main unit is located in the south of the island, so-called Massif du Sud, and
99 several tectonic klippen are spread along the West coast (**Figure 1**). All these units result from the
100 evolution of a marginal basin that opened to the east of the Norfolk Ridge during the Campanian-

101 Paleocene (90 Ma—55 Ma; Cluzel et al. 2001). This basin was inverted at 56 Ma by northeastward-
102 subduction (Cluzel et al. 2012a) and the upper plate of the system (the Loyalty Basin) was obducted
103 at ca. 34 Ma (Cluzel et al. 1998) when the Norfolk ridge entered the trench and jammed the Eocene
104 subduction. Harzburgites and dunites formed in a supra-subduction zone environment are
105 predominant, while lherzolites, inherited from the initial marginal basin are also found in the
106 northernmost massifs (Pirard et al. 2013; Secchiari et al. 2016; 2019; Ulrich et al. 2010). The
107 Peridotite Nappe bears a lateritic regolith (up to 100 m thick) that contains ~10% of the world Ni
108 reserves (McRae 2018). The Peridotite nappe overlies the Poya Terrane, which corresponds to a
109 large composite allochthon formed of two sub-units: i) tectonic slices of massive and pillow basalt
110 (Poya Terrane Basalts) of dominant MORB affinity and abyssal argillites of Campanian to Early
111 Eocene age (Aitchison et al. 1995), derived from the upper oceanic crust of the South Loyalty Basin
112 (Cluzel et al. 1997; Eissen et al. 1998) and accreted in the fore-arc region of the Loyalty Arc (Cluzel
113 et al. 2001), and ii) Coniacian-Santonian distal turbidites (Kone Facies) accumulated on the ancient
114 passive margin of the Norfolk Ridge, and intruded by lower Eocene dolerite sills of EMORB
115 affinity (Cluzel et al. 2018).

116 The serpentinization processes of the Peridotite Nappe have never been studied in-depth, while
117 peridotites are highly serpentinized. Orloff (1968) highlighted, for the first time, the decreasing
118 degree of serpentinization from bottom to the top of the ophiolite. More recently, Frost et al. (2013)
119 identified three generations of serpentine veins in a dunite sample: two-first generations of lizardite
120 and the last one of chrysotile. The transformation of lizardite to chrysotile would have been
121 accompanied by the release of Fe and the subsequent formation of magnetite. Mothersole et al. (2017)
122 used NC serpentinites as proxies of mantle wedge serpentinites and compared them with those from
123 the 15°20'N fracture zone in the Mid-Atlantic Ridge to evaluate the effect of hydrothermal alteration
124 on a budget of major and minor elements in the two different geodynamic settings (Mothersole et al.
125 2017). They concluded that serpentinization was nearly identical in the two environments, except
126 more oxidized Fe as well as enrichments in Cl, S, and C in abyssal serpentinites compared to the
127 forearc serpentinites. Serpentine-bearing faults were extensively studied i) to characterize their
128 kinematics and the mechanisms of NC ophiolite emplacement on the continental basement (Gautier
129 et al. 2016; Quesnel et al. 2016b), and ii) to constrain the carbonation and silicification of the
130 serpentinite sole in relation to meteoric fluid percolation (Quesnel et al. 2016a; 2013; Ulrich et al.
131 2014) and iii) to understand the formation of secondary Ni-rich phyllosilicates, mostly talc-like
132 phases, in serpentine-filled fractures at the top of the ophiolite (Cathelineau et al. 2016; 2015; Fritsch
133 et al. 2016; Muñoz et al. 2019). High temperature, slab-derived fluids are proposed for the origin of
134 syntectonic tremolite-antigorite veins, which are widespread in the Peridotite Nappe (Cluzel et al.

135 2019). But the source and nature of fluids in equilibrium with the main serpentinization episode that
136 affected the whole ophiolite remains, however, unconstrained.

137 138 **MATERIALS AND METHODS**

139 *Sampling and analytical strategies*

140 A collection of 30 samples, collected from five different massifs (the Massif du Sud, Kopeto,
141 Koniambo, Tiébaghi and Poum), includes serpentinized harzburgites, lherzolites and dunites referred
142 to as "upper serpentine" hereafter, as well as serpentinites from the sole of the Peridotite Nappe. They
143 represent most rock types and serpentine occurrences of the NC ophiolite. The serpentinites were
144 characterized by: 1) Raman spectroscopy, to identify serpentine species, 2) major and trace element
145 chemistry of primary minerals and serpentines crystals, to evaluate the chemical mobility during
146 fluid-rock interactions, 3) oxygen and hydrogen isotope geochemistry of each serpentine variety to
147 discuss the source of fluids involved in the serpentinization processes.

148 149 *Raman Spectroscopy*

150 Raman spectra were acquired at ENS Lyon (France) using a Horiba Jobin-Yvon LabRam
151 HR800 spectrometer and a visible ionized argon laser source with a wavelength of 514 nm. Output
152 laser power was 100 mW, and measurements were performed using an Olympus lens of 100x to focus
153 the laser beam onto an area that was 1 μm in diameter. Analyses were carried out on 30 μm polished
154 thin sections. Spectra result from the average of 5 acquisitions of 10-20 s for each point measured to
155 optimize the signal/noise ratio. Raman spectra were recorded in two spectral intervals: 200-1250 cm^{-1}
156 for structural bonding characterization and 3550-3800 cm^{-1} for the characterization of hydroxyl
157 groups. Serpentine species were mainly identified by comparing spectra with those already published
158 (Auzende et al. 2004; Lemaire 2000), focusing on the OH stretching range.

159 160 *Mineral Chemistry*

161 Electron microprobe analyses of minerals were carried out with a Cameca SX 100 at Service
162 Commun de Microscopie Électronique et de Microanalyses (SCMEM, Nancy, France). All analyses
163 of major elements, Na, Mg, Al, Si, K, Ca, Ti, Cr, Mn, Fe, Ni, were made against natural and synthetic
164 mineral standard: albite (Si, Na), corundum (Al), andradite (Ca), olivine (Mg), hematite (Fe), MnTiO_3
165 (Mn, Ti), NiO (Ni), orthoclase (K), with the exception for serpentine measurements for which Mg
166 was calibrated using natural clinocllore. Acceleration voltage and beam current were 15 kV and 12
167 nA, respectively, the counting time was 10 s, and standard correction procedures were applied. The
168 beam diameter was focused to 1 μm . Total Fe content is calculated on a divalent basis, as FeO.
169 Structural formulae were calculated based on of the following number of oxygens: olivine, 4;

170 pyroxene, 6; lizardite, chrysotile and polygonal serpentine, 7. Antigorite has a general formulae Mg_{3m-}
171 $3Si_{2m}O_{5m}(O.H.)_{4m-6}$ that differs from the idealized serpentine formula $Mg_3SiO_5(OH)_4$ by a minor
172 $Mg(OH)_2$ depletion, m being the number of tetrahedra along an entire wavelength. Structural formulae
173 for antigorite were calculated based on $m=17$.

174 Fe^{2+} and Fe^{3+} contents in serpentine were calculated using the approach described by Beard and
175 Frost (2017). Thus, in the $(Mg+Fe_T)$ pfu vs. $(Si+Al)$ pfu space, the microprobe analyses of serpentine
176 lie along a linear trend that extends from pure Mg serpentine (lizardite/chrysotile or antigorite) to
177 brucite ($Mg(OH)_2$). The trend towards brucite is a consequence of extremely fine-grained serpentine-
178 brucite intergrowths. According to Beard and Frost (2017), the deviation of a serpentine analysis from
179 the brucite trend reflects the stoichiometric effects of ferric iron substitutions in the crystal chemistry
180 of serpentine. Here, a full dioctahedral substitution is assumed, meaning that ferric iron is
181 accommodated in the serpentine structure by substitution for divalent cation plus the addition of a
182 vacancy in the octahedral sheet. In this case, a serpentine that integrates a significant amount of ferric
183 iron would deviate from the brucite trend, showing lower $(Mg+Fe_T)$ pfu at a given $(Si+Al)$ pfu.
184 Considering that this deviation is only caused by ferric iron substitution, the following equation
185 provides Fe^{3+} pfu:

$$Fe^{3+} = -x \times (Si + Al) + 7 - (Mg + Fe_T) \quad (1)$$

188 where x is the ideal number of Si cations when the serpentine formula is calculated for seven oxygens
189 (i.e., 2 in lizardite/chrysotile and 2.05 in antigorite).

191 A High-Resolution Laser Ablation Inductively Coupled-Plasma Mass Spectrometer (HR-LA-
192 ICP-MS) at the Geosciences Ocean laboratory (Brest, France) composed of a 193 nm MicroLas
193 CopexPro Coherent coupled with an Element II ICP-MS has been used for trace element analyzes.
194 Laser ablations were performed with a constant 5 Hz pulse rate, with an ablation crater of 90 to 120
195 μm in diameter. The number of pulses was 200, which is sufficient to form a long and stable signal
196 for integration. The ablated material is transported using a constant He flow and mixed with Ar in a
197 cyclone coaxial mixer before entering the ICP torch and being ionized. The ions are then sampled,
198 accelerated and focused before being separated and analyzed in the mass spectrometer. ^{29}Si content
199 — known from prior electron microprobe analyses — was used as internal standard and
200 concentrations were calibrated against the NIST 612 rhyolitic glass using reference values from
201 Pearce et al. (1997). Data reduction was carried out by using SILLIS software, following the standard
202 methods of Longerich et al. (1996). Detection limits were between <1 and 60 ppb for most trace
203 elements, <0.5 ppm for B, Li, Mn, Co, Ni, As and between 1 and 50 ppm for Mg, Ca, Ti considering
204 a spot size of 120 μm .

205

206

Stable isotope measurements

207

208

209

210

211

212

213

214

215

216

217

218

219

220

221

222

223

224

225

226

227

228

229

230

231

232

233

234

235

RESULTS

236

237

238

239

240

241

242

243

244

245

246

247

248

249

250

251

252

253

254

255

256

257

Serpentine petrography

258

259

260

261

262

263

264

265

266

267

268

269

270

271

272

273

274

275

276

277

278

279

Stable oxygen and hydrogen isotope compositions were measured from separated serpentine fragments at the Stable Isotope Laboratory at the University of Lausanne. Separated powders were obtained by micro-drilling using a drill of 500 μm of diameter for the largest veins of antigorite and chrysotile. A smaller drill of 100 μm of diameter was used to sample the mesh core of lizardite. Serpentine samples were then purified from magnetite grains by using a hand-held magnet and potential denser primary minerals were separated by settling in water. Oxygen isotopes were measured according to a method adapted after Sharp (1992). Between 1 and 2 mg of powder are loaded in a Pt sample holder and heated with a CO_2 -laser under a F atmosphere and a pressure of 50 mbar. The liberated oxygen is analyzed as O on a Finnigan MAT 253 mass spectrometer. Hydrogen isotopes were measured by applying the method of Sharp et al. (2001). Between 0.5 and 1 mg of sample powder is loaded in a tin capsule and reduced by reaction with glassy carbon at 1450°C in a helium carrier gas-producing H and CO. Produced gases are separated in a gas chromatograph and analyzed in a Finnigan MAT Delta Plus XL mass spectrometer configured to make hydrogen isotope analyses in continuous flow mode. Results are given in the standard δ -notation, expressed relative to V_{SMOW} in permil (‰). Replicate oxygen isotope analyses of the standards (UWG-2 garnet) yielded an average precision of $\pm 0.25\%$ for $\delta^{18}\text{O}$ values. The precision of the G1 biotite in-house standards for hydrogen isotope analyses was $\pm 2\%$.

In agreement with the work of Orloff (1968), whereas the degree of serpentinization is moderate to high throughout the ophiolite (>50%, "facies normal", **Figure 2a, b**), it is close to 100% near the base, giving to the rock a typical dark color ("facies de base"; **Figure 2c**). Locally, near the top of the massifs, the degree of serpentinization is less than 10% ("facies superieur"). There, serpentine occurs along fracture walls and also forms mm-thick black veins pervasively surrounding preserved grains of olivine and pyroxene.

The base of the ophiolite consists of a schistose and intensely brecciated serpentinite sole of 20 m to 300 m thick. Breccias are composed by mm to dm-scale blocks (phacoids) of totally serpentinized peridotite embedded in a matrix of sheared serpentinite. Several generations of serpentine can be identified even at naked eye: massive serpentinite is crosscut by mm to cm-thick, yellow to light-green serpentine veins (**Figure 2d**). These veins are systematically surrounded by dark seams of magnetite and the overall is frequently crosscut by mm-thick fibrous veins, the latter being occasionally replaced by veins of greenish to white serpentine (**Figure 2e, f**). This greenish to

240 white serpentine may also compose large amounts of the breccia matrix. In thin section, the latest
241 generations of serpentine occur almost exclusively as limited domains or veins formed after
242 microfracture infilling (**Figure 3b, c, d**). Larger domains of replacement can be found, but they
243 usually correspond to the strongly deformed area where secondary serpentine composes the breccia
244 matrix.

245 In the less serpentinized samples, serpentinization starts at the boundaries of olivine grains and
246 along micro-fractures (**Figure 3**). It progressively extends from the rim to the core of the grains as
247 the serpentinization degree increases, giving the rock a typical mesh texture (see S1 in **Figure 3a**). In
248 general, olivine is strongly affected by serpentinization, while orthopyroxene remains relatively
249 preserved or develop bastite rims around fresh cores. Iron released during serpentinization
250 crystallized as magnetite rimming olivine grains and along mm-scale fractures, forming dark seams
251 (**Figure 3a**).

252 Six generations of serpentine have been identified in the sole (S1-S6 in **Figure 3**). The first
253 generation of serpentine after the primary mesh texture (S1) forms homogeneous domains that display
254 the same grey color as the mesh texture under cross-polarized light (S2, **Figure 3b, d**). Black veins
255 of magnetite identical to those observed in the mesh texture are present in S2, and extend parallel to
256 the S2 borders. The limits of the S2 domain are diffuse, suggesting progressive replacements of the
257 mesh texture S1. Both serpentine generations are closely associated with μm to mm-thick veins of
258 serpentine of a characteristic bluish-grey color under cross-polarized light (S3, **Figure 3b, c, d**). S3
259 veins are made of decussate blades of tens of micrometers in size, giving these veins a typical
260 interlocking texture. The borders of S3 veins are marked by the accumulation of magnetite grains,
261 both inside and outside the veins. S4 veins occasionally crystallize in tension gashes, similarly to S5
262 veins and exhibit transitional texture between the decussate blades of S3 and the fibrous habitus that
263 characterizes S5. Fibers can reach $\sim 200 \mu\text{m}$ in size and have a grey to yellow birefringence under
264 cross-polarized light (**Figure 3b, c**). They are commonly oriented perpendicularly to the vein edges.
265 The latest serpentine generation (S6) occurs as replacement of previous serpentine generations,
266 forming veins (**Figure 3c**) or covering large domains that form the matrix of breccias as shown by
267 Ulrich et al. (2014) and Quesnel et al. (2016b).

268

269 *Nature of serpentine polymorphs*

270 The typical Raman spectra for the different generations of serpentine (i.e., from S1 to S6, as
271 previously described) are displayed in Figure 4. Their specific spectral signatures allow identifying
272 serpentine species (Figure 4; Auzende et al. 2004; Lemaire 2000). Except for minor changes in the
273 low wavenumber region, the discrimination and identification of serpentine minerals are mainly based
274 on the OH stretching bands located in the range $3600\text{-}3750 \text{ cm}^{-1}$. Lizardite characterized by peaks at

275
276
277
278
279
280
281
282
283
284
285

275 3685 and 3706 cm^{-1} , is the most abundant variety, forming the S1 and S2 generations. In contrast, the
276 typical Raman spectrum obtained for S3 veins corresponds to antigorite, with characteristic peaks at
277 3670 and 3699 cm^{-1} . S5 perfectly matches with the spectral signature of chrysotile, and S4
278 corresponds to a mixture of antigorite (S3) and chrysotile (S5). Finally, the serpentine S6 is identified
279 as polygonal serpentine, characterized by a weak band at 3648 cm^{-1} and a doublet at 3690 and
280 3697 cm^{-1} (Cathelineau et al. 2016).

281 282 *Chemistry of primary minerals*

283 The representative compositions in major and trace elements of primary minerals and each
284 serpentine variety identified are presented in Tables 1 and 2. The supplementary table S1 provides all
285 the data. Standard deviations are 2σ . Analyses of the primary minerals are consistent with those
286 previously published for the NC peridotites (Frost et al. 2013; Mothersole et al. 2017; Pirard et al.
287 2013). Olivine is Fo_{91} (**Figure 5**) and has a NiO content of ~ 0.4 wt.% (Ni=0.1 pfu) and MnO content
288 of ~ 0.16 wt.%. Olivine is also characterized by an extreme depletion in trace elements so that they
289 are usually close, or below, the detection limit. High-field strength elements (HFSE) have Primitive
290 Mantle (PM)-normalized concentrations varying between 10^{-3} and 10^{-1} (**Figure 6**). Orthopyroxene is
291 mainly enstatite and has a constant Mg# similar to olivine (0.91). CaO content ranges between 0.42
292 and 2.79 wt. % with an average value of 1.06 wt. % (Ca=0.04 pfu). Al_2O_3 and Cr_2O_3 have
293 concentrations ranging between 2.27 and 4.51 wt. % and 0.56 and 0.88 wt. %, respectively, and a
294 corresponding Cr# of ~ 0.12 and down to 0.09, reflecting a high degree of depletion of the peridotite.
295 PM-normalized trace element patterns show that orthopyroxene is strongly depleted in light rare-earth
296 elements (LREE), with $\text{Ce}_N/\text{Yb}_N < 0.05$. Clinopyroxene is diopside and is mainly present in spinel and
297 plagioclase lherzolite, although some occurrences may be observed in harzburgite, mostly from
298 exsolution in orthopyroxene. Clinopyroxene is characterized by slightly higher Mg# (~ 0.93) and
299 Al_2O_3 of ~ 4.16 wt. % (Al=0.2 pfu) and Cr_2O_3 of 0.94 wt.% (Cr# ~ 0.13). PM-normalized trace
300 element patterns show a strong fractionation of LREE relative to heavy (H)REE ($\text{Ce}_N/\text{Yb}_N < 0.01$)
301 and a nearly flat HREE pattern ($\text{Dy}_N/\text{Yb}_N \sim 0.8$). Slight Sr and Eu anomalies are observed and reflect
302 equilibrium with plagioclase.

303 304 *Chemistry of serpentine*

305 Lizardite replacing primary minerals in the upper parts of the massif (upper serpentines) has
306 been divided in four types: lizardite after olivine (i.e. in the mesh core), lizardite in the mesh rim,
307 lizardite after orthopyroxene and lizardite after clinopyroxene. All have H_2O content of ~ 13 wt. %,
308 which is consistent with the hydroxyl stoichiometry of lizardite. Lizardite after olivine shows rather
309 homogeneous compositions with ~ 41 wt. % SiO_2 and MgO (Si=2.0 pfu, Mg=2.9 pfu) and ~ 4 wt. %

310 FeO ($\text{Fe}^{2+}=0.2$ pfu). Compared to olivine, mesh cores have higher Al_2O_3 content (~ 0.3 wt. %) and
311 lower NiO content (~ 0.2 wt. %). Mesh rims are characterized by lower SiO_2 and MgO contents (38
312 wt. % and 37 wt. %, respectively). FeO content is higher (>10 wt. %, $\text{Fe}^{2+}=0.5$ pfu) and may reflect
313 the presence of minute grains of magnetite in the mesh rims. Bastite contains 38 to 42 wt. % SiO_2 ,
314 and is usually characterized by lower Si at a given $\text{Mg}+\text{Fe}_T$ compared to lizardite after olivine, and
315 displays higher Cr and Al contents. Mg# varies between 0.91 and 0.97, with an average of 0.92
316 (**Figure 5**). Bastites formed either after orthopyroxene or clinopyroxene do not show any difference
317 in the major element concentrations. Regarding the Fe oxidation state in upper serpentines, our
318 estimates show that Fe is mostly divalent ($\text{Fe}^{3+}/\text{Fe}_T < 0.1$, **Figure 5d**), consistently with previous
319 estimates made by Beard and Frost (2017).

320 Primitive Mantle normalized trace element patterns of upper serpentines are presented in
321 **Figure 6**. Despite some slight differences (particularly some enrichments in large ion lithophile
322 elements, LILE), PM-normalized trace element patterns of serpentines match well those of primary
323 minerals. Minor and trace elements in lizardite after olivine is highly depleted (Ti: 10.0-85.8 ppm;
324 Mn: 125-1059 ppm; Co: 18.7-81.1 ppm; Y: 0.060-0.375 ppm), with a strong fractionation between
325 LREE and HREE ($0.008 < (\text{Ce}/\text{Yb})_N < 0.132$). Lizardite after orthopyroxene is slightly less depleted in
326 minor and trace elements (Ti: 158-174 ppm; Mn: 568-635 ppm; Co: 26.8 ppm; Y: 0.907-0.994 ppm)
327 but still shows LREE depleted patterns and strong LREE/HREE fractionation
328 ($0.02 < (\text{Ce}/\text{Yb})_N < 0.162$) similar to lizardite after olivine. LREE are depleted in serpentine after
329 clinopyroxene. Elements such as Y (7.81 ppm), Ti (2163 ppm), Mn (1460 ppm) and Co (67.4 ppm)
330 are enriched compared to lizardite after olivine and orthopyroxene. Only one occurrence of lizardite
331 after clinopyroxene was found, confirming that the clinopyroxene is more frequently transformed into
332 amphibole (tremolite) than serpentine during the hydration processes. Regarding fluid-mobile
333 elements (FME), upper serpentines are enriched in B (4.71-24.3 ppm), Sb (0.007-0.016 ppm) and U
334 (0.854-2.74 ppm) and depleted in Li and Sr with respect to Depleted Mantle (DM) values (Figure 7).
335 More specifically, Pb and Sr concentrations are similar to those previously published for NC
336 serpentinized peridotites (Secchiari et al. 2016; 2019; Ulrich et al. 2010), and overlap the fields of
337 abyssal serpentinites and subducted serpentinites with some sedimentary contributions. Upper
338 serpentinites display B, Li and Sb concentrations lower than those of other serpentinites worldwide
339 (Figure 7). Arsenic is always below the detection limits.

340 In the serpentinite sole, all serpentine species display homogeneous major and trace element
341 compositions. They contain ~ 44 wt.% SiO_2 ($\text{Si} = 2.0$ pfu), ~ 40 wt.% MgO ($\text{Mg} = 2.8$ pfu), ~ 13 wt.%
342 H_2O and they are characterized by very low FeO (~ 2 wt.%, $\text{Fe} \leq 0.1$ pfu) and Al_2O_3 (< 0.1 wt.%, Al
343 < 0.005 pfu; **Figure 5**) and very high Mg# (~ 0.98) compared to upper serpentines. Calculated
344 $\text{Fe}^{3+}/\text{Fe}_T$ ratio shows that serpentines from the sole integrate significant amounts of ferric iron: On

345 average, lizardite and chrysotile have Fe^{3+}/Fe_T ratio of ~0.2, antigorite, 0.35, and polygonal
346 serpentine, 0.7 (up to 1). They also show HFSE depletion similar to that described in upper
347 serpentines. However, they are slightly more depleted in HREE and significantly more enriched in
348 LREE, except Ce which has a similar concentration to that of moderately serpentinized NC
349 peridotites. Serpentines from the sole display a strong Ce negative anomaly ($Ce/Ce^*=0.009-0.739$,
350 **Figure 7**). They also display enriched concentrations in FME relative to upper serpentines (B: 2.13-
351 8.52 ppm; Sb: 0.005-0.057 ppm; Li: 0.054-0.543; Cs: 0.004-0.022; Rb: 0.014-0.275 ppm; Ba: 0.066-
352 0.952 ppm; Pb: 0.002-0.133; Sr: 0.202-4.05 ppm) with a pronounced U positive anomaly (U: 0.001-
353 0.043 ppm; **Figure 6**). Similarly to upper serpentines, As concentrations in the serpentinite sole were
354 too low to be determined (**Table 2**).

356 *O and H stable isotope composition*

357 The $\delta^{18}O$ and δD values of fresh peridotites are 5.5‰ and -70‰ respectively, which are
358 consistent with mantle rock compositions (Deloule et al. 1991; Eiler 2001). Serpentines display a
359 wide range of $\delta^{18}O$ values from 1.7‰ to 13.9‰. In contrast, δD values are quite homogeneous (-107
360 to -88‰). No systematic difference can be observed between serpentine species.

361 The upper serpentines (i.e., lizardite) display a narrow range of isotopic compositions:
362 $5.4‰ < \delta^{18}O < 6.9‰$ and $-103‰ < \delta D < -97‰$. In the serpentinite sole, the $\delta^{18}O$ and δD values of
363 lizardite are somewhat broader: $\delta^{18}O_{liz} = 2.2$ to $5.7‰$ and $\delta D_{liz} = -107$ to $-97‰$. The whole range of
364 values including other serpentine species from the sole is 1.7 to 12.2‰ for oxygen, -107 to -88‰ for
365 hydrogen. Two samples (Ti 51a-1, -2, Poum 4-6, -2, -3) have traces of amorphous silica, and also the
366 highest $\delta^{18}O$ values. Such high values are likely due to amorphous silica, which has high $\delta^{18}O$ values
367 around 30‰ (Quesnel et al. 2016a). For this reason, these data will not be considered further in the
368 following discussion. The isotopic compositions of serpentines are thus assumed to range between
369 1.7 to 7.9‰ for $\delta^{18}O$, and from -107 to -88‰ for δD .

471 **DISCUSSION**

472 *Deciphering the source of serpentinization fluids and conditions of serpentinization from the* 473 *serpentine chemistry: a new modeling approach*

474 The New Caledonia serpentines plot away from the field of oceanic serpentines defined in the
475 literature (Sakai et al. 1990; Wenner and Taylor 1973), therefore excluding the involvement of
476 seawater in the serpentinization process (**Figure 8a**). Some trace element concentrations also confirm
477 this inference (**Figure 7**), since abyssal serpentines are usually characterized by a high U/Th ratio,
478 attributed to seawater interaction with peridotite (Deschamps 2010; Frisby et al. 2016). U and Th are
479

380 highly depleted in the mantle (e.g., Salters et al. 2002), but U is enriched in seawater relative to Th
381 (Chen et al. 1986), leading to a significant fractionation between these elements when seawater is
382 involved in serpentinization process. The Ce negative anomaly ($Ce/Ce^* < 1$, with Ce/Ce^* equals to
383 $Ce_N / [(La_N * Pr_N)^{1/2}]$) is typical of the seawater where Ce^{3+} is oxidized into the less soluble Ce^{4+}
384 (Elderfield and Greaves 1982). Low Ce/Ce^* is also a common feature in abyssal serpentines
385 (Delacour et al. 2008; Frisby et al. 2016; Rouméjon et al. 2015). Frisby et al. (2016) have recently
386 shown that seawater influences the LREE budget of serpentine through the addition of La and Pr, and
387 that Ce/Ce^* decreases in abyssal serpentines with increasing U/Th. NC serpentines, more specifically
388 those from the serpentinite sole, are characterized by high U/Th and low Ce/Ce^* ratios compared to
389 moderately serpentinized NC peridotites (**Figure 7**). However, U/Th ratio never exceeds 10 in our
390 samples whereas it is $\gg 10$ in abyssal serpentines (up to 10,000). Also, most of our samples display
391 much larger Ce negative anomalies than that of abyssal serpentines, thus providing additional
392 evidence that seawater was unlikely involved in the formation of NC serpentines.

393 Serpentine with δD values as low as -100‰ have been identified in other places worldwide,
394 forming the "Ophiolite serpentines" field defined by Wenner and Taylor (1973) where NC serpentines
395 plot (**Figure 8a**). These Ophiolite serpentines are commonly assumed to result from the interaction
396 of peridotite with meteoric or metamorphic fluids either during obduction or during exhumation and
397 retrograde re-equilibration of the peridotites (Früh-Green et al. 1996; 2001; Kyser et al. 1999;
398 O'Hanley 1996). Typically, very low δD values for serpentine minerals (< -100 ‰) are attributed to
399 late serpentinization events due to the circulation of meteoric waters under subsurface conditions. On
400 the other hand, δD values in the range of -100 to -70‰ are better explained by the presence of
401 composite fluids (Burkhard and O'Neil 1988; Früh-Green et al. 2001).

402 The O and H isotope compositions of a given serpentine depend on three main parameters: 1)
403 the isotopic composition of the serpentinizing fluid ($\delta^{18}O_{fluid}$ and δD_{fluid}), 2) the serpentinization
404 temperature (T), and 3) the water-rock ratio (W/R) during the reaction. The complex relationships
405 between these three parameters on the one hand, and the isotopic fractionation factors on the other
406 hand, have been characterized experimentally and from the study of natural samples (e.g. Saccocia et
407 al. 2009; Sakai and Tsutsumi 1978; Savin and Lee 1988; Wenner and Taylor 1973; Zheng 1993). The
408 isotopic compositions of serpentinizing fluids may be calculated using calibrated serpentine-water
409 isotopic fractionation factors, and assuming W/R values and temperature (e.g., Alt et al. 2012; Alt
410 and Shanks Iii 2006; Früh-Green et al. 2001; Kyser et al. 1999; Rouméjon et al. 2015; Sakai et al.
411 1990; Thakurta et al. 2009). Alternatively, W/R can be determined if the composition of the
412 serpentinizing fluid is known (Agrinier and Cannat 1997; Alt et al. 2007; Burkhard and O'Neil 1988;
413 Magaritz and Taylor 1974; Rouméjon et al. 2015; Wenner and Taylor 1973). Conversely, the
414 approximative temperature of serpentinization can be estimated by using the serpentine-magnetite

415 geothermometer, based on the oxygen isotope fractionation between these two co-genetic minerals
 416 (Wenner and Taylor 1971). Actually, this approach is somewhat unsatisfactory because it requires
 417 knowing or arbitrarily setting at least one of the parameters listed above. For example, in the oceanic
 418 context, serpentine fluids are relatively well constrained because they are either seawater or seawater
 419 modified by hydrothermal fluids (Agrinier and Cannat 1997). But for fluids derived from ancient
 420 lithospheric remnants, $\delta^{18}\text{O}_{\text{fluid}}$ and $\delta\text{D}_{\text{fluid}}$ are generally unknown and need to be assumed or
 421 calculated. It follows that the serpentine-magnetite geothermometer can hardly be used in the case of
 422 multiple serpentinization events since the related generations of magnetite are challenging to identify
 423 and separate.

424 In this study we developed a new approach based on Monte Carlo simulations to constrain the
 425 source of fluids in equilibrium with NC serpentines based on their oxygen and hydrogen isotope
 426 compositions. Figure 8 (b to d) shows the result of one million Monte Carlo simulations using the
 427 isotopic fractionation factors of Wenner and Taylor (1973) (as modified by O'Hanley 1996) for
 428 oxygen isotopes:

$$1000\ln\alpha_{\text{serpentine-water}}^{18\text{O}-16\text{O}} = 1.69 \times 10^6/T^2 - 4.23 \quad (2)$$

429 and of Saccocia et al. (2009) for hydrogen isotopes:

$$1000\ln\alpha_{\text{serpentine-water}}^{D-H} = 3.436 \times 10^6/T^2 - 34.736 \times 10^3/T + 21.67 \quad (2)$$

432 where T is the temperature in Kelvin. It should be noticed that the use of oxygen isotope fractionation
 433 factors from Saccocia et al. (2009) provides quite similar results to those of Wenner and Taylor (1971)
 434 in the temperature range of 250-450°C. However the serpentine-water $^{18}\text{O}-^{16}\text{O}$ fractionation factor
 435 of Wenner and Taylor (1971) is applicable for a wide range of temperature, contrarily to the
 436 experimental approach of Saccocia et al. (2009) whose fractionation factor was calibrated for
 437 temperatures >250°C. As a consequence, the use of the Wenner and Taylor fractionation factor was
 438 found more consistent with calculating the $\delta^{18}\text{O}$ composition of serpentinizing fluids when no other
 439 constraint on serpentinization temperature is available.

440 The O and H isotope compositions of a serpentine can be calculated by applying Sheppard et
 441 al. (1969) mass-balance equation:

$$\delta_{\text{serpentine}} = \frac{\delta_{\text{mantle}} + W/R \times (\delta_{\text{fluid}} + 1000\ln\alpha_{\text{serpentine-water}})}{1 + W/R} \quad (4)$$

449 with $\delta_{serpentine}$, δ_{mantle} and δ_{fluid} are the O and H isotope compositions of the serpentine, the mantle and
 450 the serpentinizing fluid, respectively, W/R is the fluid-rock ratio and $1000\ln\alpha$ is the fractionation
 451 factor calculated with equations (2) and (3). Mantle values of $\delta^{18}\text{O} = +5.5\text{‰}$ and $\delta\text{D} = -80\text{‰}$ have
 452 been chosen for the composition of the starting material (Deloule et al. 1991; Eiler 2001). Other
 453 parameters are defined randomly for each simulation in the following ranges: $50 < T^{\circ}\text{C} < 450$,
 454 $0.13 < \text{WR} < 1000$, $-40 < \delta^{18}\text{O}_{\text{fluid}} (\text{‰}) < 40$ and $-200 < \delta\text{D}_{\text{fluid}} (\text{‰}) < 20$ (see **Figure 8**). Although
 455 serpentine can be stable at temperature up to $\sim 700^{\circ}\text{C}$, the temperature of serpentinization rarely
 456 exceeds 350°C at spreading centers and $400\text{-}500^{\circ}\text{C}$ in subduction zones (e.g., Evans 2004; Klein et
 457 al. 2013; Ulmer and Trommsdorff 1995). Low-temperature serpentinization remains poorly
 458 documented, even though some authors argued for serpentinization might occur at temperature lower
 459 than 80°C (e.g., Agrinier et al. 1995; Bonatti et al. 1984). Thus, a low-temperature threshold of 50°C
 460 was chosen arbitrarily. The range of fluid-rock ratios was chosen considering that 0.13 is the
 461 minimum ratio required to convert an olivine into a serpentine stoichiometrically, and $\delta_{serpentine}^{WR=1000} \approx$
 462 $\delta_{serpentine}^{WR=\infty} \cdot \delta_{\text{fluid}}$ thresholds were chosen so that almost all compositions of terrestrial fluids were
 463 covered (Hoefs 2009). In our modeling approach, a simulation is considered to be valid when the
 464 modeled serpentine displays $\delta^{18}\text{O}$ and δD compositions that are in the range of NC serpentinites
 465 ($1.7\text{‰} < \delta^{18}\text{O} < 7.9\text{‰}$; $-107\text{‰} < \delta\text{D} < -88\text{‰}$). Results are provided in supplementary materials and
 466 are presented in **Figure 8: Figure 8b** reports the calculated $\delta^{18}\text{O}$ and δD compositions of fluids that
 467 are able to reproduce a serpentine that matches the O and H compositions of NC serpentines. Among
 468 1 million random simulations, ~ 6500 were consistent with the O and H signatures of NC serpentines.
 469 **Figure 8c** and **Figure 8d** show, respectively, the calculated $\delta^{18}\text{O}_{\text{fluid}}$ and $\delta\text{D}_{\text{fluid}}$ as a function of the
 470 correspondent temperatures of serpentinization. Results of Monte-Carlo simulations show that fluids
 471 in equilibrium with NC serpentines extend between the meteoric water line and an area defined
 472 between 3‰ and 8‰ in $\delta^{18}\text{O}$ and -80‰ and -60‰ in δD in which most of the results plot ($\sim 40\%$ of
 473 6500 simulations, see the red, white cross-hatched area in Figure 8b). Fluids that fall into this area
 474 have interacted with the mantle at temperatures between $\sim 250^{\circ}$ and 430°C (the white cross-hatched
 475 areas in Figure 8c,d), while interactions with fluids showing negative $\delta^{18}\text{O}$ and higher δD signatures
 476 ($> -60\text{‰}$) occurred at lower temperatures ($100\text{-}200^{\circ}\text{C}$; **Figure 8c, d**). With a few exceptions, our
 477 calculations show that NC serpentines were formed at relatively high W/R (>1) (see Figure S1 in
 478 supplementary materials).

Origin of NC serpentinites

From deep serpentinization...

482 Based on the new petrological, mineralogical, geochemical and modeling data presented here,
 483 the chronology of serpentinization of NC peridotites would be as follows. First, the decreasing

484 serpentinization degree from bottom to the top of the Peridotite nappe is good evidence for a fluid
485 circulation mainly located at the base of the ophiolite. Since the NC ophiolite was in the forearc
486 position for ~20 Ma before its obduction on the Norfolk Ridge, the most likely source of the fluids
487 forming pervasive lizardite S1 would come from dehydration of the subducting slab. As our results
488 fall into the Alpine Ophiolite-type field of Wenner and Taylor (1973), they are consistent with this
489 assumption. Consequently, three potential sources of fluids present in the recycled oceanic
490 lithosphere can contribute to hydrating the mantle wedge: the altered oceanic crust (AOC), the
491 subducted sediments and the subducted abyssal serpentinites. The fluids in equilibrium with all of
492 these components have distinct signatures in trace elements and stable isotopes that also sharply differ
493 from the composition of the mantle wedge (Eiler et al. 1998; Kodolanyi et al. 2012; Peters et al.
494 2017). One of the best examples documented worldwide is provided by the formation of serpentine
495 mud volcanoes along the Marianna Trench (Fryer 1992). The geodynamics in this region
496 approximates the one assumed for the South Loyalty Basin at the subduction time, and the occurrence
497 of serpentinite seamounts provide a unique window for studying fluid circulations into the forearc
498 mantle. Alt and Shanks III (2006) used typical $\delta^{18}\text{O}$ and δD values for the AOC, oceanic sediments,
499 and abyssal serpentinites to predict the isotopic compositions of fluids in equilibrium with each
500 subducted component, and determine the source of serpentinizing fluids in the Marianna forearc
501 mantle. In their modeling, they assumed that the metasomatized basaltic basement has $\delta^{18}\text{O} = +8$ to
502 $+11\text{‰}$ and $\delta\text{D} = -90$ to -120‰ (Alt 2003), and used a simplified AOC mineralogy with 49% albite,
503 49% chlorite and 2% calcite. The dehydration of metabasalts having these isotopic compositions and
504 mineralogy would produce, therefore, fluids with $\delta^{18}\text{O}$ values of $+2$ to $+8\text{‰}$ (up to $+10\text{‰}$ at 400°C)
505 and δD values of -50‰ to -90‰ . Similarly, the authors calculated higher $\delta^{18}\text{O}$ ($+12$ to $+16\text{‰}$) and
506 δD (-20 to -40‰) values for sediment-derived fluids and $\delta^{18}\text{O}$ and δD in the range of $+5$ to $+9\text{‰}$ and
507 -5 to -30‰ respectively for serpentine-derived fluids at $\sim 200\text{-}350^\circ\text{C}$ (**Figure 8b**). By comparison,
508 the main O and H isotope values calculated for fluids in equilibrium with NC serpentinites (the red,
509 white cross-hatched area in Figure 8b) are consistent with fluids coming from the dehydration of an
510 AOC. On the contrary, neither sediment-derived fluids nor serpentine-derived fluids fit our modeled
511 serpentinizing fluids. Our simulations also predict that AOC-derived fluids interacted with the forearc
512 peridotites at temperatures of $250\text{-}430^\circ\text{C}$ (**Figure 8c, d**). These temperatures are close to those of
513 AOC dehydration usually proposed in forearc settings ($200\text{-}450^\circ\text{C}$; Alt and Shanks Iii 2006; Rüpke
514 et al. 2004). Additionally, the maximum temperature of 430°C estimated by our simulations may be
515 lowered to $\sim 350^\circ\text{C}$ based on field observations: lizardite is commonly replaced by antigorite at
516 temperature $>350^\circ\text{C}$ in (supra)-subduction environments (Evans et al. 1976; Evans 2004; Ulmer and
517 Trommsdorff 1995; 1999). This replacement has never been observed in the NC ophiolite, where

518 lizardite is the dominant serpentine variety, while antigorite is mainly restricted to synkinematic crack
519 seals (Cluzel et al. 2019; Quesnel et al. 2016b).

520 Regarding trace elements, the evolution of the mantle wedge composition interacting with slab-
521 derived fluids is evaluated by proposing a single-step process where the fluids that migrate from the
522 descending slab are mixed with the overlying forearc mantle. Trace element concentrations of a slab-
523 derived fluid C_f can be estimated by applying the following equation:

$$524 \quad C_f = \frac{C_0 \times M}{F} \quad (5)$$

525 where C_0 is the concentration of an element in the subducted component (i.e., the AOC, the sediments
526 or the serpentinites), M is the mobility (in percent) of an element during the dehydration of a
527 subducted component, and F is the weight fraction of fluid extracted from the subducted component
528 (Sano et al. 2001). All parameters used for the modeling of trace elements, references and results of
529 calculations are summarized in **Table 4**. The weight fraction of fluids released from the AOC and
530 sediments is assumed to be 1.5 and 3 wt.% respectively, in agreement with estimates previously
531 published (Peacock 1990; Rüpke et al. 2004). The lizardite-antigorite transition in the subducting slab
532 could have released fluids at temperatures below 350°C in the forearc subducted slab. Thus, pure Mg-
533 lizardite contains 13 wt.% H₂O, while pure Mg-antigorite (m=17) only contains 12.3 wt.% H₂O.
534 Consequently, the weight fraction of serpentine-derived fluids was set to ~0.7 wt.%. Data of element
535 mobility during dehydration processes are taken from experimental studies on natural pelite for
536 sediments (Aizawa et al. 1999), natural amphibolite for AOC (Kogiso et al. 1997; Sano et al. 2001)
537 and natural antigorite for serpentinite (Tenthorey and Hermann 2004). U, Th, B and Zr are used
538 because of their behavior during dehydration and their respective concentrations in the slab
539 components: Th and Zr mobilities are rather low in hydrous fluids, while B is highly mobile. U
540 mobility depends on its oxidation state: it is immobile in its reduced form U⁴⁺ while it is mobile in its
541 oxidized form U⁶⁺ (Brenan et al. 1995). Actually, the high solubility of uranium in subduction zone
542 fluids has been reported by several studies (e.g., Bailey and Ragnarsdottir 1994; Bali et al. 2010). All
543 of these elements are enriched in sediments (Plank 2014) and depleted in the mantle (Salters and
544 Stracke 2004; Secchiari et al. 2019). The U/Th ratio is low in sediments, but is roughly similar in
545 AOC and abyssal serpentinites (**Table 4**). However, the U/Th ratio is more fractionated during
546 serpentine dehydration than during AOC dehydration (Kogiso et al. 1997; Tenthorey and Hermann
547 2004). As a consequence, the U/Th ratio is higher in serpentine-derived fluids than in AOC fluids,
548 and is the lowest in sediment-derived fluids (**Figure 9**). Subducted serpentinites have a high B/Zr
549 ratio (>20), contrarily to subducted sediments and AOC, which are characterized by low (<1) to very
550 low (<0.1) B/Zr ratios, respectively. Considering these ratios and the high mobility of B in fluids
551

553 compared to Zr, the addition of subduction zone fluids in the mantle wedge leads to an increase of
554 B/Zr ratio towards ~50 for AOC-derived fluids, ~370 for sediment-derived fluids and up to ~8,200
555 for serpentine-derived fluids. Consistently with the conclusions drawn from the stable isotope study,
556 the trace element modeling suggests that NC upper serpentines were likely formed by the interaction
557 with AOC-derived fluids, with nevertheless some addition of sediment-derived fluids (<30%, **Figure**
558 **9**). This result is consistent with the highly radiogenic strontium isotope compositions of some NC
559 serpentines from which a metasedimentary contribution was inferred (Cluzel et al. 2019). The
560 modeling also indicates that the amount of slab-derived fluids that interacted with NC peridotites in
561 the forearc was low, in the range of <0.1-3 wt.% (**Figure 9**). The amount of sediment-derived fluids
562 in the mantle wedge was consequently in the order of 0.9 wt.% or less. Such a low amount of
563 sediment-derived fluids is unresolvable by our modeling approach based on stable isotopes (**Figure**
564 **8**). On the contrary, the Sr budget of sediments is high compared to the mantle so that a minute amount
565 of sediments can buffer the Sr isotope system. These results together with the very low concentrations
566 of As and Sb, which are proxies of the sedimentary contribution in serpentine chemistry (Deschamps
567 et al. 2013; Deschamps et al. 2011; Hattori and Guillot 2007), imply that the amount of subducted
568 sediments was low at the time of forearc peridotite hydration. The limited influence of sediment-
569 derived fluids in the serpentine signature is also inferred by the lack of sedimentary prism, the latter
570 being replaced by slices of basaltic rocks (i.e., the future Poya Terrane) scrapped off the down going
571 plate during the Eocene NE-dipping subduction of the SLB (Cluzel et al. 2001; 2012b). In Figure 9,
572 the domain of the serpentinite sole is more widespread than that of upper serpentines, with some
573 samples plotting away from the modeling trends. This could reflect the effects of a later episode of
574 fluids circulation (see the next section below) rather than those of slab-derived fluids contribution.

575 The subduction inception occurring at (or near to) the ridge axis in the SLB led to the
576 development of a forearc magmatic activity from 55 to 47 Ma (Cluzel et al. 2006; 2016). During this
577 period, thermal conditions in the forearc were high, causing the melting of the mantle wedge rather
578 than its hydration. The continuous influx of fluids released from the dehydration of the oceanic crust
579 of the subducting slab progressively cooled the forearc mantle, leading to the cessation of the forearc
580 magmatism about 10 Ma after subduction inception (Cluzel et al. 2012a; Cluzel et al. 2016; Ulrich et
581 al. 2010; Whattam et al. 2008). This period was long enough to alter significantly the oceanic crust
582 exposed at the seafloor (Staudigel et al. 1981) Then, the AOC entering the subduction zone releases
583 fluids in the overlying mantle wedge. Such fluids finally cause the massive serpentinization of the
584 future NC ophiolite (**Figure 10a**). It is worth noting that based on these results, no trace of oceanic
585 serpentinization related to the opening of the SLB was identified so far. It is possible however that
586 the serpentinized upper part of the upper plate (the Loyalty Basin) was removed early (i.e., soon after
587 subduction inception) when the hot and buoyant lower plate had to force its way beneath the future

588 Loyalty fore-arc. Such a feature could account for the absence of MORB-type basaltic crust on top
589 of the peridotites in the Massif du Sud and the occurrence of fore-arc cumulates directly overlying
590 highly depleted harzburgites and dunites.

591
592 *... to (sub-) surface serpentinization.*

593 The development of multiple serpentine generations in the tectonic sole likely reflects changes
594 in crystallization conditions, including the fluid composition and the formation events, both being
595 connected with the tectonic history of the Peridotite Nappe. Consistently, the significant differences
596 in the chemical compositions from S1 to S2 serpentines (e.g., increasing Mg#, different trace element
597 patterns) may reveal a change in the elemental budget of serpentinizing fluids. On the other hand, the
598 transition from the lizardite-antigorite assemblage (S2-S3/S4) to chrysotile-polygonal serpentine (S5-
599 S6) without significant changes in the serpentine chemistry is in favour of a sole development under
600 cooling temperatures. Our modeling approach of stable isotopes suggests that AOC-derived fluids
601 alone cannot explain the formation of the serpentinite sole. Low temperature fluids (~100-250°C) of
602 a meteoric origin can be considered (**Figure 8b**). The involvement of meteoric fluids is also suggested
603 by major and trace element compositions of sole serpentines. The high $\text{Fe}^{3+}/\text{Fe}_T$ ratio in serpentines
604 from the sole (**Figure 5**) indicates a formation under more oxidizing conditions than in the upper
605 system, which may be interpreted in term of formation depth.

606 Interestingly, Muñoz et al. (2019) showed that secondary serpentines, which are formed close
607 to the surface by the circulation of meteoric fluids during the early stages of laterization display an
608 increasing amount of ferric iron from lizardite ($\text{Fe}^{3+}/\text{Fe}_T = 0.4$) to polygonal serpentine
609 ($\text{Fe}^{3+}/\text{Fe}_T = 0.95$). $\text{Fe}^{3+}/\text{Fe}_T$ ratios in serpentines from the sole are very comparable to those measured
610 in the regolith. Polygonal serpentine was also the latest serpentine variety to form and it has the
611 highest $\text{Fe}^{3+}/\text{Fe}_T$. We thus interpret the increase of ferric iron in serpentines from the sole as evidence
612 of their formation under near-surface conditions (i.e., low temperature, high $f\text{O}_2$). The behavior of
613 LREE provides additional proof of meteoric fluid involvement in the formation of the serpentinite
614 sole. Serpentines from the serpentinite sole are LREE-enriched, except Ce. The exact opposite, i.e.,
615 LREE depletion and strong Ce positive anomaly (**Figure 7**), is observed in laterites on top of the NC
616 regolith and is explained by the very low mobility of Ce^{4+} relative to all other REE (Ulrich et al.
617 2019). Also, the downslope migration of elements from the regolith can explain the high U/Th ratio
618 in serpentines from the sole. Indeed, U is mobile under oxidizing surface conditions, while Th is
619 insoluble (e.g., Dequincey et al. 2002). As a consequence, U/Th ratio is lower in laterites than in the
620 initial peridotite (**Figure 7**). Meteoric fluids may thus transport LREE, and potentially other FME,
621 released during weathering. A high U/Th ratio and a low Ce/Ce* ratio in serpentine is therefore not
622 necessarily a marker for the influence of seawater solely.

623 Lateritization has been considered as rather early and was active during or slightly after the
624 ophiolite emplacement by Quesnel et al. (2013), based on a coupled isotopic and structural analysis
625 of magnesite veins. Following our Monte-Carlo simulations, the O and H isotope signatures of the
626 meteoric fluids involved during serpentinization ($\delta^{18}\text{O} = -6 \pm 2\text{‰}$, $\delta\text{D} = -40 \pm 10\text{‰}$; **Figure 8b**) are
627 comparable with present-day rainwater (Nicolini et al. 2016). The current discharge of H_2 , CH_4 , and
628 N_2 -enriched hyperalkaline spring waters reveals active and low-temperature serpentinization at the
629 base of the NC ophiolite (Deville and Prinzhofer 2016; Monnin et al. 2014). Thus, the serpentinization
630 of the serpentinite sole was partly formed in response to the circulation of meteoric fluids during the
631 late stages of its emplacement (**Figure 10b**). After the crystallization of lizardite 2 in microfracture
632 networks, antigorite veins may have crystallized under moderate temperatures ($<250^\circ\text{C}$), and high
633 deformation conditions, such as documented by Ribeiro Da Costa et al. (2008). Finally, as the
634 obduction proceeded, the progressive cooling temperatures may have led to the replacement of
635 antigorite into lower temperature species, such as chrysotile and polygonal serpentine, as shown by
636 Quesnel et al. (2016b).

637 638 **CONCLUSIONS**

639 The new mineralogical and geochemical data presented here, on the serpentinites from the
640 peridotite nappe and the sole of NC ophiolite, provide evidence for a polyphasic history of fluid-rock
641 interactions. By using trace element concentrations and a new modeling approach based on Monte
642 Carlo simulations applied on oxygen and hydrogen isotope compositions, we propose that the main
643 serpentinization event (lizardite formation) mostly occurred during the NE-dipping subduction in the
644 SLB due to slab dehydration and subsequent hydration of forearc mantle wedge (i.e., the future
645 Peridotite Nappe). Also, our simulations shift serpentinization temperatures in the fore-arc mantle in
646 the range of $250\text{--}450^\circ\text{C}$, with an upper threshold that may be lowered to $\sim 350^\circ\text{C}$, as inferred by the
647 lack of antigorite.

648 Other serpentine species present in the serpentinite sole recorded retrogression during fore-arc
649 cooling and obduction. These serpentinization events occurred under high strain conditions and at
650 lower temperature, from $\sim 250^\circ\text{C}$ to $< 100^\circ\text{C}$. From the oxygen and hydrogen isotope composition of
651 these serpentines, we suggest a meteoric contribution for the late stage serpentinizing fluids. Thus,
652 this study demonstrates that serpentine in ophiolite may record a long history of fluid-rock
653 interactions, from early fluid circulations deep into the forearc mantle to late meteoric fluid
654 percolation at shallow depth during obduction

655 656 **Acknowledgements**

657
658
659
660
661
662
663
664
665

657 We thank Claire Bassoulet for her help during LA-ICP-MS measurements at Géosciences
658 Ocean laboratory (Brest, France). We also thank Olivier Rouer (SCMEM, Nancy, France) for his help
659 during electron microprobe analyses. Marie-Camille Caumon (Géoresources, Nancy, France), and
660 Gilles Montagnac (Laboratoire de Géologie, ENS Lyon, France) are thanked for their contributions
661 during Raman spectroscopy analyses. Benita Putlitz and Thorsten Wennemann (ISTE, University of
662 Lausanne, Switzerland) are acknowledged for their help during the measurement of O and H isotopes.

663 Sampling in New Caledonia was partly funded by the National Centre for Technological
664 Research CNRT "Nickel et son environnement" based in Nouméa, New Caledonia (Project grant:
665 8PS2013-CNRT.CNRS/SCANDIUM) and Labex Ressources21 (supported by the French National
666 Research Agency through the National Program Investissements d'Avenir, reference ANR-10-
667 LABX-21-LABEXRESSOURCES 21). The fieldwork benefited from the help of Koniambo S.A..

668 Juan Carlos de Obeson, an anonymous reviewer and the editor Othmar Müntener are warmly
669 acknowledged for their detailed and constructive suggestions that helped to improve the manuscript.

670

24

25

26

27

28

29

30

31

32

33

34

35

36

37

38

39

40

41

42

43

44

45

46

47

48

49

50

51

52

53

54

55

56

57

58

59

60

61

62

63

64

65

671
672
673
674
675
676
677
678
679
680
681
682
683
684
685
686
687
688
689
690
691
692
693
694
695
696
697
698
699
700
701
702
703
704
60
61
62
63
64
65

Figure Captions

Figure 1: Simplified geological map of New Caledonia, showing the exposures of Paleocene-Eocene terranes, (adapted from Maurizot and Vende-Leclerc, 2009). Pre-obduction situation is modified from Cluzel et al. (2012).

Figure 2: a, b. Slightly (<20%) to moderately (~50%) serpentinized peridotite, respectively corresponding to the "facies supérieur" (b) and "facies intermediaire" (a) described in Orloff (1968). **c.** Serpentinite from the base of the ophiolite nappe, just above the serpentinite sole. **d, e, f.** Serpentinite from the serpentinite sole showing multiple generations of serpentine in the form of veins and fracture infilling. These serpentines include centimeter-scale greenish veins (d) that are crosscut by millimeter-scale veins filled by fibrous serpentine and/or light green to white-colored massive serpentine (e, f).

Figure 3: a. Microphotography (cross-polarized) of the typical mesh texture (S1) observed in serpentinized peridotite and serpentinites from the upper parts of the Peridotite Nappe. Black veins correspond to magnetite (sample MS60). **b.** Microphotography (cross-polarized) of the serpentinite sole showing the primary mesh texture (S1) crosscut by 4 successive generations of serpentine veins (S2 to S5; sample xx3786). **c.** Microphotography (cross-polarized) of the serpentinite sole showing the primary mesh texture (S1) crosscut by S3 veins, itself crosscut by fiber-habitus S5 veins and the close association between S5 and S6 serpentines (sample xx3758). **d.** Schematic representation of (b). mgt: magnetite; chr: chromite.

Figure 4: Raman spectra of the main serpentine species identified in this study.

Figure 5: Plots of **a.** Si+Al cations vs. Mg+Fe_T cations; **b.** Mg cations vs. Fe_T cations; **c.** Fe_T cations vs. Al cations; and **d.** Mg# ($Mg^{2+}/(Mg^{2+}+Fe^{2+})$) vs. Fe³⁺/Fe_T (lower right), showing that serpentine from the sole integrates less Al and Fe_T and more oxidized iron than upper serpentines. Compositions of primary minerals are also shown. Ol: olivine; Opx: orthopyroxene; Cpx: clinopyroxene. Atoms per formula units are calculated based on 7 oxygens for serpentine minerals, except for antigorite which is calculated based on 6.823 oxygens. Olivine and pyroxene structural formulas are calculated based on 4 and 6 oxygens, respectively, and then converted to 7 oxygens for comparison with serpentine minerals. Brucite and Fe³⁺ dioctahedral substitution trends are from Beard and Frost (2017).

705 **Figure 6:** PM-normalized extended trace element patterns of serpentine minerals. **a.** Lizardite from
706 upper serpentines compared to their magmatic mineral precursors (olivine, orthopyroxene,
707 clinopyroxene). The first serpentine generation (lizardite S1) preserves the initial trace element
708 patterns. **b.** Trace element patterns of lizardite from the serpentinite sole (S2) compared to lizardite
709 S1. **c.** Trace element patterns of antigorite (S3) from the serpentinite sole compared to lizardite S2.
710 **d.** Trace element patterns of chrysotile (S5) and polygonal serpentine (S6) from the serpentinite sole
711 compared to lizardite S2. S1 to S2 transition is marked by an enrichment in fluid-mobile elements (in
712 blue), especially with a pronounced U positive anomaly and an enrichment in LREE except for Ce.
713 S2 to S6 transitions occurred isochemically. Primitive-mantle values are from McDonough and Sun
714 (1995).

715
716 **Figure 7:** Plots of concentrations of selected fluid-mobile elements (B, Li, Sb, Pb, and Sr), U/Th and
717 Ce/Ce* ratios in serpentines from Upper serpentinites and from the serpentinite sole. Primitive and
718 depleted mantle values are from McDonough and Sun (1995) and from Workman and Hart (2005),
719 respectively, except for B, Li and Sb concentrations in the depleted mantle which are from Salters
720 and Stracke (2004). Global subducted sediments (GLOSS II) concentrations are from Plank (2014).
721 Other concentration ranges are from Frisby et al. (2016) and Peters et al. (2017) for abyssal
722 serpentinites; Lafay et al. (2013) and Peters et al. (2017) for serpentines with sedimentary imprints;
723 Ulrich et al. (2010) and Secchiari et al. (2016; 2019) for NC serpentinitized peridotites; Ulrich et al.
724 (2019) for laterites. $Ce/Ce^* = C_{eN} / [(La_N * Pr_N)^{1/2}]$.

725
726 **Figure 8: a.** δD vs. $\delta^{18}O$ of NC serpentines. Blue and green fields represent the isotopic compositions
727 of oceanic serpentinites and ophiolite serpentinites, respectively (Wenner and Taylor, 1973; Früh-
728 Green et al., 2001). The black arrow shows the trend formed by samples contaminated by supergene
729 silica ($\delta^{18}O > 29\%$; Quesnel et al., 2016). Grey areas indicate the range of mantle compositions in
730 $\delta^{18}O$ and δD , with average values of 5.5‰ and -80‰ respectively (Deloule et al., 1991; Eiler et al.,
731 2001). **b.** Calculated δD vs. $\delta^{18}O$ compositions of serpentinizing fluids (represented as a density field)
732 in equilibrium with NC serpentines (~6500 positive results, i.e., consistent with the isotopic
733 compositions of NC serpentines, over 1 000 000 Monte-Carlo simulations, see the main text for more
734 details about the modeling). The O and H compositions of fluids in equilibrium with the altered
735 oceanic crust at 200-400°C, with subducted sediments (sed. fluids) and with subducted serpentinites
736 (serp. fluids) at 200-350°C are calculated according to the modeling approach of Alt and Shanks III
737 (2006). NC meteoric rainwater compositions are from Nicolini et al. (2016). **c. and d.** Calculated
738 $\delta^{18}O_{fluid}$ and δD_{fluid} vs. temperature of serpentinization. The white cross-hatched area indicates
739 simulations that fall into the red area in (b) (~40% of >6500 simulations). Colorbar values correspond

740
741
742
743
744
745
746
747
748
749
750
751
752
753
754
755

740 to the number of pixels in one grid cell of a size of 1‰ ($\delta^{18}\text{O}$) by 10‰ (δD) in (b), 50°C (T) by 1‰
741 ($\delta^{18}\text{O}$) in (c) and 50°C (T) by 10‰ (δD) in (d).

742
3
743 **Figure 9:** Plots of **a.** U/Th vs. U and **b.** B/Zr vs. B of NC serpentines. Thick solid lines represent the
5 bulk mixing between the NC mantle wedge and sediment-derived fluids (in orange), with AOC-
744 derived fluids (in blue) and with serpentine-derived fluids (in green). Thin dotted lines represent the
745 bulk mixing between the NC mantle wedge and AOC-derived fluids mixed with various amounts of
9 sediment-derived fluids (in orange) and serpentine-derived fluids (in green). Grey dotted lines
10 correspond to the percentage additions of slab-derived fluids to the mantle wedge. Compositions of
11 the NC mantle wedge and AOC, sediment and serpentine-derived fluids and respective sources are
12 listed in Table 4.

18
19
20
21 **Figure 10: a.** A simple model for the serpentinization of the New Caledonia ophiolite. **a.** Massive
22 hydration of the forearc mantle related to the dehydration of the altered oceanic basement of the
23 subducted plate, leading to the formation of fully serpentinized peridotites (including pyroxenes) at
24 the slab interface, where fluid flows are the most intense, and partially serpentinized peridotites at
25 shallower depths where fluid flows are less expressed. **b.** Conceptual model of the serpentinite sole
26 formation in response to the percolation of meteoric fluids at the base of the NC ophiolite during its
27 emplacement on the Norfolk continental basement. Note that these meteoric fluids previously
28 interacted with peridotite the top of the ophiolite, forming a thick regolith since the ophiolite emersion
29 at 34 Ma. (modified after Lagabrielle et al., 2013). The legend is the same as in Figure 1.

30
31
32
33
34
35
36
37
38
39
40
41
42
43
44
45
46
47
48
49
50
51
52
53
54
55
56
57
58
59
60
61
62
63
64
65

762
763
1
764
3
765
5
766
7
767
768
10
769
12
770
14
771
16
772
18
773
19
20
21
22
775
23
24
25
26
27
28
29
30
31
32
33
34
35
36
37
38
39
40
41
42
43
44
45
46
47
48
49
50
51
52
53
54
55
56
57
58
59
60
61
62
63
64
65

Table Captions

Table 1: Representative major element concentrations of primary minerals (olivine, orthopyroxene and clinopyroxene) and serpentines from NC peridotites.

Table 2: Representative trace element concentrations of primary minerals (olivine, orthopyroxene and clinopyroxene) and serpentines from NC peridotites.

Table 3: Oxygen and hydrogen compositions of NC serpentines (US: upper serpentinites; Lhz: lherzolite; Hz: harzburgite; Du: dunite; lz: lizardite; atg: antigorite; ctl: chrysotile; pol: polygonal serpentine; BR: bulk rock).

Table 4: Chemical compositions, mobilities and references used for trace element modeling.

777

~~778~~

3

~~749~~

5

~~780~~~~781~~~~782~~~~783~~~~784~~

11

~~785~~~~786~~~~787~~~~788~~~~789~~~~790~~

19

~~791~~~~792~~

21

~~793~~~~794~~~~795~~

25

~~796~~~~797~~~~798~~~~799~~

30

~~800~~~~801~~~~802~~

34

~~803~~~~804~~~~805~~

38

~~806~~~~807~~~~808~~~~809~~

43

~~810~~~~811~~~~812~~

47

~~813~~~~814~~

50

~~815~~~~816~~

52

~~817~~~~818~~

55

~~819~~~~820~~~~821~~

58

~~822~~~~823~~

61

62

63

64

65

- Agard P, Yamato P, Soret M, Prigent C, Guillot S, Plunder A, Dubacq B, Chauvet A, Monié P (2016) Plate interface rheological switches during subduction infancy: Control on slab penetration and metamorphic sole formation. *Earth Planet Sci Lett* 451:208-220
- Agrinier P, Cannat M (1997) Oxygen-isotope constraints on serpentinization processes in ultramafic rocks from the Mid-Atlantic Ridge (23 °N). *Proceedings of Ocean Drilling Program, Scientific Results* 153:381-388
- Agrinier P, Hékinian R, Bideau D, Javoy M (1995) O and H stable isotope compositions of oceanic crust and upper mantle rocks exposed in the Hess Deep near the Galapagos Triple Junction. *Earth Planet Sci Lett* 136(3-4):183-196
- Aitchison JC, Clarke GL, Meffre S, Cluzel D (1995) Eocene arc-continent collision in New Caledonia and implications for regional southwest Pacific tectonic evolution. *Geology* 23(2):161
- Aizawa Y, Tatsumi Y, Yamada H (1999) Element transport by dehydration of subducted sediments: Implication for arc and ocean island magmatism. *Island Arc* 8(1):38-46
- Alt JC (2003) Stable isotopic composition of upper oceanic crust formed at a fast spreading ridge, ODP Site 801. *Geochem Geophys Geosyst* 4(5)
- Alt JC, Garrido CJ, Shanks III WC, Turchyn A, Padrón-Navarta JA, Sánchez-Vizcaíno VL, Pugnaire MTG, Marchesi C (2012) Recycling of water, carbon, and sulfur during subduction of serpentinites: A stable isotope study of Cerro del Almirante, Spain. *Earth and Planetary Science Letters* 327-328:1-11
- Alt JC, Shanks III WC (2003) Serpentinization of abyssal peridotites from the MARK area, Mid-Atlantic Ridge: sulfur geochemistry and reaction modeling. *Geochimica et Cosmochimica Acta* 67(4):641-653
- Alt JC, Shanks III WC (2006) Stable isotope compositions of serpentinite seamounts in the Mariana forearc: Serpentinization processes, fluid sources and sulfur metasomatism. *Earth Planet Sci Lett* 242(3):272-285
- Alt JC, Shanks WC, Bach W, Paulick H, Garrido CJ, Beaudoin G (2007) Hydrothermal alteration and microbial sulfate reduction in peridotite and gabbro exposed by detachment faulting at the Mid-Atlantic Ridge, 15 degrees 20 ' N (ODP Leg 209): A sulfur and oxygen isotope study. *Geochem Geophys Geosyst* 8
- Andréani M, Escartin J, Delacour A, Ildefonse B, Godard M, Dymont J, Fallick AE, Fouquet Y (2014) Tectonic structure, lithology, and hydrothermal signature of the Rainbow massif (Mid-Atlantic Ridge 36° 14' N). *Geochemistry Geophysics Geosystems* 15(9):3543-3571
- Andréani M, Mével C, Boullier AM, Escartin J (2007) Dynamic control on serpentine crystallization in veins: Constraints on hydration processes in oceanic peridotites. *Geochemistry Geophysics Geosystems* 8(2):24
- Auzende AL, Daniel I, Reynard B, Lemaire C, Guyot Fo (2004) High-pressure behaviour of serpentine minerals: a Raman spectroscopic study. *Physics and Chemistry of Minerals* 31(5):269-277
- Avias J (1967) Overthrust structure of the main ultrabasic new caledonian massives. *Tectonophysics* 4(4-6):531-541
- Bailey EH, Ragnarsdottir KV (1994) Uranium and thorium solubilities in subduction zone fluids. *Earth Planet Sci Lett* 124(1-4):119-129
- Bali E, Audétat A, Keppler H (2010) The mobility of U and Th in subduction zone fluids: an indicator of oxygen fugacity and fluid salinity. *Contrib Mineral Petrol* 161(4):597-613
- Beard JS, Frost BR (2017) The stoichiometric effects of ferric iron substitutions in serpentine from microprobe data. *International Geology Review* 59(5-6):541-547
- Bonatti E, Lawrence JR, Morandi N (1984) Serpentinization of oceanic peridotites: temperature dependence of mineralogy and boron content. *Earth Planet Sci Lett* 70:88-94
- Brenan JM, Shaw HF, Ryerson FJ, Phinney DL (1995) Mineral-aqueous fluid partitioning of trace elements at 900°C and 2.0 GPa: Constraints on the trace element chemistry of mantle and deep crustal fluids. *Geochim Cosmochim Acta* 59(16):3331-3350
- Burkhard DJM, O'Neil JR (1988) Contrasting serpentinization processes in the eastern Central Alps. *Contrib Mineral Petrol* 99(4):498-506

- 824 Burkhard DJM, O'Neil JR (1988) Contrasting serpentinization processes in the eastern Central Alps. *Contributions to*
825 *Mineralogy and Petrology* 99(4):498-506
- 826 Cannat M, Mevel C, Maia M, Deplus C, Durand C, Gente P, Agrinier P, Belarouchi A, Dubuisson G, Humler E (1995)
827 Thin crust, ultramafic exposures, and rugged faulting patterns at the Mid-Atlantic Ridge (22–24°N). *Geology*
828 23(1):49-52
- 829 Cathelineau M, Myagkiy A, Quesnel B, Boiron M-C, Gautier P, Boulvais P, Ulrich M, Truche L, Golfier F, Drouillet M
830 (2016) Multistage crack seal vein and hydrothermal Ni enrichment in serpentinized ultramafic rocks (Koniambo
831 massif, New Caledonia). *Miner Deposita* 52(7):1-16
- 832 Cathelineau M, Quesnel B, Gautier P, Boulvais P, Couteau C, Drouillet M (2015) Nickel dispersion and enrichment at
833 the bottom of the regolith: formation of pimelite target-like ores in rock block joints (Koniambo Ni deposit, New
834 Caledonia). *Miner Deposita* 51(2):271-282
- 835 Chen JH, Edwards RL, Wasserburg GJ (1986) ²³⁸U, ²³⁴U and ²³²Th in seawater. *Earth Planet Sci Lett* 80(3-4):241-251
- 836 Chenin P, Manatschal G, Picazo S, Müntener O, Karner G, Johnson C, Ulrich M (2017) Influence of the architecture of
837 magma-poor hyperextended rifted margins on orogens produced by the closure of narrow versus wide oceans.
838 *Geosphere* 13(2)
- 839 Cluzel D, Aitchison JC, Picard C (2001) Tectonic accretion and underplating of mafic terranes in the Late Eocene
840 intraoceanic fore-arc of New Caledonia (Southwest Pacific): geodynamic implications. *Tectonophysics* 340(1-
841 2):23-59
- 842 Cluzel D, Boulvais P, Iseppi M, Lahondère D, Lesimple S, Maurizot P, Paquette J-L, Tarantola A, Ulrich M (2019) Slab-
843 derived origin of tremolite–antigorite veins in a supra-subduction ophiolite: the Peridotite Nappe (New Caledonia)
844 as a case study. *International Journal of Earth Sciences*:1-26
- 845 Cluzel D, Chiron D, Courme M-D (1998) Discordance de l'Éocène supérieur et événements pré-obduction en Nouvelle-
846 Calédonie. *Comptes Rendus de l'Académie des Sciences - Series IIA - Earth and Planetary Science* 327(7):485-
847 491
- 848 Cluzel D, Jourdan F, Meffre S, Maurizot P, Lesimple S (2012a) The metamorphic sole of New Caledonia ophiolite:
849 ⁴⁰Ar/³⁹Ar, U-Pb, and geochemical evidence for subduction inception at a spreading ridge. *Tectonics* 31(3):3016-
850 n/a
- 851 Cluzel D, Maurizot P, Collot J (2012b) An outline of the Geology of New Caledonia; from Permian-Mesozoic Southeast
852 Gondwanaland active margin to Cenozoic obduction and supergene evolution. *Episodes* 35(1):72-86
- 853 Cluzel D, Meffre S, Maurizot P, Crawford AJ (2006) Earliest Eocene (53 Ma) convergence in the Southwest Pacific:
854 evidence from pre-obduction dikes in the ophiolite of New Caledonia. *Terra Nova* 18(6):395-402
- 855 Cluzel D, Picard C, Aitchison JC, Laporte C, Meffre S, Parat F (1997) La nappe de Poya (ex-formation des Basaltes) de
856 Nouvelle-Calédonie (Pacifique Sud-Ouest) : un plateau océanique Campanien-Paléocène supérieur obducté à
857 l'Eocène supérieur. *Comptes Rendus de l'Académie des Sciences de Paris* 324(6):443-451
- 858 Cluzel D, Ulrich M, Jourdan F, Meffre S, Paquette J-L, Audet M-A, Secchiari A, Maurizot P (2016) Early Eocene
859 clinostatite boninite and boninite-series dikes of the ophiolite of New Caledonia; a witness of slab-derived
860 enrichment of the mantle wedge in a nascent volcanic arc. *Lithos* 260:429-442
- 861 Cluzel D, Whitten M, Meffre S, Aitchison JC, Maurizot P (2018) A Reappraisal of the Poya Terrane (New Caledonia):
862 Accreted Late Cretaceous-Paleocene Marginal Basin Upper Crust, Passive Margin Sediments, and Early Eocene
863 E-MORB Sill Complex. *Tectonics* 37(1):48-70
- 864 Debret B, Andréani M, Godard M, Nicollet C, Schwartz S, Lafay R (2013) Trace element behavior during
865 serpentinization/de-serpentinization of an eclogitized oceanic lithosphere: A LA-ICPMS study of the Lanzo
866 ultramafic massif (Western Alps). *Chemical Geology* 357:117-133
- 867 Delacour A, Früh-Green GL, Frank M, Gutjahr M, Kelley DS (2008) Sr- and Nd-isotope geochemistry of the Atlantis
868 Massif (30°N, MAR): Implications for fluid fluxes and lithospheric heterogeneity. *Chemical Geology* 254(1-2):19-
869 35
- 870 Deloule E, Albarede F, Sheppard SMF (1991) Hydrogen Isotope Heterogeneities in the Mantle from Ion Probe Analysis
871 of Amphiboles from Ultramafic Rocks. *Earth and Planetary Science Letters* 105(4):543-553
- 872 Dequincey O, Chabaux F, Clauer N, Sigmarsson O, Liewig N, Leprun JC (2002) Chemical mobilizations in laterites:
873 evidence from trace elements and ²³⁸U-²³⁴U-²³⁰Th disequilibria. *Geochim Cosmochim Acta* 66(7):1197-1210
- 874 Deschamps F (2010). Université Joseph Fourier

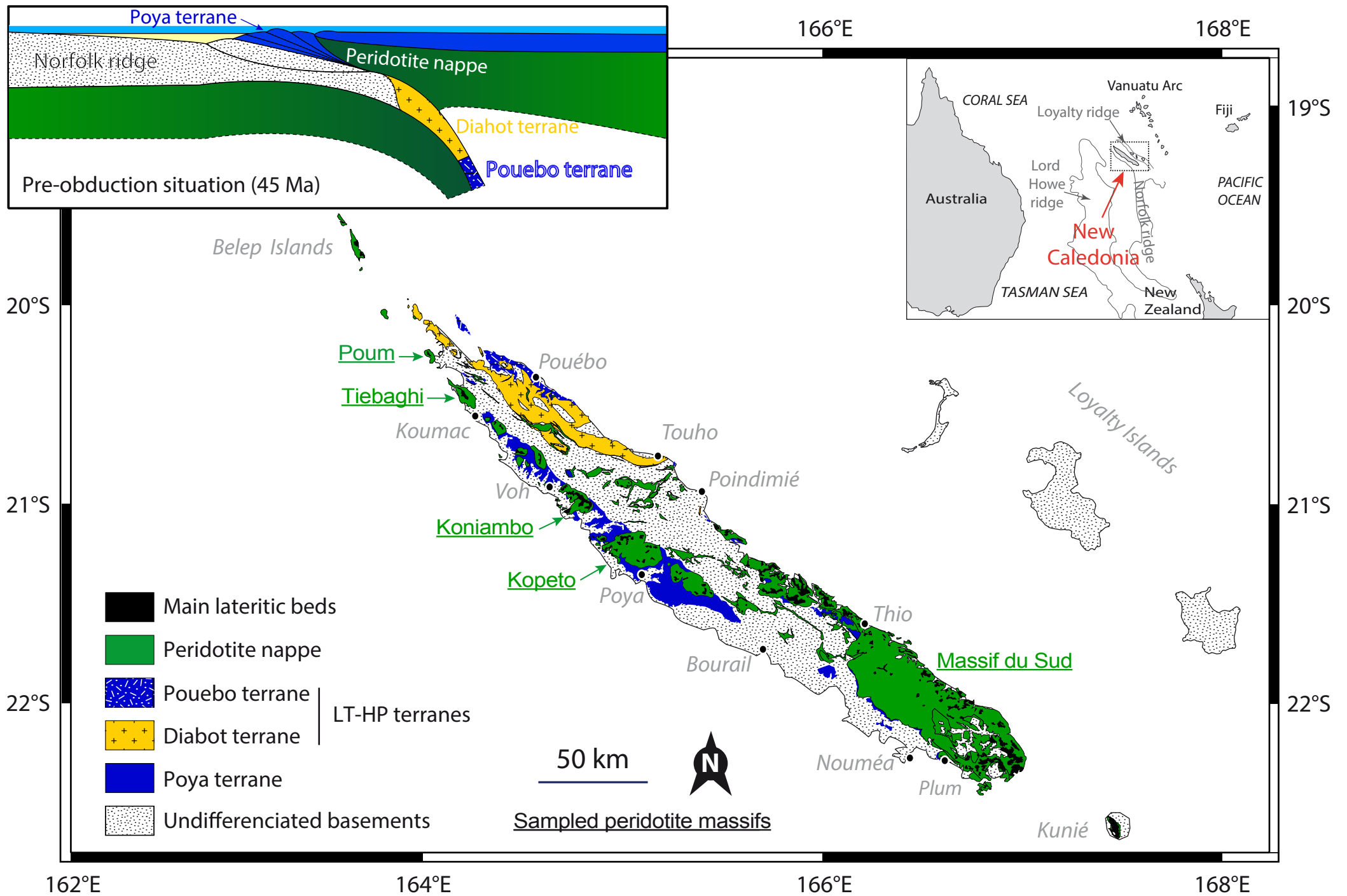
- 875 Deschamps F, Godard M, Guillot S, Chauvel C, Andréani M, Hattori KH, Wunder B, France L (2012) Behavior of fluid-
876 mobile elements in serpentines from abyssal to subduction environments: Examples from Cuba and Dominican
877 Republic. *Chemical Geology* 312-313:93-117
- 878 Deschamps F, Godard M, Guillot S, Hattori KH (2013) Geochemistry of subduction zone serpentinites: A review. *Lithos*
879 178:96-127
- 880 Deschamps F, Guillot S, Godard M, Andréani M, Hattori KH (2011) Serpentinites act as sponges for fluid-mobile
881 elements in abyssal and subduction zone environments. *Terra Nova* 23(3):171-178
- 882 Deville E, Prinzhofer A (2016) The origin of N₂-H₂-CH₄-rich natural gas seepages in ophiolitic context: A major and
883 noble gases study of fluid seepages in New Caledonia. *Chemical Geology* 440:139-147
- 884 Eiler JM (2001) Oxygen isotope variations of basaltic lavas and upper mantle rocks. *Stable Isotope Geochemistry* 43:319-
885 364
- 886 Eiler JM, McInnes B, Valley JW, Graham CM, Stolper EM (1998) Oxygen isotope evidence for slab-derived fluids in
887 the sub-arc mantle. *Nature* 393(6687):777-781
- 888 Eissen J-P, Crawford AJ, Cotten J, Meffre S, Bellon H, Delaune M (1998) Geochemistry and tectonic significance of
889 basalts in the Poya Terrane, New Caledonia. *Tectonophysics* 284(3-4):203-219
- 890 Elderfield H, Greaves MJ (1982) The rare earth elements in seawater. *Nature* 296(5854):214-219
- 891 Evans B, Johannes W, Oterdoom H, Trommsdorff V (1976) Stability of chrysotile and antigorite in the serpentine
892 multisystem. *Schweizerische Mineralogische und Petrographische Mitteilungen* 56:79-93
- 893 Evans BW (2004) The serpentinite multisystem revisited: Chrysotile is metastable. *International Geology Review*
894 46(6):479-506
- 895 Frisby C, Bizimis M, Mallick S (2016) Seawater-derived rare earth element addition to abyssal peridotites during
896 serpentinitization. *Lithos* 248-251:432-454
- 897 Fritsch E, Juillot F, Dublet G, Fonteneau L, Fandeur D, Martin E, Caner L, Auzende AL, Grauby O, Beaufort D (2016)
898 An alternative model for the formation of hydrous Mg/Ni layer silicates ('deweylite/'garnierite') in faulted
899 peridotites of New Caledonia: I. Texture and mineralogy of a paragenetic succession of silicate infillings. *European*
900 *Journal of Mineralogy* 28(2):295-311
- 901 Frost BR, Evans KA, Swapp SM, Beard JS, Mothersole FE (2013) The process of serpentinitization in dunite from New
902 Caledonia. *Lithos* 178:24-39
- 903 Früh-Green G, Plas A, Lécuyer C (1996) Petrologic and stable isotope constraints on hydrothermal alteration and
904 serpentinitization of the EPR shallow mantle at Hess Deep(Site 895). *Proceedings of the Ocean Drilling Program*
905 *Scientific Results* 147:255-291
- 906 Früh-Green G, Scambelluri M, Vallis F (2001) OH isotope ratios of high pressure ultramafic rocks: implications for fluid
907 sources and mobility in the subducted hydrous mantle. *Contributions to Mineralogy and Petrology* 141(2):145-
908 159
- 909 Fryer P (1992) A synthesis of Leg 125 drilling of serpentine seamounts on the Mariana and Izu-Bonin forearcs. In, vol
910 Fryer, P., Pearce, J.A., Stokking, L.B., et al., 1992. *Proc. ODP, Sci. Results*, 125: College Station, TX (Ocean
911 Drilling Program). pp 593-614
- 912 Gautier P, Quesnel B, Boulvais P, Cathelineau M (2016) The emplacement of the Peridotite Nappe of New Caledonia
913 and its bearing on the tectonics of obduction. *Tectonics* 35(12):3070-3094
- 914 Gillard M, Tugend J, Müntener O, Manatschal G, Karner G, Autin J, Sauter D, Figueredo PH, Ulrich M (2019) The role
915 of serpentinitization and magmatism in the formation of decoupling interfaces at magma-poor rifted margins. *Earth*
916 *Science Reviews* 196:102882
- 917 Guillot S, Hattori KH, Agard P, Schwartz S, Vidal O (2009) Exhumation processes in oceanic and continental subduction
918 contexts: a review. In: *Subduction zone geodynamics*, vol. Springer, pp 175-205
- 919 Guillot S, Hattori KH, de Sigoyer J (2000) Mantle wedge serpentinitization and exhumation of eclogites: insights from
920 eastern Ladakh, northwest Himalaya. *Geology* 28(3):199
- 921 Guillot S, Schwartz S, Reynard B, Agard P, Prigent C (2015) Tectonic significance of serpentinites. *Tectonophysics*
922 646:1-19
- 923 Hattori KH, Guillot S (2003) Volcanic fronts form as a consequence of serpentinite dehydration in the forearc mantle
924 wedge. *Geology* 31(6):525-528

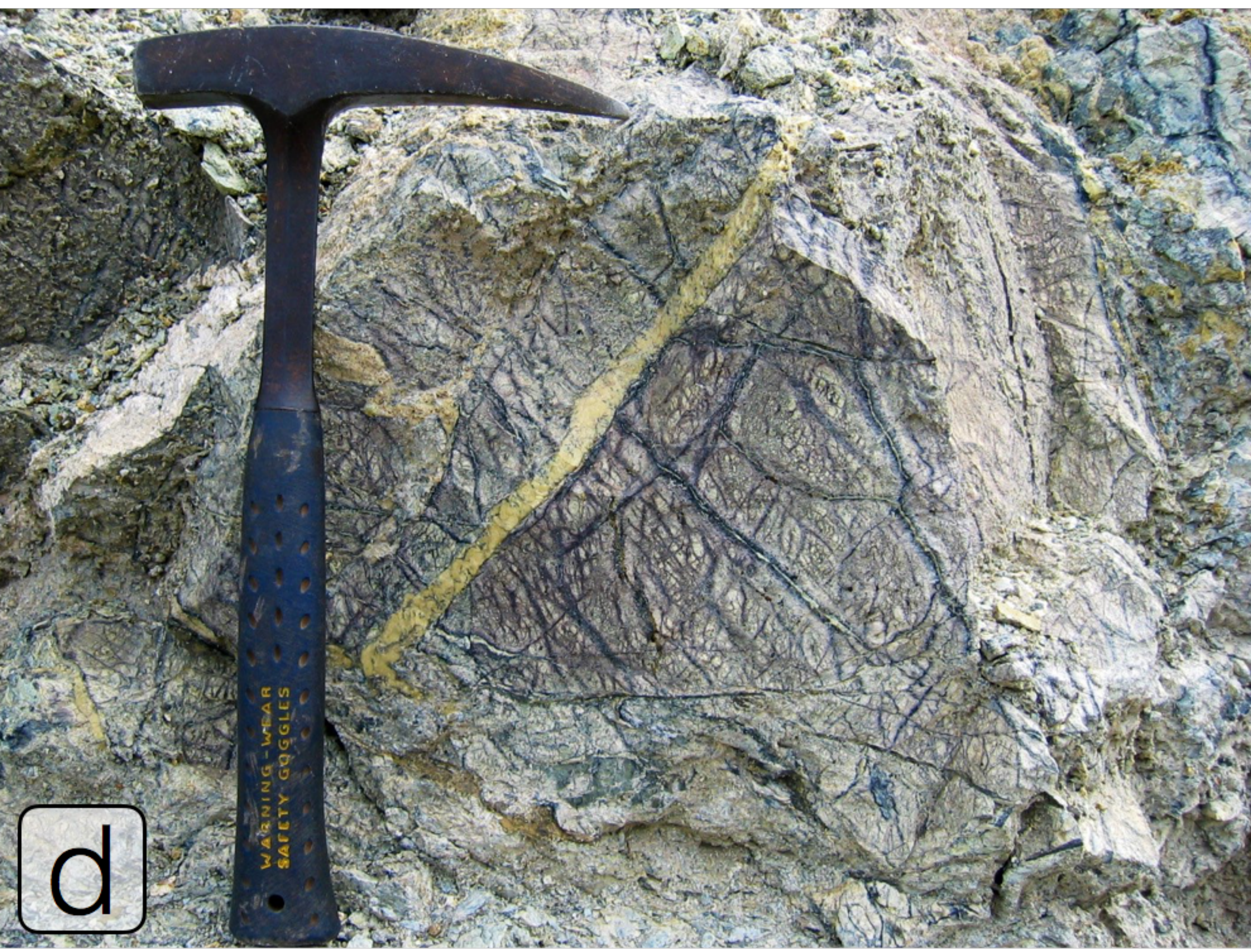
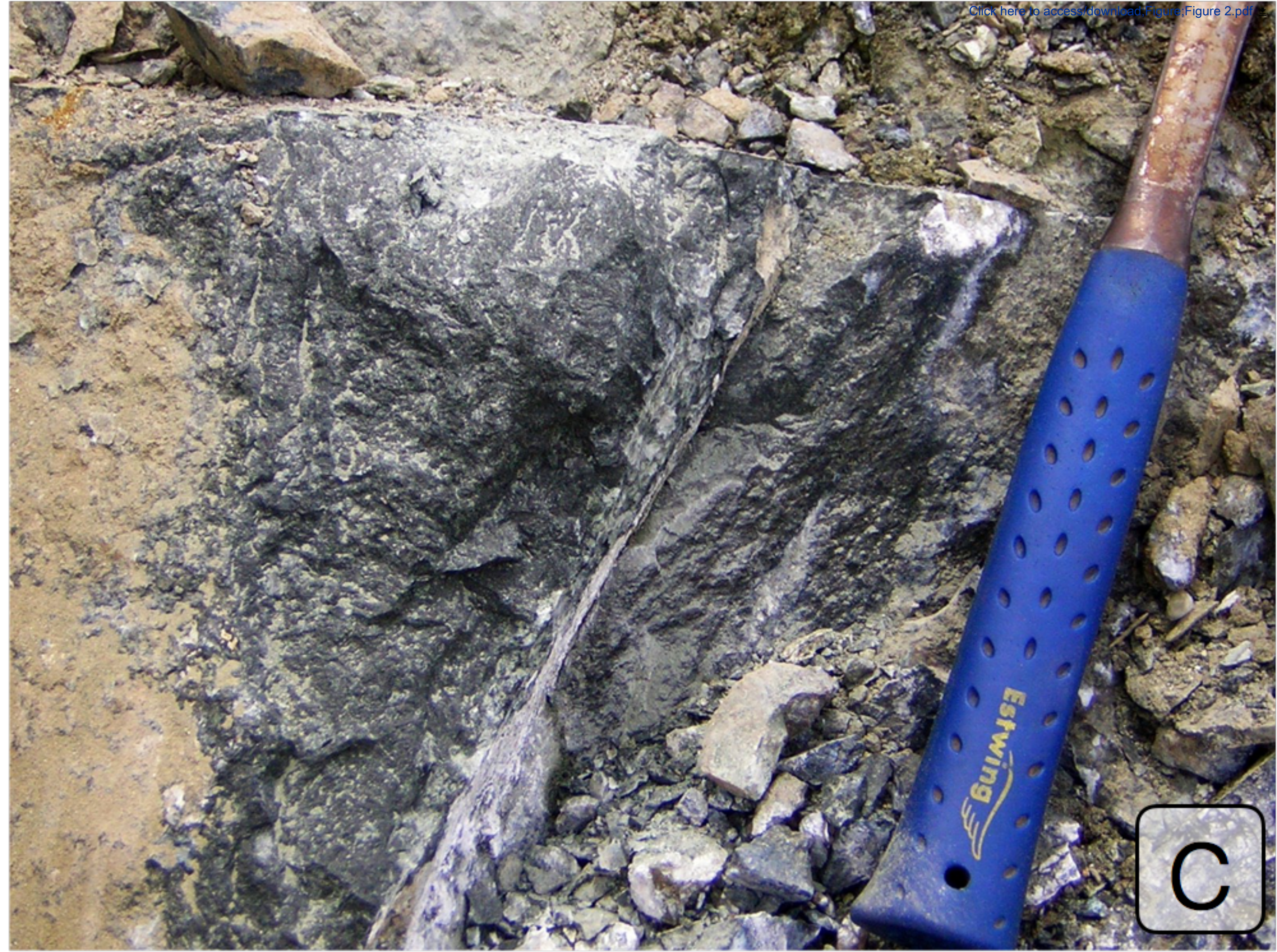
- 925 Hattori KH, Guillot S (2007) Geochemical character of serpentinites associated with high- to ultrahigh-pressure
926 metamorphic rocks in the Alps, Cuba, and the Himalayas: Recycling of elements in subduction zones.
927 *Geochemistry Geophysics Geosystems* 8(9):n/a-n/a
- 928 Hoefs J (2009) *Stable Isotope Geochemistry*. Springer, Berlin
- 929 Hyndman RD, Peacock SM (2003) Serpentinization of the forearc mantle. *Earth Planet Sci Lett* 212(3-4):417-432
- 930 Iwamori H (1998) Transportation of H₂O and melting in subduction zones. *Earth and Planetary Science Letters* 160(1):65-
931 80
- 932 Iyer K, Austrheim H, John T, Jamtveit B (2008) Serpentinization of the oceanic lithosphere and some geochemical
933 consequences: Constraints from the Leka Ophiolite Complex, Norway. *Chemical Geology* 249(1-2):66-90
- 934 Klein F, Bach W, McCollom TM (2013) Compositional controls on hydrogen generation during serpentinization of
935 ultramafic rocks. *Lithos* 178:55-69
- 936 Klein F, Marschall HR, Bowring SA, Humphris SE, Horning G (2017) Mid-ocean ridge serpentinite in the Puerto Rico
937 Trench: From seafloor spreading to subduction. *J Petrology* 58(9):1729-1754
- 938 Kodolanyi J, Pettke T, Spandler C, Kamber BS, Gmeling K (2012) Geochemistry of Ocean Floor and Fore-arc
939 Serpentinites: Constraints on the Ultramafic Input to Subduction Zones. *J Petrology* 53(2):235-270
- 940 Kogiso T, Tatsumi Y, Nakano S (1997) Trace element transport during dehydration processes in the subducted oceanic
941 crust: 1. Experiments and implications for the origin of ocean island basalts. *Earth Planet Sci Lett* 148(1-2):193-
942 205
- 943 Kyser TK, O'Hanley DS, Wicks FJ (1999) The origin of fluids associated with serpentinization processes: evidence from
944 stable-isotope compositions. *The Canadian Mineralogist* 37(1):223-237
- 945 Lafay R, Deschamps F, Schwartz S, Guillot S, Godard M, Debret B, Nicollet C (2013) High-pressure serpentinites, a
946 trap-and-release system controlled by metamorphic conditions: Example from the Piedmont zone of the western
947 Alps. *Chemical Geology* 343:38-54
- 948 Lemaire C (2000) *Application des spectroscopies vibrationnelles à la détection d'amiante dans les matériaux et à l'étude
949 des serpentines*. Université de Paris 7
- 950 Longerich HP, Jackson SE, Günther D (1996) Laser ablation inductively coupled plasma mass spectrometric transient
951 signal data acquisition and analyte concentration calculation. *Journal of Analytical Atomic Spectrometry*
952 11(9):899-904
- 953 Magaritz M, Taylor HP (1974) Oxygen and hydrogen isotope studies of serpentinization in the Troodos ophiolite
954 complex, Cyprus. *Earth and Planetary Science Letters* 23(1):8-14
- 955 McDonough WF, Sun SS (1995) The composition of the Earth. *Chemical Geology* 120(3-4):223-253
- 956 McRae ME (2018) Nickel. In: *US Geological Survey, Mineral Commodity Summaries, vol., U.S. Geological Survey,
957 Mineral Commodity Summaries*, pp 112-113
- 958 Mével C (2003) Serpentinization of abyssal peridotites at mid-ocean ridges. *Comptes Rendus Geosciences* 335(10-
959 11):825-852
- 960 Monnin C, Chavagnac V, Boulart C, Ménez B, Gérard M, Gérard E, Pisapia C, Quéméneur M, Erauso G, Postec A,
961 Guentas-Dombrowski L, Payri C, Pelletier B (2014) Fluid chemistry of the low temperature hyperalkaline
962 hydrothermal system of Prony Bay (New Caledonia). *Biogeosciences* 11(20):5687-5706
- 963 Mothersole FE, Evans K, Frost BR (2017) Abyssal and hydrated mantle wedge serpentinised peridotites: a comparison
964 of the 15°20'N fracture zone and New Caledonia serpentinites. *Contrib Mineral Petrol* 172(8):69
- 965 Muñoz M, Ulrich M, Cathelineau M, Mathon O (2019) Weathering processes and crystal chemistry of Ni-bearing
966 minerals in saprock horizons of New Caledonia ophiolite. *Journal of Geochemical Exploration* 198:82-99
- 967 Nicolini E, Rogers K, Rakowski D (2016) Baseline geochemical characterisation of a vulnerable tropical karstic aquifer;
968 Lifou, New Caledonia. *Biochemical Pharmacology* 5:114-130
- 969 O'Hanley DS (1996) *Serpentinites: records of tectonic and petrological history*. Oxford University Press,
- 970 Orloff O (1968) *Etude géologique et géomorphologique des massifs d'ultrabasites compris entre Houailou et Canala
971 (Nouvelle-Calédonie)*.
- 972 Peacock SM (1990) Fluid Processes in Subduction Zones. *Science* 248(4):329-337
- 973 Peacock SM, Hyndman RD (1999) Hydrous minerals in the mantle wedge and the maximum depth of subduction thrust
974 earthquakes. *Geophysical Research Letters* 26(16):2517-2520

- 975 Pearce NJG, Perkins WT, Westgate JA, Gorton MP, Jackson SE, Neal CR, Chenery SP (1997) A Compilation of New
976 and Published Major and Trace Element Data for NIST SRM 610 and NIST SRM 612 Glass Reference Materials.
977 *Geostandards and Geoanalytical Research* 21(1):115-144
- 978 Peters D, Bretscher A, John T, Scambelluri M, Pettke T (2017) Fluid-mobile elements in serpentinites: Constraints on
979 serpentinisation environments and element cycling in subduction zones. *Chemical Geology* 466:654-666
- 980 Picazo S, Cannat M, Delacour A, Escartín J, Rouméjon S, Silantsev S (2012) Deformation associated with the denudation
981 of mantle-derived rocks at the Mid-Atlantic Ridge 13°-15°N: The role of magmatic injections and hydrothermal
982 alteration. *Geochemistry Geophysics Geosystems* 13(9):n/a-n/a
- 983 Pinto VH, Manatschal G, Karpoff AM, Ulrich M, Viana AR (2016) Seawater storage and element transfer associated
984 with mantle serpentinization in magma-poor rifted margins: A quantitative approach. *Earth and Planetary Science
985 Letters* 459:1-11
- 986 Pirard C, Hermann J, O'Neill HSC (2013) Petrology and Geochemistry of the Crust-Mantle Boundary in a Nascent Arc,
987 Massif du Sud Ophiolite, New Caledonia, SW Pacific. *J Petrology* 54(9):1759-1792
- 988 Plank T (2014) The chemical composition of subducted sediments. In: *Treatise on geochemistry*, vol 4. Elsevier, pp 607-
989 629
- 990 Poli S, Schmidt MW (2002) Petrology of subducted slabs. *Annual Review of Earth and Planetary Sciences* 30(1):207-235
- 991 Quesnel B, Boulvais P, Gautier P, Cathelineau M, John CM, Dierick M, Agrinier P, Drouillet M (2016a) Paired stable
992 isotopes (O, C) and clumped isotope thermometry of magnesite and silica veins in the New Caledonia Peridotite
993 Nappe. *Geochim Cosmochim Acta* 183:234-249
- 994 Quesnel B, Boulvais P, Gautier P, Cathelineau M, Maurizot P, Cluzel D, Ulrich M, Guillot S, Lesimple S, Couteau C
995 (2013) Syn-tectonic, meteoric water-derived carbonation of the New Caledonia peridotite nappe. *Geology*
996 41(10):1063-1066
- 997 Quesnel B, Gautier P, Cathelineau M, Boulvais P, Couteau C, Drouillet M (2016b) The internal deformation of the
998 Peridotite Nappe of New Caledonia: A structural study of serpentine-bearing faults and shear zones in the
999 Koniambo Massif. *Journal of Structural Geology* 85:51-67
- 1000 Reynard B (2013) Serpentine in active subduction zones. *Lithos* 178:171-185
- 1001 Ribeiro Da Costa I, Barriga FJAS, Viti C, Mellini M, Wicks FJ (2008) Antigorite in deformed serpentinites from the Mid-
1002 Atlantic Ridge. *European Journal of Mineralogy* 20:563-572
- 1003 Rouméjon S, Cannat M, Agrinier P, Godard M, Andréani M (2015) Serpentinization and Fluid Pathways in Tectonically
1004 Exhumed Peridotites from the Southwest Indian Ridge (62-65 E). *J Petrology* 56(4):703-734
- 1005 Rüpke LH, Morgan JP, Hort M, Connolly JAD (2004) Serpentine and the subduction zone water cycle. *Earth Planet Sci
1006 Lett* 223(1-2):17-34
- 1007 Saccocia PJ, Seewald JS, Shanks III WC (2009) Oxygen and hydrogen isotope fractionation in serpentine-water and talc-
1008 water systems from 250 to 450°C, 50MPa. *Geochimica et Cosmochimica Acta* 73(22):6789-6804
- 1009 Sakai H, Tsutsumi M (1978) D-H Fractionation Factors Between Serpentine and Water at 100°C to 500°C and 2000 Bar
1010 Water-Pressure, and D-H Ratios of Natural Serpentines. *Earth and Planetary Science Letters* 40(2):231-242
- 1011 Sakai R, Kusakabe M, Noto M, Ishii T (1990) Origin of waters responsible for serpentinization of the Izu-Ogasawara-
1012 Mariana forearc seamounts in view of hydrogen and oxygen isotope ratios. *Earth and Planetary Science Letters*
1013 100(1-3):291-303
- 1014 Salters VJM, Longhi JE, Bizimis M (2002) Near mantle solidus trace element partitioning at pressures up to 3.4 GPa.
1015 *Geochem Geophys Geosystems* 3(7):1-23
- 1016 Salters VJM, Stracke A (2004) Composition of the depleted mantle. *Geochem Geophys Geosyst* 5(5):n/a-n/a
- 1017 Sano T, Hasenaka T, Shimaoka A, Yonezawa C, Fukuoka T (2001) Boron contents of Japan Trench sediments and Iwate
1018 basaltic lavas, Northeast Japan arc: estimation of sediment-derived fluid contribution in mantle wedge. *Earth
1019 Planet Sci Lett* 186(2):187-198
- 1020 Savin SM, Lee M (1988) Isotopic studies of phyllosilicates. In: Bailey S (ed) *Hydrous Phyllosilicates (exclusive of micas)*,
1021 vol 19. Mineralogical Society of America, pp 189-223
- 1022 Savov IP, Ryan J, D'Antonio M, Kelley K, Mattie P (2005) Geochemistry of serpentinized peridotites from the Mariana
1023 Forearc Conical Seamount, ODP Leg 125: Implications for the elemental recycling at subduction zones.
1024 *Geochemistry Geophysics Geosystems* 6(4):-

- 1025 Scambelluri M, Fiebig J, Malaspina N, Müntener O, Pettke T (2004) Serpentinite subduction: implications for fluid
1026 processes and trace-element recycling. *International Geology Review*:595-613
- 1027 Schmidt MW, Poli S (1998) Experimentally based water budgets for dehydrating slabs and consequences for arc magma
1028 generation. *Earth and Planetary Science Letters* 163(1):361-379
- 1029 Schwartz S, Allemand P, Guillot S (2001) Numerical model of the effect of serpentinites on the exhumation of eclogitic
1030 rocks: insights from the Monviso ophiolitic massif (Western Alps). *Tectonophysics* 342(1-2):193-206
- 1031 Schwarzenbach EM, Caddick MJ, Beard JS, Bodnar RJ (2015) Serpentinization, element transfer, and the progressive
1032 development of zoning in veins: evidence from a partially serpentinized harzburgite. *Contributions to Mineralogy
1033 and Petrology* 171(1):1-22
- 1034 Secchiari A, Montanini A, Bosch D, Macera P, Cluzel D (2016) Melt extraction and enrichment processes in the New
1035 Caledonia lherzolites: Evidence from geochemical and Sr–Nd isotope data. *Lithos* 260:28-43
- 1036 Secchiari A, Montanini A, Bosch D, Macera P, Cluzel D (2019) Sr, Nd, Pb and trace element systematics of the New
1037 Caledonia harzburgites: tracking source depletion and contamination processes in a SSZ setting. *Geoscience
1038 Frontiers*
- 1039 Sharp Z (1992) In situ laser microprobe techniques for stable isotope analysis. *Chemical Geology* 101:3-19
- 1040 Sharp Z, Atudorei V, Durakiewicz T (2001) A rapid method for determination of hydrogen and oxygen isotope ratios
1041 from water and hydrous minerals. *Chemical Geology* 178(1-4):197-210
- 1042 Sheppard SMF, Nielsen RL, Taylor HP (1969) Oxygen and hydrogen isotope ratios of clay minerals from porphyry
1043 copper deposits. *Economic Geology* 64(7):755-777
- 1044 Staudigel H, Hart SR, Richardson SH (1981) Alteration of the oceanic crust: Processes and timing. *Earth and Planetary
1045 Science Letters* 52(2):311-327
- 1046 Stern RJ (2002) Subduction zones. *Reviews of Geophysics* 40(4):1012
- 1047 Tenthoery E, Hermann J (2004) Composition of fluids during serpentinite breakdown in subduction zones: Evidence for
1048 limited boron mobility. *Geology* 32(1):865
- 1049 Thakurta J, Ripley EM, Li C (2009) Oxygen isotopic variability associated with multiple stages of serpentinization, Duke
1050 Island Complex, southeastern Alaska. *Geochimica et Cosmochimica Acta* 73(20):6298-6312
- 1051 Ulmer P, Trommsdorff V (1995) Serpentine Stability to Mantle Depths and Subduction-Related Magmatism. *Science*
1052 268(5212):858-861
- 1053 Ulmer P, Trommsdorff V (1999) Phase relations of hydrous mantle subducting to 300km. *Geochemical Society Special
1054 Publication* 6:259-281
- 1055 Ulrich M, Cathelineau M, Muñoz M, Boiron M-C, Teitler Y, Karpoff AM (2019) The relative distribution of critical (Sc,
1056 REE) and transition metals (Ni, Co, Cr, Mn, V) in some Ni-laterite deposits of New Caledonia. *Journal of
1057 Geochemical Exploration* 197:93-113
- 1058 Ulrich M, Muñoz M, Guillot S, Cathelineau M, Picard C, Quesnel B, Boulvais P, Couteau C (2014) Dissolution–
1059 precipitation processes governing the carbonation and silicification of the serpentinite sole of the New Caledonia
1060 ophiolite. *Contributions to Mineralogy and Petrology* 167(1):952-919
- 1061 Ulrich M, Picard C, Guillot S, Chauvel C, Cluzel D, Meffre S (2010) Multiple melting stages and refertilization as
1062 indicators for ridge to subduction formation: The New Caledonia ophiolite. *Lithos* 115(1):223-236
- 1063 Wenner D, Taylor H (1971) Temperatures of serpentinization of ultramafic rocks based on O 18/O 16 fractionation
1064 between coexisting serpentine and magnetite. *Contributions to Mineralogy and Petrology* 32(3):165-185
- 1065 Wenner DB, Taylor HP (1973) Oxygen and hydrogen isotope studies of the serpentinization of ultramafic rocks in oceanic
1066 environments and continental ophiolite complexes. *American Journal of Science* 273(3):207
- 1067 Whattam SA, Malpas J, Ali JR, Smith IEM (2008) New SW Pacific tectonic model: Cyclical intraoceanic magmatic arc
1068 construction and near-coeval emplacement along the Australia-Pacific margin in the Cenozoic. *Geochemistry
1069 Geophysics Geosystems* 9(3):n/a-n/a
- 1070 Workman RK, Hart SR (2005) Major and trace element composition of the depleted MORB mantle (DMM). *Earth Planet
1071 Sci Lett* 231(1-2):53-72
- 1072 Wunder B, Wirth R, Gottschalk M (2001) Antigorite: Pressure and temperature dependence of polysomatism and water
1073 content. *European Journal of Mineralogy* 13(3):485
- 1074 Zheng Y (1993) Calculation of oxygen-Isotope Fractionation in Hydroxyl-Bearing Silicates. *Earth and Planetary Science
1075 Letters* 120:247-263

Figure 1





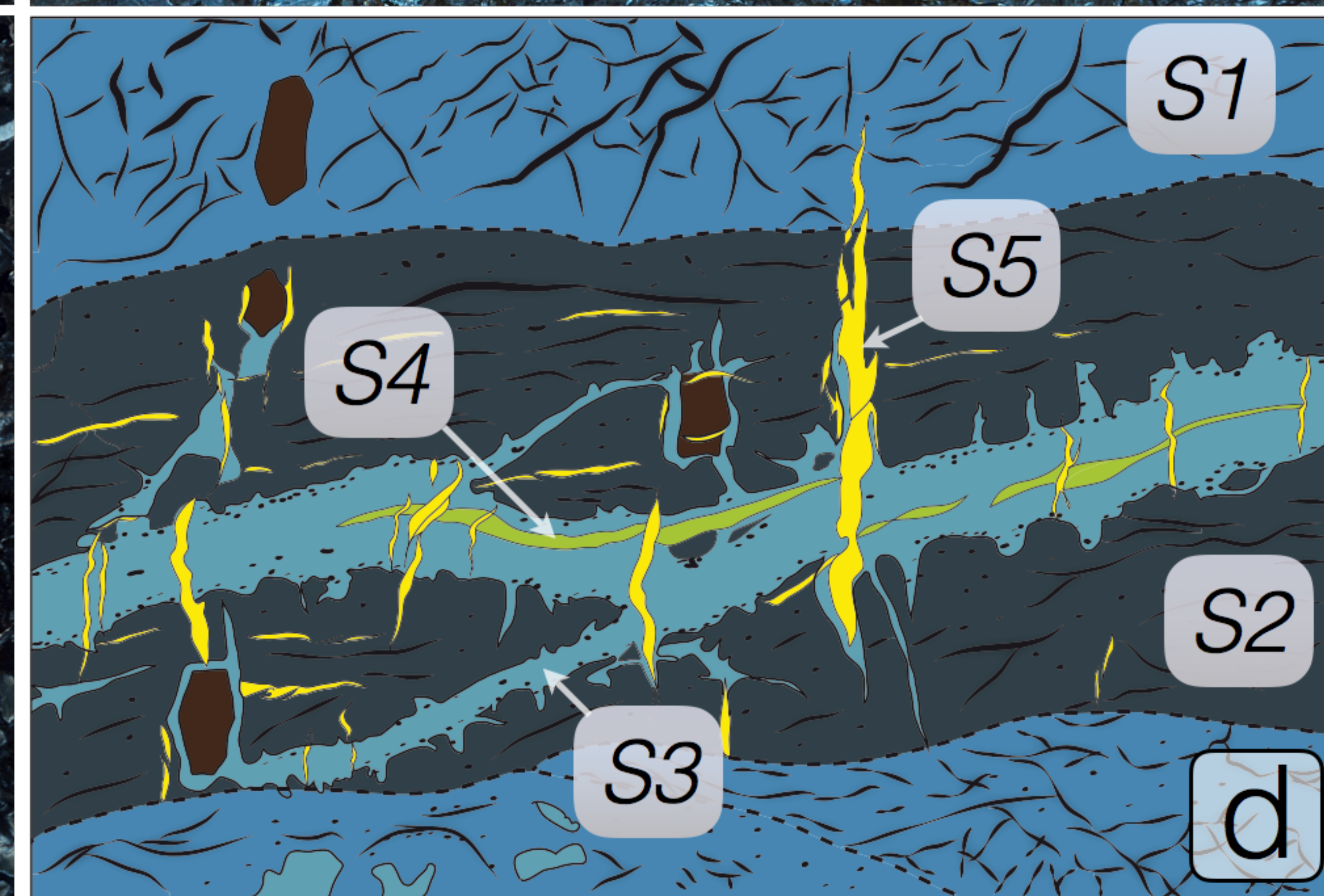
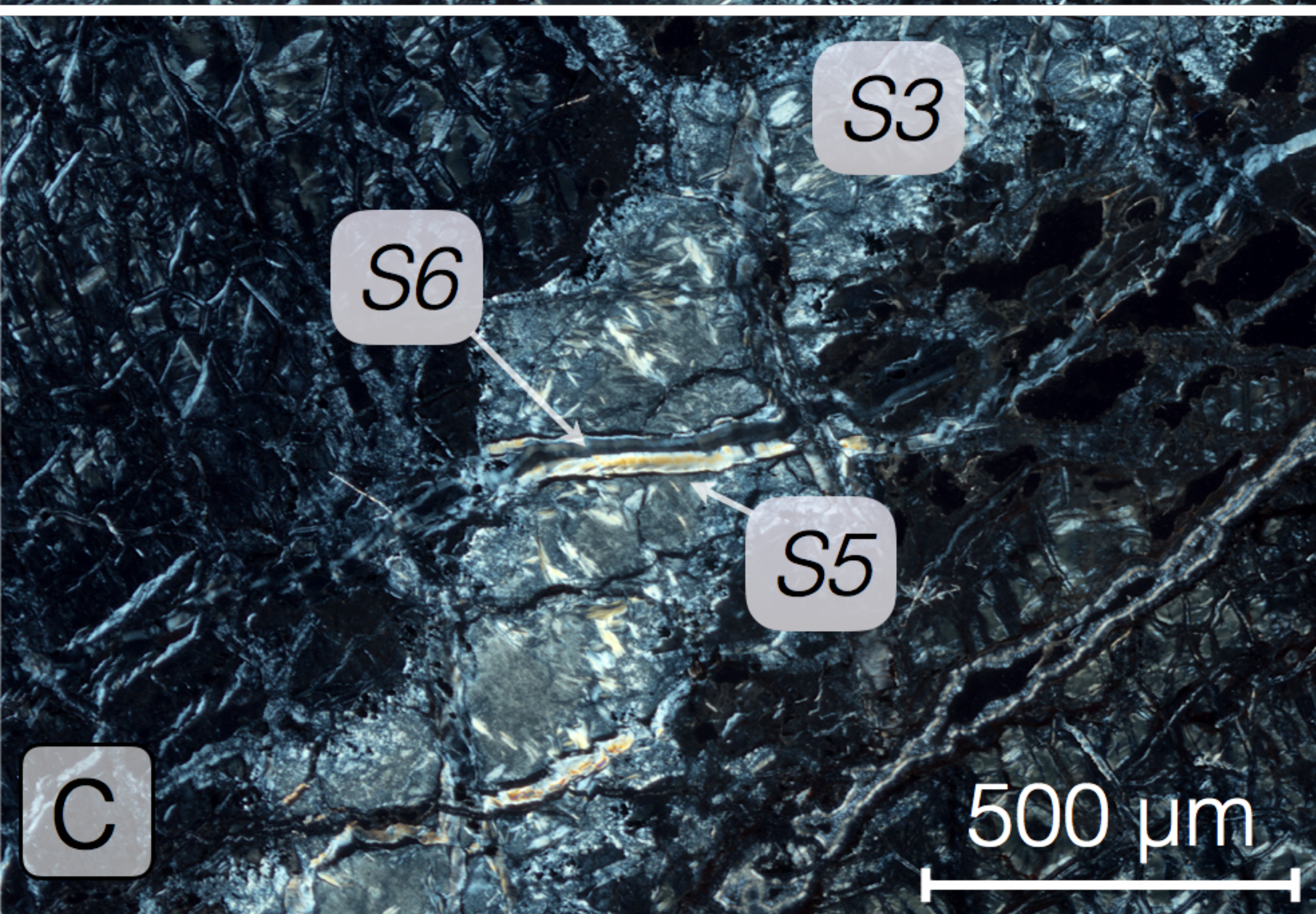
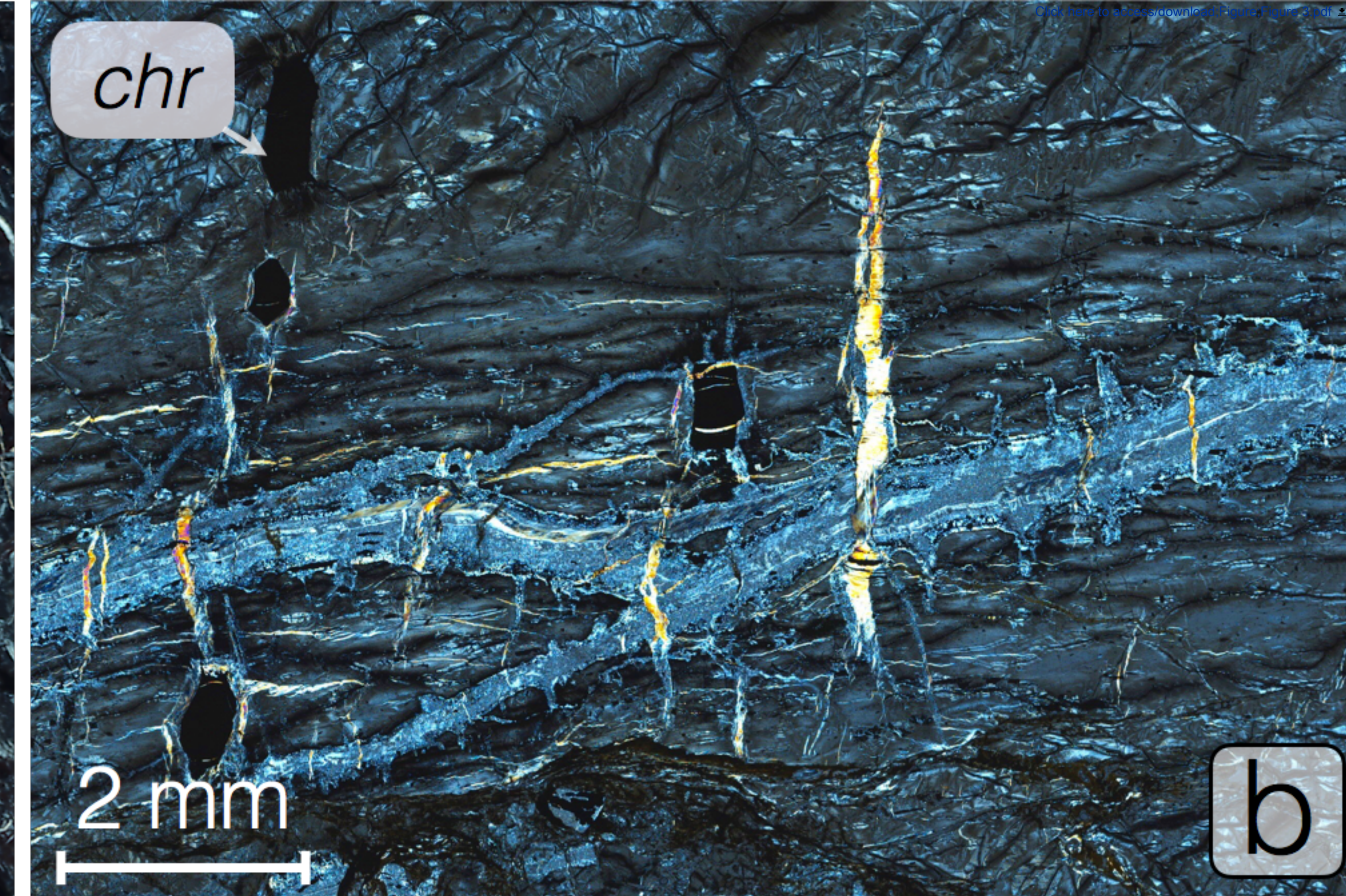
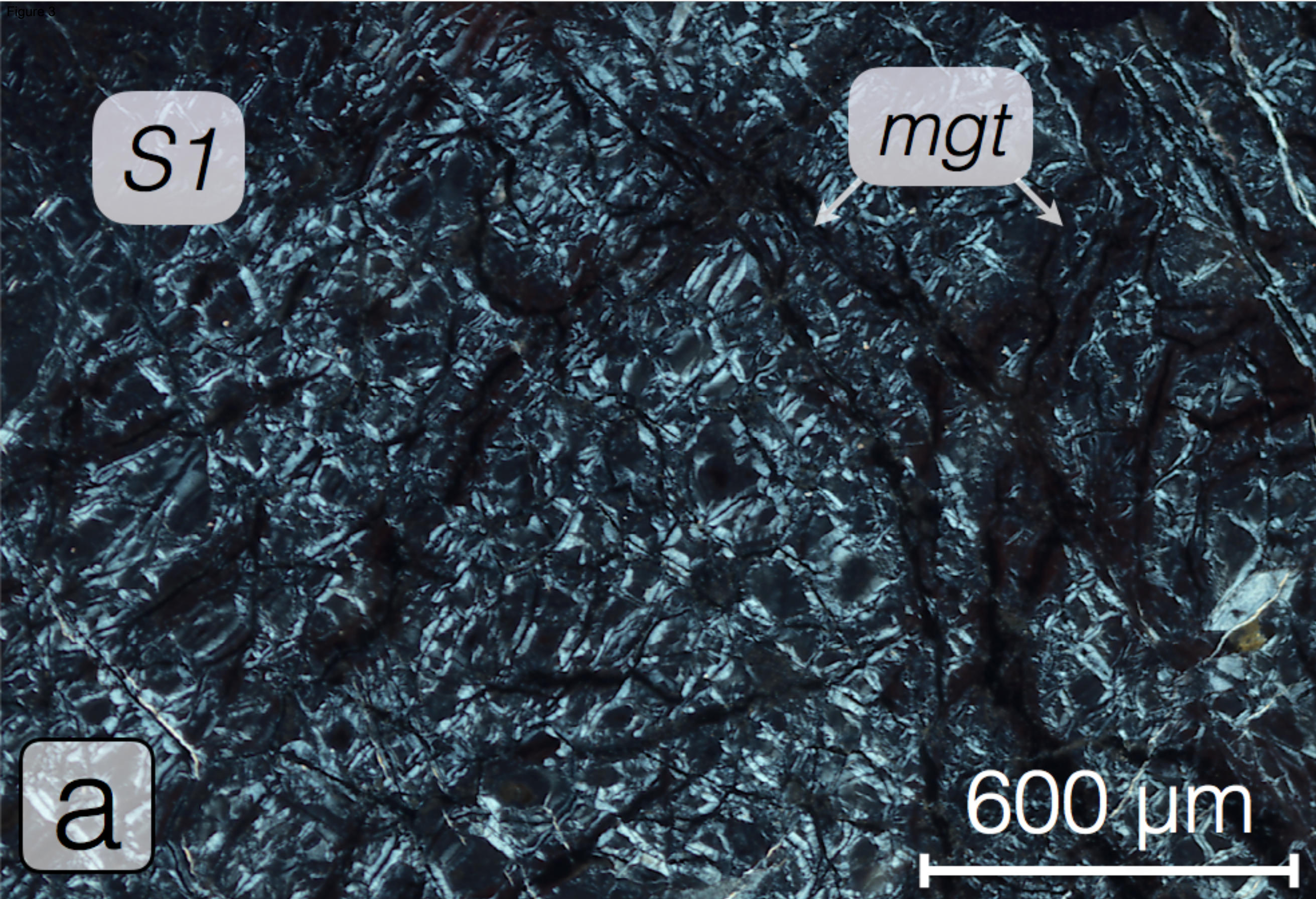


Figure 4

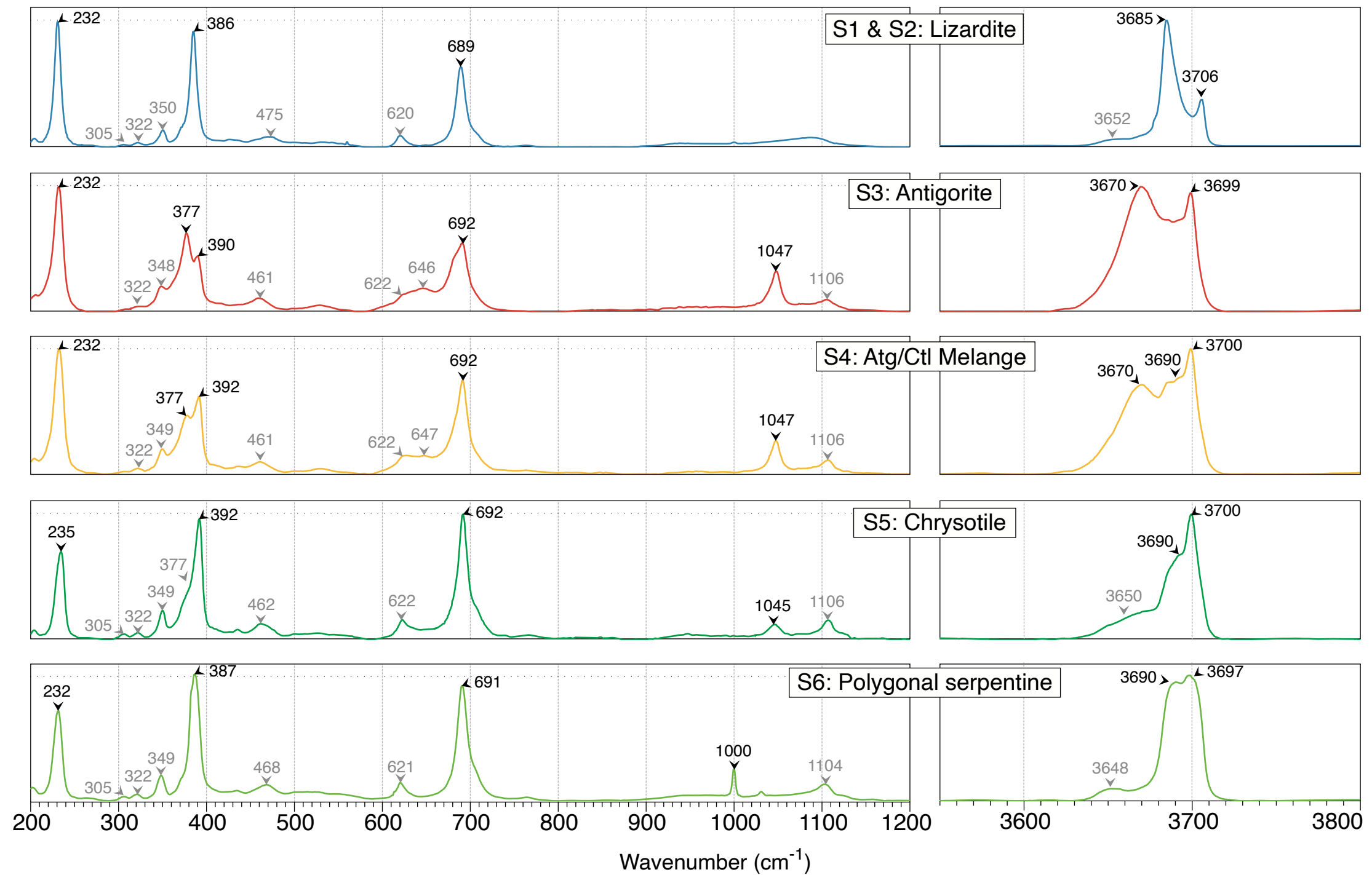
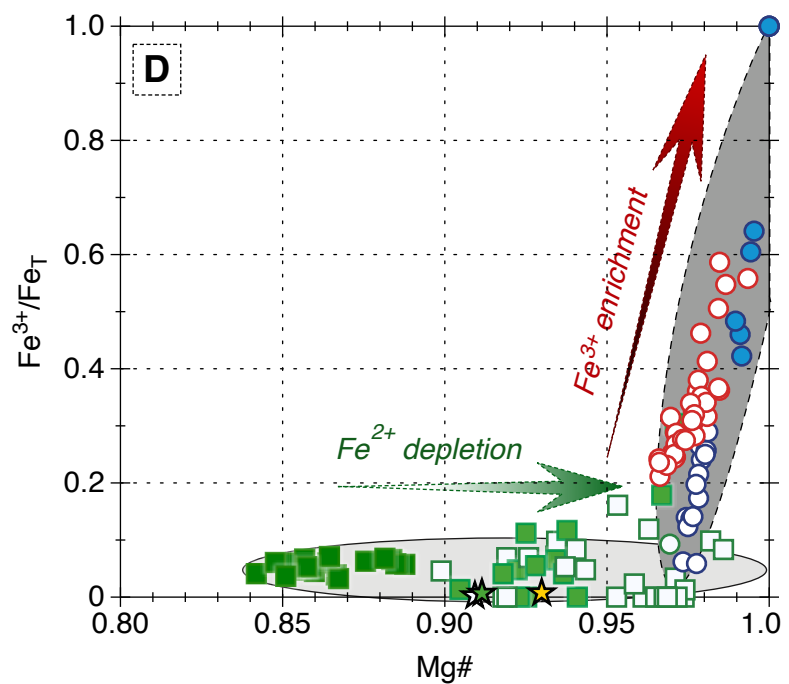
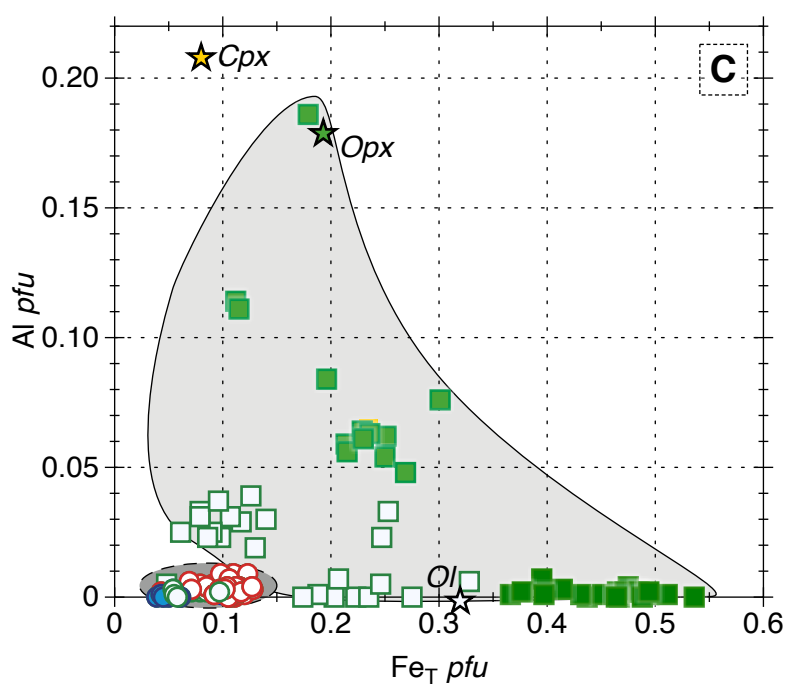
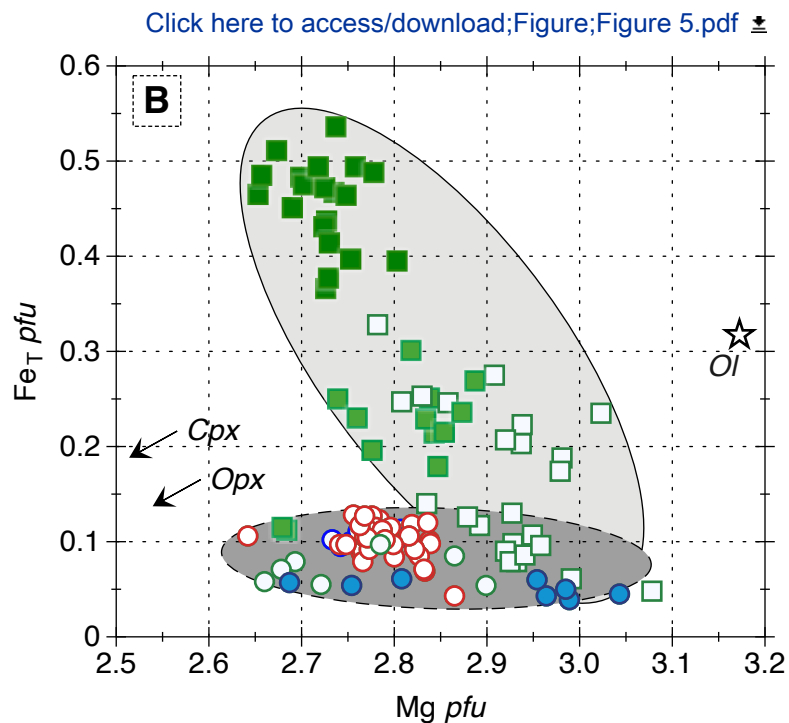
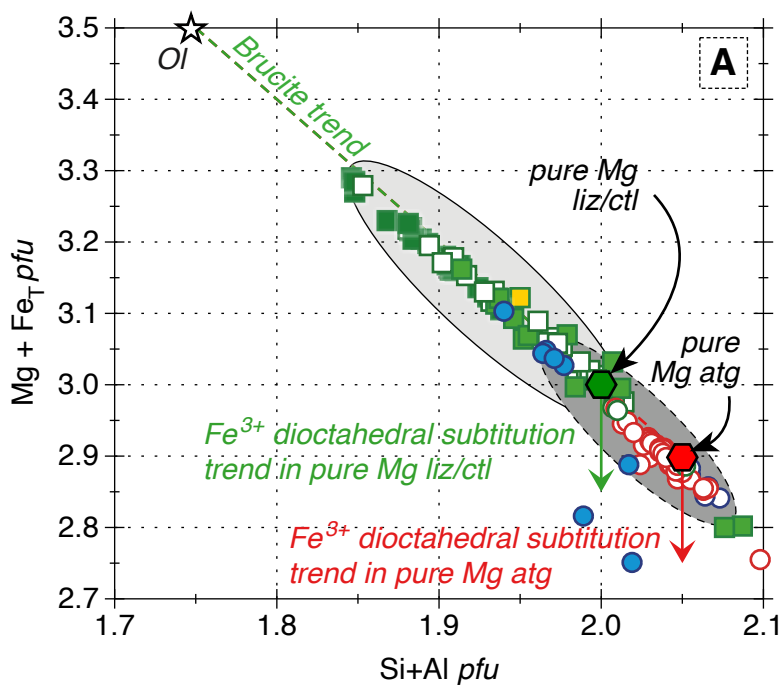


Figure 5

**Upper Serpentines**

- Lizardite (after olivine)
- Lizardite (after orthopyroxene)
- Lizardite (after clinopyroxene)
- Lizardite (mesh)

Serpentinite sole

- Lizardite
- Antigorite
- Chrysotile
- Polygonal

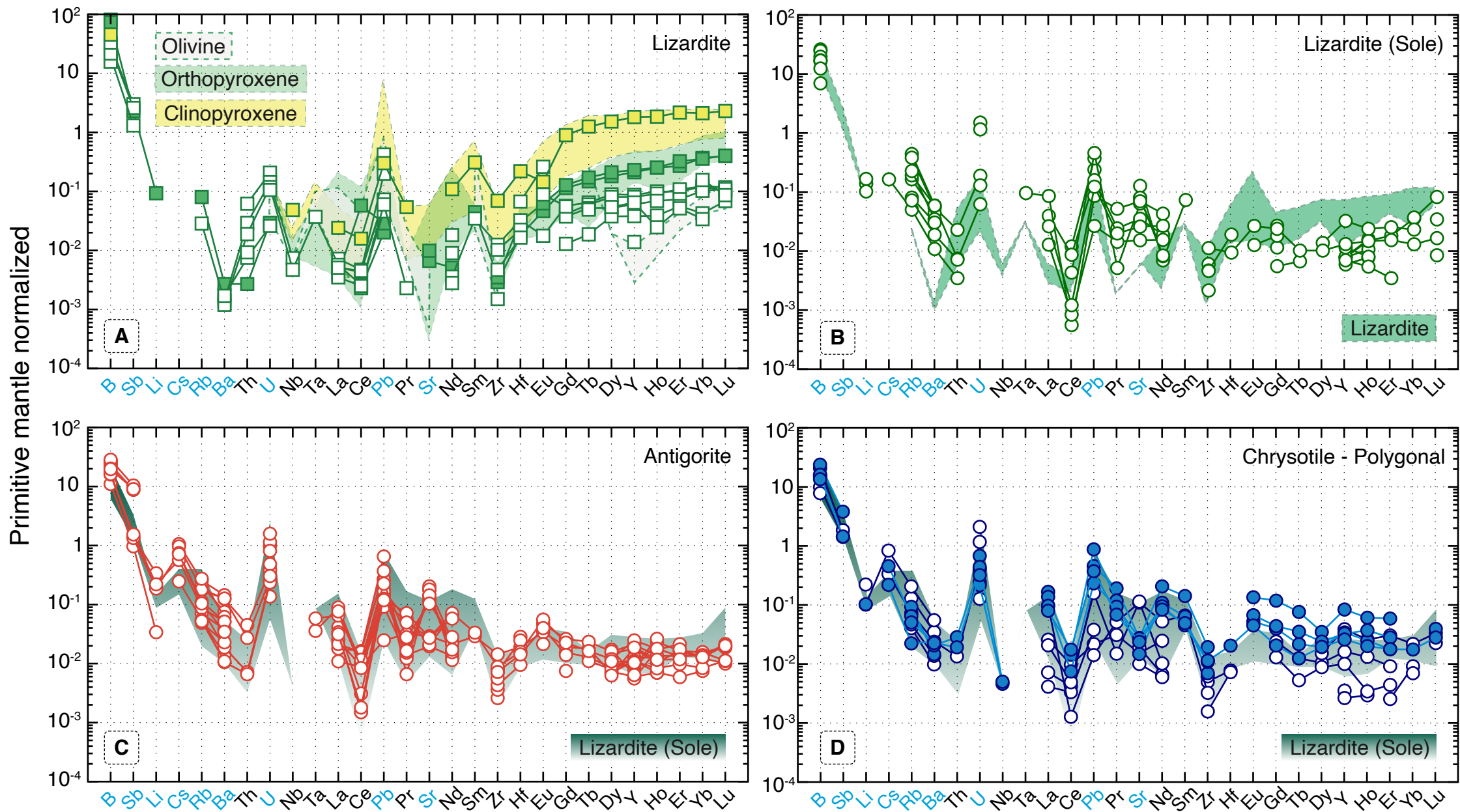
Primary minerals

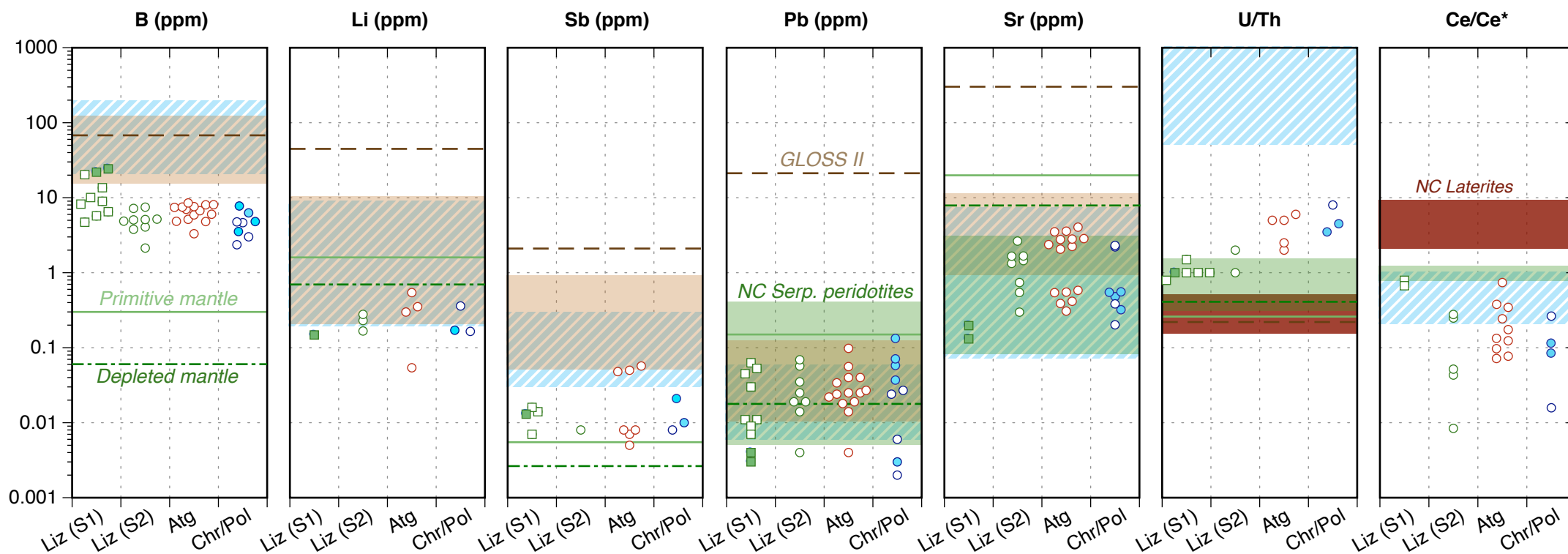
- ☆ Olivine
- ☆ Orthopyroxene
- ☆ Clinopyroxene

Fields

- Upper part of the massifs
- Serpentinite sole

Figure 6



**Upper serpentines**

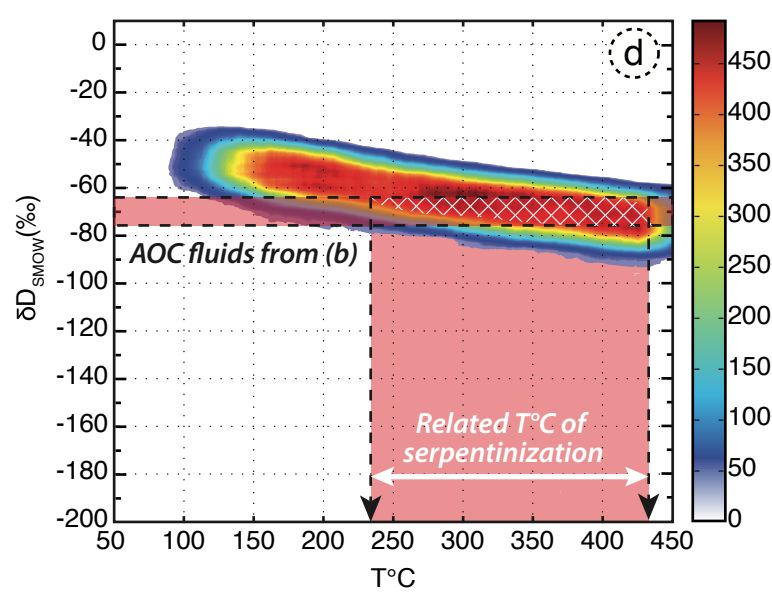
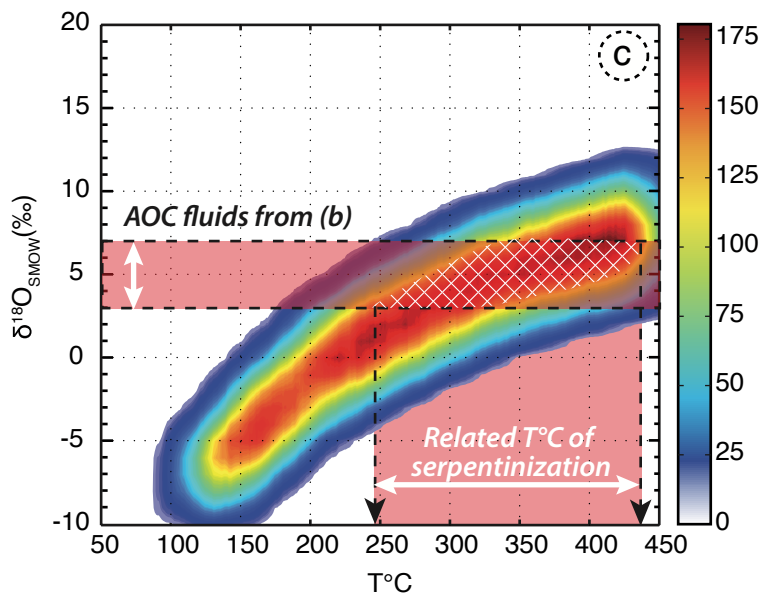
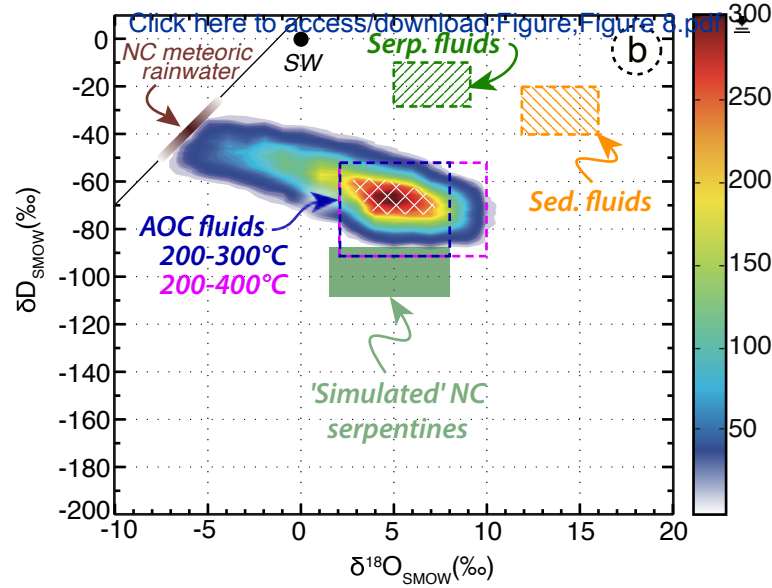
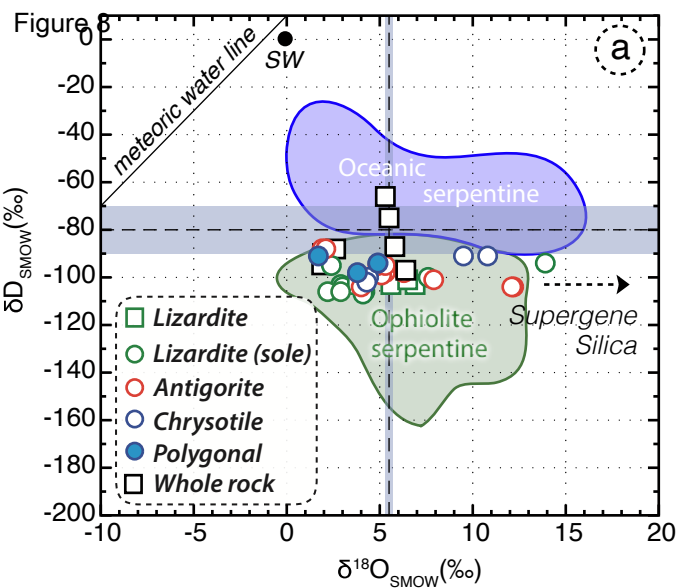
- Lizardite (S1)
- Lizardite (after opx)

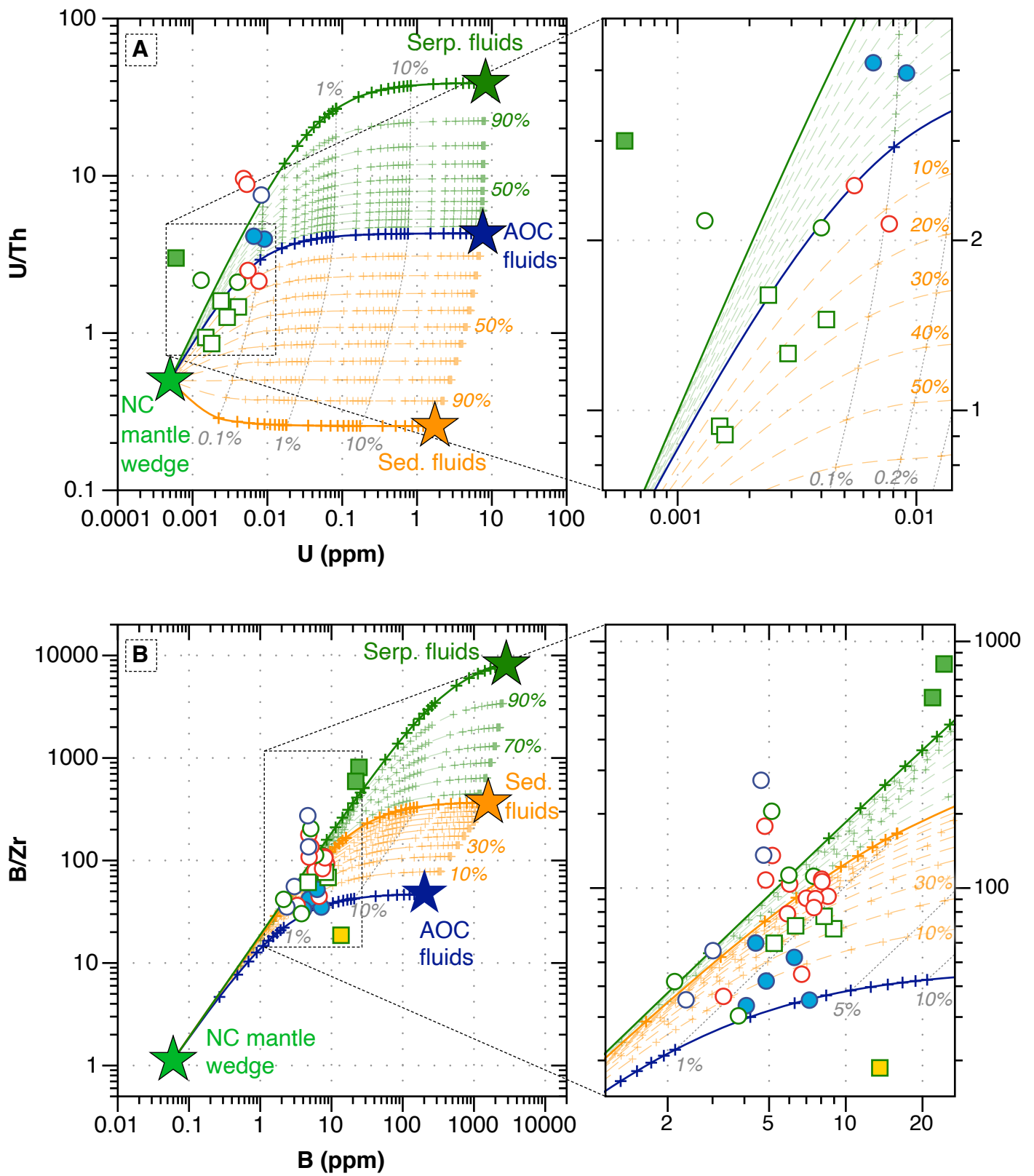
Serpentinite sole

- Lizardite (S2)
- Antigorite (S3)
- Chrysotile (S5)
- Polygonal serpentine (S6)

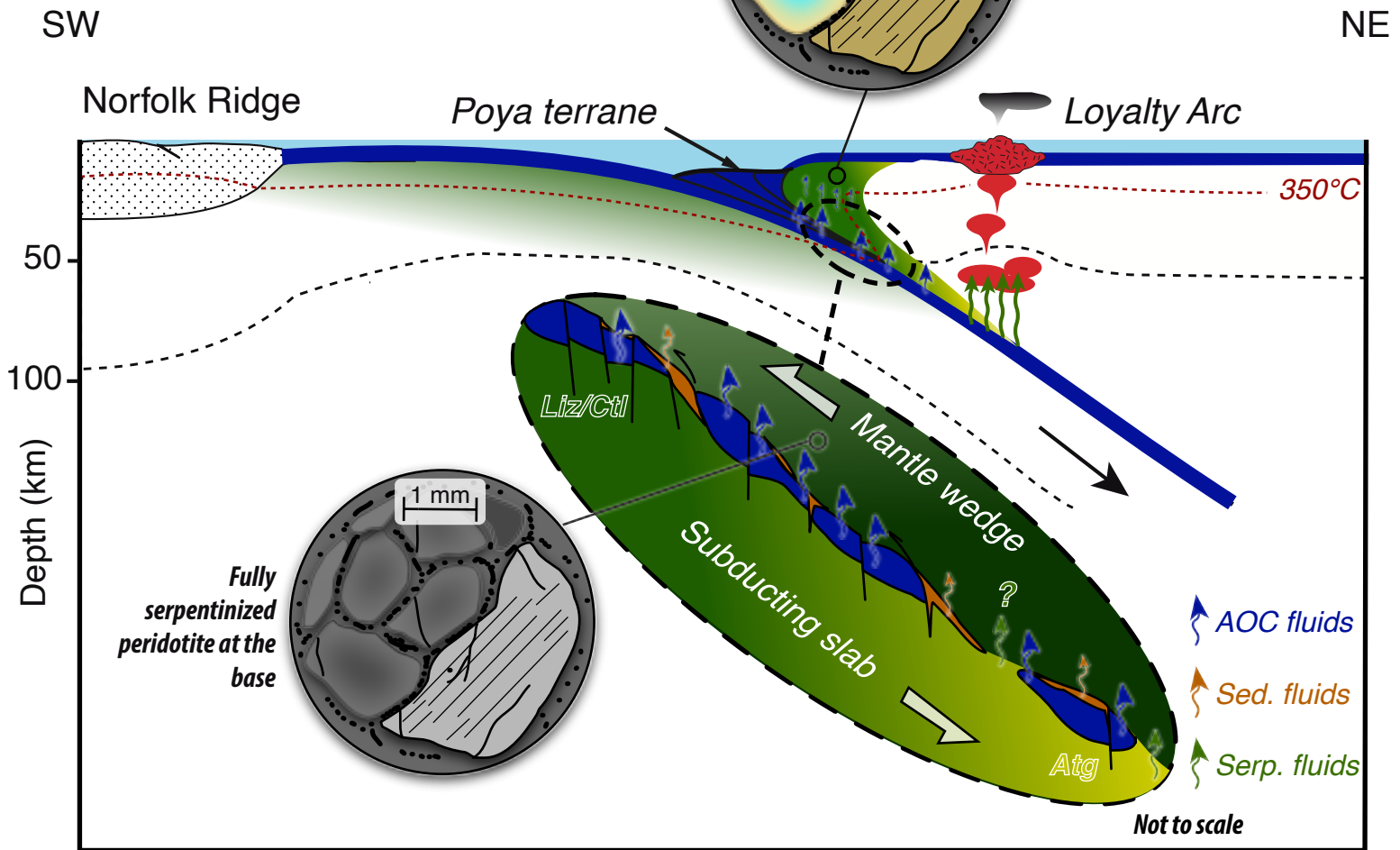
Literature references

- ▨ Abyssal serpentinites
- ▨ Serpentinized peridotites
- ▨ NC laterites

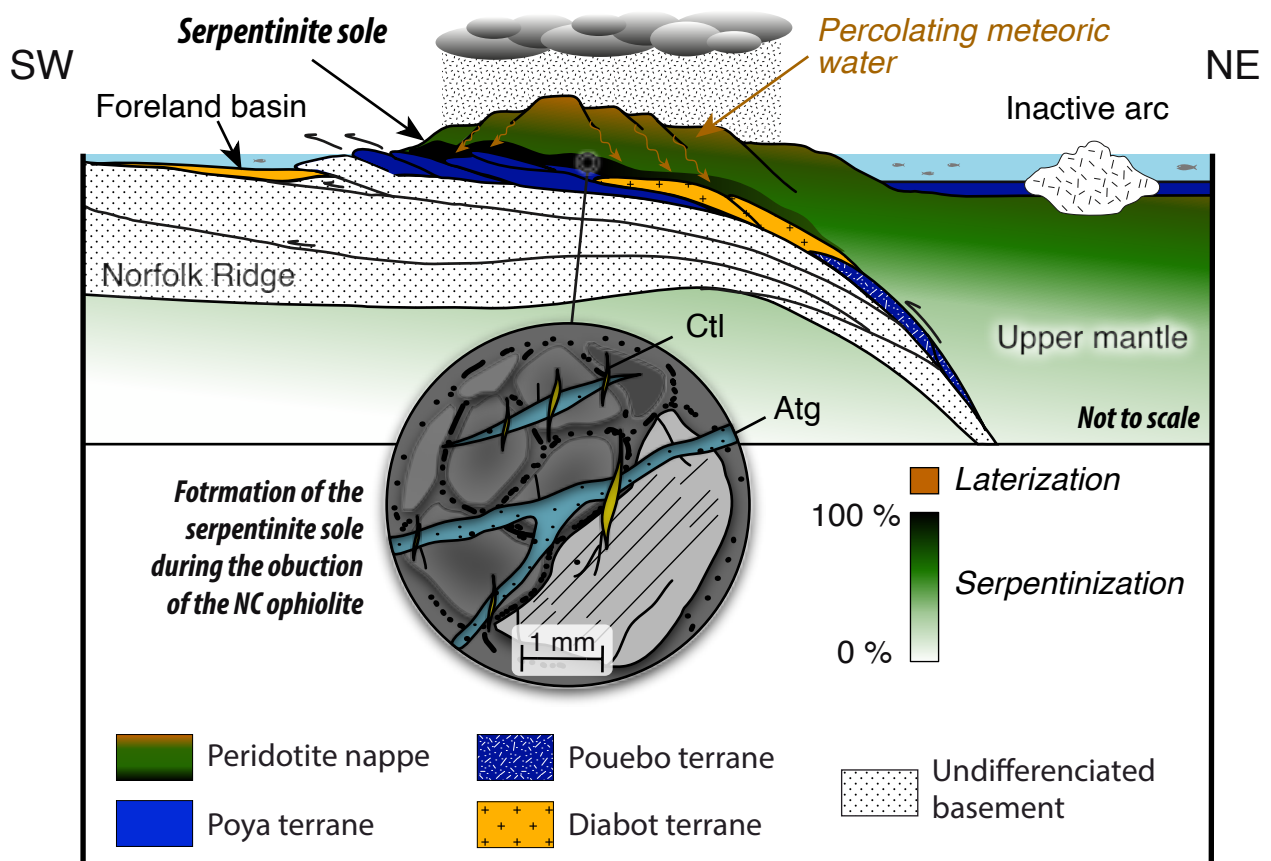




A : Forearc serpentinitization (45 Ma)



B: Serpentinite sole formation (~40 Ma)



Structural position	Upper part of the ophiolite												
	MS60-1	Ti6-3	Ti50A-07-6	Ti50A-07-9	Ti6-1	Ti50A-07-3	Ti50-2	Ti48	Poum 17	Ti-48	Ti48-06	Poum-13	xx3786A-7
Sample id													
Type	Lizardite		Lizardite		Lizardite	Lizardite	Olivine		Orthopyroxene		Clinopyroxene		Lizarc
Texture	Mesh core		Mesh rim		Bastite	Bastite							Clast and matr
Primary minerals	Olivine		Olivine		Opx	Cpx							
SiO₂	40.0	41.7	38.9	38.5	42.4	39.4	41.0	40.8	55.2	55.1	51.9	51.7	43.2
TiO₂	-	-	-	0.01	0.07	0.04	-	-	0.09	0.11	0.30	0.27	0.04
Al₂O₃	-	0.57	0.01	-	2.07	1.15	-	-	4.20	3.56	4.77	4.26	0.04
FeO	5.58	2.75	10.97	11.41	2.86	5.88	8.75	8.83	6.01	5.88	2.44	2.07	2.21
MnO	0.02	-	0.19	0.04	0.15	0.18	0.16	0.14	0.16	0.15	0.10	0.12	0.08
MgO	41.3	42.4	36.7	37.5	38.7	40.3	50.0	49.8	33.5	33.1	16.3	16.3	41.4
CaO	-	-	-	-	0.11	-	0.04	0.02	0.47	1.06	23.11	23.01	-
Na₂O	0.01	0.02	-	-	0.03	-	-	-	0.01	-	0.29	0.38	-
K₂O	-	-	-	-	0.01	-	-	-	-	-	-	-	0.02
Cr₂O₃	-	-	-	-	0.95	-	0.01	0.01	0.66	0.88	1.01	1.11	-
NiO	0.38	0.11	0.49	0.47	0.15	0.40	0.41	0.38	0.10	0.10	0.05	0.05	0.48
Total	87.3	87.5	87.3	87.9	87.5	87.3	100.3	99.9	100.4	99.9	100.2	99.3	87.4
<i>Number of oxygen p.f.u.</i>	7		7		7	7	4		6		6		7
Si	1.92	1.95	1.91	1.88	1.97	1.86	1.00	1.00	1.90	1.91	1.88	1.89	2.00
Ti	-	-	-	-	0.002	-	-	-	0.002	0.003	0.008	0.007	0.001
Al	0.018	0.031	0.001	-	0.114	0.064	-	-	0.170	0.146	0.203	0.183	0.002
Fe³⁺	-	-	0.027	0.021	0.020	-	-	-	-	-	-	-	0.023
Fe²⁺	0.212	0.107	0.424	0.446	0.092	0.313	0.178	0.181	0.173	0.170	0.074	0.063	0.062
Mn	0.002	-	0.008	0.002	0.006	0.007	-	-	0.005	0.005	0.003	0.004	0.003
Mg	2.90	2.95	2.69	2.73	2.68	2.84	1.81	1.81	1.72	1.71	0.88	0.89	2.86
Ca	-	-	-	-	0.006	-	<0.001	<0.001	0.017	0.039	0.897	0.900	-
Na	0.002	0.002	-	-	0.002	-	-	-	<0.001	-	0.020	0.027	-
K	-	-	-	-	0.001	-	-	-	-	-	-	-	0.001
Cr	-	-	-	-	0.035	-	<0.001	<0.001	0.018	0.024	0.029	0.032	-
Ni	0.008	0.004	0.019	0.018	0.006	0.015	0.008	0.007	0.003	0.003	0.001	0.001	0.018
Mg#	0.93	0.96	0.86	0.86	0.97	0.90	0.91	0.91	0.91	0.91	0.92	0.93	0.98
Fe³⁺/(Fe²⁺+Fe³⁺)	-	-	0.06	0.04	0.18	-	-	-	-	-	-	-	0.27

Serpentinite sole

KOP-13	xx3786A-13	KOP3-5	xx3758-7	xx3786B-2	KOP3-3	KOP3-4
lite	Antigorite		Chrysotile		Polygonal	
breccia	Vein		Vein		Vein and breccia	
ix					matrix	
44.0	43.5	44.4	44.1	43.5	44.6	45.5
0.01	-	-	0.02	-	-	-
0.05	0.02	0.01	0.06	0.05	0.05	0.01
1.42	2.85	2.42	2.01	2.08	1.46	1.54
0.05	0.01	0.03	0.06	0.02	0.02	-
42.6	39.9	41.4	40.0	40.4	41.5	40.7
0.07	-	0.09	0.11	0.08	0.04	-
0.03	0.06	0.01	0.02	0.05	0.02	0.02
0.01	-	-	0.02	0.01	-	0.02
-	-	0.01	-	0.10	-	0.08
0.29	0.23	0.10	0.05	0.12	0.21	0.21
88.5	86.6	88.4	86.4	86.4	87.9	88.1
	6.823		7		7	
2.01	1.98	1.98	2.06	2.04	1.99	2.02
-	-	-	0.001	-	-	-
0.003	0.001	0.001	0.003	0.003	0.003	0.001
0.017	0.027	0.026	0.011	0.016	0.054	0.057
0.037	0.082	0.065	0.067	0.065	0	0
0.002	0.000	0.001	0.002	0.001	0.001	-
2.90	2.72	2.75	2.78	2.82	2.75	2.69
0.003	-	0.004	0.006	0.004	0.002	-
0.003	0.005	0.001	0.002	0.005	0.002	0.002
0.001	-	-	0.001	0.001	-	0.001
-	-	<0.001	-	0.004	-	0.003
0.011	0.008	0.004	0.002	0.005	0.008	0.007
0.99	0.97	0.98	0.98	0.98	1.00	1.00
0.31	0.25	0.28	0.14	0.20	1.00	1.00

Structural position	Upper serpentinite											
Type	Lizardite		Lizardite	Lizardite	Olivine		Orthopyroxene		Clinopyroxene		Lizardite	
Texture	Mesh core		Bastite	Bastite							Clast and breccia	
Primary minerals	Olivine		Opx	Cpx								
Sample name	Ti-6	Ti 50	Ti-6	Ti-50	TI-50	Poum-13	TI-48	Poum-11	Ti 50	Poum-11	xx-3786a	Ti-47
Li	<0.071	<0.561	<0.088	<0.684	n.d.	n.d.	n.d.	n.d.	n.d.	n.d.	<0.088	<0.215
B	5.72	9.89	24.3	13.6	n.d.	n.d.	n.d.	n.d.	n.d.	n.d.	3.79	5.98
Ti	60.1	60.3	159	2163	14.0	14.0	646	239	1766	542	<1.80	b.d.l.
Mn	166.712	847	635	1460	1057	1004	1090	1096	747	638	80.8	116
Co	31.8628	81.1	27.3	67.4	147	146	63.0	59.0	28.0	24.0	18.2	45.3
Ni	783	4350	576	3068	3127	3179	806	725	415	415	1488	1424
As	<0.156	<2.19	<0.461	<1.85	n.d.	n.d.	n.d.	n.d.	n.d.	n.d.	<0.454	<1.23
Rb	<0.010	<0.062	<0.031	<0.113	<0.013	<0.014	<0.017	<0.015	0.054	0.085	0.045	0.120
Sr	<0.032	<0.218	0.131	<0.357	0.02	0.02	1.16	<0.015	0.39	0.92	0.545	1.334
Y	0.260	0.060	0.907	7.809	0.012	0.014	1.72	0.189	8.709	2.053	0.060	0.037
Zr	0.049	<0.084	0.030	0.729	0.025	<0.01	0.022	0.018	0.164	0.137	0.125	0.053
Nb	0.003	<0.021	<0.003	0.032	<0.005	<0.004	0.011	<0.006	0.015	<0.007	<0.002	<0.006
Sn	<0.0512	<0.318	<0.048	<0.526	n.d.	n.d.	n.d.	n.d.	n.d.	n.d.	<0.045	<0.212
Sb	0.007	<0.033	<0.008	<0.040	n.d.	n.d.	n.d.	n.d.	n.d.	n.d.	<0.009	<0.016
Cs	<0.003	<0.035	<0.008	<0.049	<0.006	<0.009	<0.007	<0.013	<0.006	0.01	<0.008	<0.014
Ba	0.008	<0.044	0.012	<0.039	0.243	<0.018	0.283	0.055	0.864	0.248	0.131	0.406
La	0.004	<0.008	<0.002	0.016	0.006	<0.002	0.133	<0.003	0.041	0.032	0.018	<0.003
Ce	0.004	<0.006	0.004	0.027	0.226	<0.001	0.195	<0.003	0.029	0.038	0.002	0.008
Pr	<0.0007	<0.003	<0.0007	0.014	0.003	<0.002	<0.003	<0.001	0.014	0.01	0.005	0.001
Nd	0.003	0.011	0.006	0.137	<0.017	<0.008	<0.013	<0.013	0.074	0.111	0.035	<0.007
Sm	<0.012	<0.147	<0.014	0.126	<0.008	<0.037	0.015	<0.015	0.152	0.03	<0.017	<0.032
Eu	<0.001	0.040	0.007	0.022	<0.003	<0.003	0.009	0.003	0.105	0.011	0.004	<0.005
Gd	0.005	0.005	0.015	0.124	<0.013	<0.008	0.05	<0.008	0.684	0.116	0.001	<0.005
Tb	0.020	<0.022	0.062	0.488	<0.001	<0.001	0.018	<0.002	0.186	0.026	0.014	<0.012
Dy	0.035	<0.013	0.122	1.028	0.007	<0.005	0.2	0.023	1.307	0.282	0.007	<0.011
Ho	0.010	<0.003	0.037	0.275	<0.003	<0.002	0.053	0.006	0.355	0.075	0.002	0.002
Er	0.032	<0.014	0.118	0.951	<0.008	0.005	0.263	0.039	1.05	0.275	0.007	<0.011
Yb	0.045	0.069	0.162	0.932	<0.027	<0.013	0.453	0.099	1.059	0.388	0.006	<0.015
Lu	0.007	0.006	0.027	0.155	0.002	0.003	0.072	0.017	0.144	0.056	0.001	<0.003
Hf	0.005	0.019	0.005	0.062	<0.006	<0.003	<0.007	<0.003	0.052	0.008	0.003	0.006
Ta	0.001	<0.013	<0.005	<0.019	<0.003	<0.001	<0.001	<0.003	0.003	0.006	<0.003	<0.005
Pb	0.007	0.063	0.003	0.045	0.055	0.028	<0.026	0.039	0.732	0.158	0.019	0.071
Th	0.002	<0.007	<0.001	<0.005	0.006	<0.001	<0.002	<0.001	0.004	0.005	0.001	<0.002
U	0.002	0.002	<0.0004	<0.004	<0.003	0.002	<0.004	<0.001	0.003	0.002	0.001	0.003

Serpentinite sole

matrix	Antigorite Vein			Chrysotile Vein		Polygonal Vein and breccia matrix	
	xx-3758	KOP-3	Ti-47	xx-3758	xx-3786a	xx-3758	KOP-3
0.170749	<0.069	<0.209	0.352	<0.048	0.165	<0.173	<0.072
5.12	7.00	8.07	4.85	3.01	4.65	7.20	6.28
2.71	<1.81	12.7	1.95	<1.64	<1.60	<4.56	7.36
84.5	206	289	119	168	158	139	267
7.62289	22.8	85.2	19.9	9.59	14.3	48.1	33.2
905	908	2146	938	471	526	2756	904
<0.259	<0.366	<1.05	<0.209	<0.326	<0.180	<1.20	<0.316
0.051	0.029	0.164	0.053	0.044	0.125	0.057	0.025
1.454	0.416	2.245	2.847	0.384	2.306	0.556	0.308
0.147	0.090	0.028	0.047	0.016	0.044	0.365	0.070
0.025	0.077	0.076	0.045	0.054	0.017	0.205	0.120
<0.002	<0.002	<0.015	<0.001	<0.001	<0.001	<0.009	<0.003
<0.043	<0.070	<0.341	<0.047	<0.051	<0.034	<0.115	<0.037
<0.005	0.048	<0.028	0.008	0.008	<0.005	0.021	0.010
<0.005	<0.005	<0.019	0.012	0.007	0.018	<0.008	<0.007
0.211	0.151	0.405	0.339	0.163	0.370	0.098	0.066
0.058	0.043	<0.008	0.020	0.005	0.014	0.110	0.017
0.001	0.017	<0.010	0.003	0.007	0.008	<0.007	0.017
0.014	0.014	<0.003	0.004	<0.001	0.004	0.049	0.008
0.057	0.082	<0.018	0.021	0.009	0.013	0.262	0.031
<0.008	<0.026	<0.038	<0.012	<0.007	<0.011	0.058	<0.009
0.002	0.007	<0.011	<0.002	<0.002	<0.001	0.021	<0.003
<0.0007	0.002	<0.002	0.001	<0.0008	0.001	0.008	0.001
0.010	0.014	<0.025	<0.005	<0.005	0.007	0.065	0.013
0.010	0.011	0.012	0.005	<0.004	0.006	0.024	0.007
0.004	0.002	<0.002	0.001	<0.0007	0.001	0.009	0.002
0.012	0.006	<0.007	0.004	0.001	0.002	0.026	0.004
0.011	0.006	<0.019	0.004	0.004	<0.008	<0.018	<0.008
<0.001	<0.001	<0.003	0.001	<0.0003	<0.001	<0.005	0.002
<0.004	<0.005	0.007	0.003	0.002	0.002	<0.010	<0.003
0.004	<0.005	<0.010	<0.003	<0.002	<0.003	<0.015	<0.002
0.014	0.025	0.027	0.025	0.027	0.024	0.069	0.003
<0.0003	<0.0008	<0.002	<0.002	0.001	<0.0008	<0.002	<0.0005
0.024	0.010	<0.003	0.016	0.008	0.043	0.014	0.003

Sample	Location	Protolith	Position	Type	$\delta^{18}\text{O}_{\text{SMOW}}$	$\text{OD}_{\text{SMOW}} (\text{‰})$
Por12-1	Massif du sud	Du	US	liz	2.2	-106
Por12-2	Massif du sud	Du	US	liz	4.2	-106
Por12-3	Massif du sud	Du	US	liz	2.9	-106
Por6	Massif du sud	HZ	US	WR	5.3	-66
Por11	Massif du sud	HZ	US	WR	5.5	-75
Por12	Massif du sud	Du	US	WR	2.2	-95
Kop6-1	Kopéto	HZ	Sole	liz	4.1	-107
Kop6-2	Kopéto	HZ	Sole	ant	6.3	-98
Kop6-3	Kopéto	HZ	Sole	ant	3.8	-98
Kop6-4	Kopéto	HZ	Sole	ant	5.3	-98
xx3758	Koniambo	HZ	Sole	ant	4.0	-104
xx3773	Koniambo	HZ	Sole	ant	1.7	-91
xx3778	Koniambo	HZ	Sole	ant	5.1	-
Ko-05-1	Koniambo	HZ	Sole	chrys	4.4	-100
Ko-05-2	Koniambo	HZ	Sole	chrys	4.3	-102
Ti 24-1	Tiébaghi	Lhz	Sole	liz	2.9	-103
Ti 47-2	Tiébaghi	Lhz	Sole	liz	5.7	-97
Ti 48.06-1	Tiébaghi	Lhz	US	liz	5.4	-97
Ti 48.06-2	Tiébaghi	Lhz	US	liz	5.6	-103
Ti 5-1	Tiébaghi	HZ	Sole	liz	2.4	-95
Ti 51c-1	Tiébaghi	Lhz	Sole	liz	3.0	-104
Ti 47-3	Tiébaghi	Lhz	Sole	ant	1.9	-88
Ti 47-3 dup	Tiébaghi	Lhz	Sole	ant	2.1	-88
Ti 52E	Tiébaghi	Lhz	Sole	ant	4.9	-95
Ti 52E dup	Tiébaghi	Lhz	Sole	ant	5.3	-95
Ti 5-3	Tiébaghi	HZ	Sole	chrys	1.7	-
Ti 51a-1	Tiébaghi	Lhz	Sole	chrys	9.5	-91
Ti 51a-2	Tiébaghi	Lhz	Sole	chrys	10.8	-91
Ti 54b	Tiébaghi	Lhz	Sole	chrys	4.9	-94
Ti 51c	Tiébaghi	Lhz	Sole	WR	2.6	-88
Ti 24	Tiébaghi	Lhz	Sole	WR	1.9	-90
Ti 47	Tiébaghi	Lhz	Sole	WR	5.8	-87
Ti 48.06	Tiébaghi	Lhz	US	WR	6.4	-97
Poum 17-1	Poum	Lhz	US	liz	6.8	-103
Poum 17-1 dup	Poum	Lhz	US	liz	6.9	-103
Poum 18-1	Poum	Lhz	US	liz	6.5	-101
Poum 4-5	Poum	HZ	Sole	liz	7.6	-100
Poum 4-6	Poum	HZ	Sole	liz	13.9	-94
Poum 4-1	Poum	HZ	Sole	ant	7.9	-101
Poum 4-2	Poum	HZ	Sole	ant	12.2	-104

Poum 4-3	Poum	Hz	Sole	ant	12.1	-104
UwG-2 gnt (n= 16; valeur theorique: 5.8 ‰)					5.78 ± 0.25	-
G1 Biotite (n=16; valeur théorique: -66 ‰)					-	-67 ± 2

Element	B	Th	U	Zr	U/Th	B/Zr	References
NC mantle wedge	0.06	0.001	0.0005	0.053	0.5	1.13	U, Th, Zr: Secchiari et al. (2016; 2019); B: Salters and Stracke (2004)
AOC	5.2	0.070	0.300	66.5	4.29	0.078	U, Th, Zr: Staudigel et al; (1996); B: Smith et al. (1995)
Mobility (%)	60	37.7	29.1	0.1			Kogiso (1998); Sano et al. (2001)
AOC-derived fluid (F = 1.5%)	208	1.76	5.82	4.43	3.31	46.9	Weight fraction of fluid F: Peacock (1990); Rüpke et al. (2004)
GLOSS II	67.9	8.10	1.73	129	0.214	0.526	Plank (2014)
Mobility (%)	70	2.5	3.0	0.1			Aizawa et al. (1999)
Sed-derived fluid (F = 3%)	1584	6.75	1.73	4.3	0.256	368	Weight fraction of fluid F: Peacock (1990); Rüpke et al. (2004)
Abyssal serpentines	50	0.073	0.569	2.4	7.79	20.8	Peters et al. (2017)
Mobility (%)	39.2	2	10	0.1			Tenthorey and Hermann (2004)
Serp-derived fluid (F = 0.69%)	2841	0.212	8.25	0.348	39.0	8167	Weight fraction of fluid F: Water loss during Lz/Ctl to Atg (2004)

[Click here to view linked References](#)

Marc ULRICH

June, 25 2020

Dear Pr Othmar Müntener,

Please find attached the corrected version of the manuscript written by by myself, Manuel Muñoz, Philippe Boulvais, Michel Cathelineau, Stéphane Guillot and Christian Picard entitled "Serpentinization of New Caledonia peridotites: from depth to (sub-)surface" that we submitted for publication to Contributions to Mineralogy and Petrology.

Following the very helpful comments made by yourself and the two reviewers, we made some substantial changes in the manuscript. They are listed below:

Dear Marc,

I have now received two reviews of your paper. Both reviewers are generally supportive of publication of your paper, but there are numerous issues to be resolved. The recommendation is between moderate to major revisions. I have also read your paper and agree mostly with their evaluations. Both reviewers provided many detailed comments for improving the overall presentation. Please follow their advice. There are, however, several major points that need careful attention. In brief you present a nice dataset, but you have not fully exploited its potential, which is reflected in a relatively general narrative, which lacks rigor of process discussion. This needs improvement along the following lines

- (i) The paper needs generally a better organisation, more clearly defined research questions, a thorough discussion and then conclusions that take into account this discussion. Looking at the introduction, you invoke large scale processes (non-specific, see problems how you cite below), but in the discussion and conclusions these aspects have not been re-visited. This is too bad, because a reader will not get what are the novel things that one can learn from your study. You need to exploit the data in a more thorough way in order to make your study interesting for the reader.*
- (ii) The introduction on line 78 is poorly formulated, questions about the origin and nature of serpentinizing fluids can mean virtually everything. Please rewrite and be more specific what kind of research question do you want to address with your contribution and then discuss these in terms of the relevant processes. Otherwise a reader will get the impression of a local study. The general relevance of your findings should then be thoroughly discussed.*

[Answer to comments \(i\) and \(ii\): We agree with these comments. The introduction has been rewritten accordingly, and we tried to be more specific on the questions we addressed in this study. The large scale processes we invoked in the introduction are now re-visited in the discussion and the conclusions \(see also our \[detailed answers to reviewers comments below\]\(#\)\).](#)

(iii) Problems of correctly citing papers, somehow related to point (ii) above. I do not think that listing many many references is necessary. A few key references in the right place are in order. In particular you should cite the original and most important work of Ulmer and Trommsdorff (Science 1995, and Geochemical Society 1999) The works cited on line 70 and 71 refer all to these experimental studies but have not added new insights to this. When you talk about the importance of serpentine then a few papers that address the rheology of serpentine should be incorporated, not only geochemical literature. So focus on a few key references in the right place and do not provide long lists. Be specific when you add citations.

An effort has been done in correctly citing papers. Original and most important works have been cited (e.g., Ulmer and Trommsdorff papers). A paragraph dealing specifically with the serpentine rheology and its role on rock exhumation has been added to the introduction (lines 79-84).

(iv) Some of the modelling needs serious rethinking and rewriting as outlined by reviewer #1, and the methods how you have done the calculations needs to be better described and thoroughly discussed

The modeling has been rewritten and is now described in details (see answer to reviewer #1).

(v) The discussion of the trace elements and its relationship with the stable isotopes needs to be expanded. As is, this is insufficient. On the one hand you use As, Sb and call these sedimentary traces that are low, but Sr and Sr isotopes are high, derived from sediments. What is the importance of U spikes in panel b,c,d and the Th/U ratio? How important is the high Fe³⁺ in sole serpentinites? What is the Ce anomaly telling you? You need to milk these data more thoroughly, and then decide what you can say and what you cannot say. Mobility of incompatible elements depends on many parameters (Eh, pH of fluids) but you associate some anomalies to laterite formation, fair enough. But forming the sole in response to meteoric fluid circulation is not evident and the role of deformation on the trace element composition might be important. Retrogression of antigorite to chrysotile and polygonal serpentine is not isochemical, so what are the changes that you observe?

A new paragraph dealing with the behavior of trace elements has been added to the discussion, with 2 additional figures (lines 375-392). In addition, we have developed a new modeling that predict the evolution of the mantle wedge budget in trace element during slab dehydration. The results are compared with those of Monte Carlo simulations made on stable isotopes. The origin of U spikes (high U/Th ratios), low Ce/Ce* (i.e., Ce negative anomaly) and high Fe³⁺ in serpentine from the serpentinite sole have been extensively discussed (lines 612-622).

(vi) The final version needs to be read very carefully by a native English speaker. There are numerous franglisms in the paper, which need to be eliminated.

Done

From an editorial point of view, you need to complete the Table in the Electronic Appendix by providing GPS coordinates of all samples. So far I have not found any information where exactly the samples are collected.

Tables: It is not appropriate to report values in Tables that are 0.00 or 0.01 with std dev of 0.02. Please replace these by the detection limit of your analysis. (e.g. TiO₂ < 0.01). Relevant digits should be given only, e.g. SiO₂ 41.0 and not 41.04. Bdl in Table 2 should be replaced by the calculated limit of detection (e.g. Li < 0.3 ppm).

Figures: please add relevant error bars in the figures. Not on all samples, but representative ones. Figure 5: I do not understand why you plot Fe³⁺/Fetot up to values of 1.1. The range is limited between 0 and 1, the same is true for Mg#, the grey field cannot exceed 1. So the axis should be limited to 1.

Figures: In general needs labels for individual panels and these need proper description in the figure caption (see reviewer #2 for improvement). Fig. 8 needs improvement (see reviewer#1)

All your editorial suggestions have been taken into account and corrected accordingly. In most diagrams, the error bars are not reported because they are smaller than the size of the points.

Note that Contributions to Mineralogy and Petrology has no title numbering and you should consult the webpage for correct formatting of the manuscript, figures, figure captions and tables.

Done

Reviewer 1

Overall the paper presents interesting work that provides insights into the serpentinization process of the Peridotite Nappe of New Caledonia. The integration of mineralogical, major and trace element geochemistry, and particularly the isotope geochemistry and Monte Carlo and AOC fluid composition modeling is a creative way to develop an interpretation of the serpentinization process. However, there is a general lack of detailed description of the methods and some of the figures need substantial modification to be most effective.

Considering these limitations, I cannot recommend publication until after substantial revision and potential re-review.

Major comments:

In the introduction, as justification for the work, the significance of the work in general, in regard to understanding plate tectonics and global geochemical cycles is stated. However, these ideas are not revisited in the discussion or conclusions of the manuscript. Thus, the broader significance of what has been learned from this work needs to be developed in more detail.

We agree with this comment, and the discussion has been revisited accordingly. In particular, we have added a paragraph dealing with and modelling the behavior of some trace elements during the dehydration of subducted slab components and subsequent hydration of the overlying mantle wedge. The behavior of trace elements during late serpentinization events has been discussed more thoroughly, and how serpentines participate to the global geochemical cycles is now better described (e.g., lines 520-574)

The methods section does not contain enough detailed information. Particularly the methods for the modeling of the $\delta^{18}O/\delta^D$ are not addressed in the methods section of the paper and are mostly constrained to the caption of Figure 7. This is not adequate and the methods must be much more fully described within the main body text. Similarly, the method for determining Fe^{3+}/Fe^T is not stated in the method section and needs to be described and/or referenced.

We do not find appropriate to develop our modeling approach in the Materials and Methods section, particularly because the first paragraph of the Discussion deals with the main limitations of modeling approaches that were previously published in the literature and highlights the benefits of our original approach. However, we agree that the modeling methods have to be better and fully developed, which is now the case in the present version: a new paragraph has been added at the beginning of the Discussion where the modeling approach is fully developed, including the equations used to calculate fractionation factors, the main equation used to calculate the isotopic compositions of serpentine as a function of mantle and fluids compositions, fractionation factors and fluid-rock ratio, and the proper references (lines 424-478).

The method for determining Fe^{3+}/Fe^T (Beard and Frost, International Geology Reviews, 2016) have been described in details in the Materials and Methods section (lines 174-190).

Figure 7. Modeling methods should be removed from caption/figure and stated more completely in a dedicated section in the manuscript text. It is not clear enough that there are a couple of different models, that to some degree iterate on one another, involved in determining the temperature of the serpentinizing fluids. There is no justification of using Alt and Shanks 2006 to model the AOC isotopic composition which was then used to narrow the results from the Monte Carlo simulations.

We agree with this comment and the figure caption has been modified accordingly. In addition, as stated above, the manuscript now includes a section developing the modeling approach. The use of Alt and Shanks III study

(2006) is argued on the basis of the regional geodynamics in the Marianna, which is assumed to be relatively similar to that expected for the South Loyalty Basin at the subduction time. In addition, the Marianna region is the only one so far providing an "access" to fluid circulations in the forearc mantle via the occurrence of serpentinite seamounts. This is now clearly stated in the text (lines 494-519).

7b – It's not clear if the boundaries of the black box are significant. Please clarify. If they are, please somehow make it easier to interpret the values from the outline of the box.

Please list the isotopic values of fluid you are inferring on the plot, as these are the actual results and are difficult to read off of the plot as presented. Remove the AOC crustal mineralogy/composition info from Alt and Shanks, 2006, as this belongs in a better developed methods section in the text vs. only shown on the plot itself.

The AOC composition and mineralogy has been removed from the figure 7b, and details about the AOC modeling is now given in the text (lines 494-519). Basically, the black box symbolizes the range of O and H isotope compositions of fluids in equilibrium with metabasalts, assuming that the metasomatised basaltic basement has $\delta^{18}\text{O} = 8\text{-}11\text{‰}$ and $\delta\text{D} = -90$ to -120‰ (Alt, Gcubed, 2003), and a simple mineralogy of 48% albite, 48% chlorite and 2% calcite. The dehydration of metabasalts having these isotopic compositions and mineralogy would produce fluids with $\delta^{18}\text{O}$ values of 2-8‰ δD values of -50‰ to -90‰. Clearly, the boundaries of the black box are dependent of the chosen parameters. However, by keeping the AOC stable isotope composition as defined by Alt (2003), the variation of other parameters (i.e., the mineralogy and the temperature) would lead to increase or reduce the size of the box without significantly moving it. In the modified version of Figure 7, the black box is now in dashed blue lines, and we add a supplementary purple box showing the fluids in equilibrium with the AOC at 200-400°C, which illustrates that increasing the temperature leads to increase the $\delta^{18}\text{O}$ range up to -10‰ without changing the range of δD . O and H isotopic compositions of subducted serpentinite and sediment-derived fluids as calculated by Alt and Shanks have been also added to the Figure.

The list of isotopic values of fluids inferred on the plot is now provided in a supplementary table. This table also includes T, fluid-rock ratios and isotopic compositions of serpentinite for each simulation.

7c/7d – Please define directly what the cross-hatch pattern indicates. Please directly state why the cross-hatch pattern is constrained to the red area of the density plot of the Monte Carlo simulation results. Please indicate what proportion of total number of simulations is included in that hatched area vs. in the red AOC fluid window.

The white cross-hatched pattern in Figure 7c/7d corresponds to simulations that plot in the red area in 7b. It represents about 40% of ~6500 random simulations. This is now indicated in the main text and in the figure caption.

Figure 8 – Either more detailed labelling or indications of process (e.g. labeled arrows) need to be included on the figure itself and/or a more detailed description of the take home message of the figure needs to be included in the caption to make this figure useful. A description of how the rocks and processes from (A) are related to the rocks and processes in (B) would also make this figure more useful.

The Figure caption has been modified accordingly: It now includes a more detailed description of the take home message.

The paper needs to be thoroughly reviewed and corrected specifically for English grammar.

Done

Line-by-line comments:

Line 32 – 'admitted' is a strange word choice here

Deleted

Line 34-35 – ‘their possible association’ what is this referring to? Please state directly.

Done

Line 59 – Is ‘mantellic’ actually a word?

Corrected

Line 67 – What is ‘huge’ and what are the implications on the geologic system of this water getting into the mantle? It is this that will make the process important.

The sentence has been modified as follow: "Thus, the uppermost part of the oceanic lithosphere is hydrothermally altered before entering subduction zones. Then, the dehydration of the subducting slab favors the formation of forearc serpentine, which hosts a large amount of water (up to ~13 wt.%). The circulation of such an amount of aqueous fluids may, in turn, transport fluid-mobile elements (FME) deep into the mantle down to ~150 km (Ulmer and Trommsdorff 1995; Wunder et al. 2001). At temperature above ~650°C, serpentine is no longer stable and aqueous fluids are liberated by serpentine breakdown triggered mantle wedge melting that gives rise to arc volcanism (Hattori and Guillot 2003; Iwamori 1998; Reynard 2013; Schmidt and Poli 1998; Ulmer and Trommsdorff 1995; 1999)."

Line 113-114 – awkwardly worded in English.

The sentence has been rewritten.

Line 133 – what exactly does the term “upper serpentine” refer to? The whole package of serpentinitized harz/lherz/dun? Please state this clearly.

Indeed the term “upper serpentine” refers to the whole package, this is now specified.

Section 3.1

No mention of a method for Fe^{3+}/Fe_T

No mention of the isotope model parameters, etc. in the methods section – they are only briefly touched on in the Discussion section and caption of Figure 7. More development of this is necessary.

The Fe^{3+}/Fe_T method is now fully developed (lines 174-190)

Line 232 – Clearly some Fe but how much compared to the Fe content of the primary olivine? E.g. how much Fe is in the serpentine?

Considering atom per formula unit calculations on the basis of 7 oxygens for both serpentine and olivine in order to compare, $Fe=0.2$ in average in lizardite vs. $Fe=0.32$ in average in olivine, which confirms the loss of Fe during serpentinization. This information is available in the supplementary table S1.

Line 253-255 – awkwardly worded.

Rephrased

Line 301-303 – Fe_2/Fe_3 estimated by eprobe analyses. A statement describing this method in more detail and its limitations should be included here or in the methods section. However, it does seem reasonable to use this method if the interpretations are limited and broad as they are in this work.

Done (see the answer on Major comments above)

Line 332-334 – serpentines have a wide range of $\delta^{18}\text{O}$ while $\delta^{16}\text{O}$ are homogeneous. Why? No systematic difference between serpentine varieties. Why? Upper serpentines (i.e. liz) have a narrow isotope composition while Lizardite in the serpentinite sole have a wider range of isotopic compositions. Why the difference between the two?

We do not find it appropriate to discuss the reasons why serpentines exhibit chemical heterogeneities in the Results section. The origin of these heterogeneities is widely discussed and addressed in the Discussion section of the manuscript.

Line 390-392 – The authors state that they do not use the fractionation factors of Saccocia because they are limited to $T > 250^\circ\text{C}$. Yet, as stated on lines 403-405, the fluids have been interpreted to have mainly been at 250-430C (which is $> 250^\circ\text{C}$)? Additionally, the fractionation factors from all the mentioned sources do converge at T of x - x . ask Eric for plot.

As it is now specified in the manuscript, the use of oxygen isotope fractionation factors from Saccocia et al. (2009) provides quite similar results to that of Wenner and Taylor (1971) in the temperature range of 250-450°C. However the serpentine–water ^{18}O – ^{16}O fractionation factor of Wenner and Taylor (1971) is applicable at a wide range of temperature, contrarily to the experimental approach of Saccocia et al. (2009) of which fractionation factor was calibrated only for temperatures $> 250^\circ\text{C}$. As a consequence, the use of Wenner and Taylor fractionation factor was found more consistent in the aim of calculating the $\delta^{18}\text{O}$ composition of serpentinizing fluids without any other constraints on serpentinization temperature. Who is Erik?

Line 404-406 – It isn't at all clear how the Monte Carlo simulations are used to get from the isotope space the values fall into (stated on line 403) to interpreting/knowing that the fluids interacted with the mantle at T of 250-430C? This isn't clearly described anywhere in the manuscript and must be developed.

Following the reviewer's recommendations, how the Monte-Carlo simulations have been calculated is now fully developed (see the detailed answer in Major comments and the new section in the manuscript, lines 424-478)

Line 414-416 – The base is more serpentinized, correct? (At least, it is stated to be such on lines 108-109.) So, this isn't worded correctly because it's saying the serpentinization degree increases from bottom to top thus the bottom is less serpentinized and the top is more serpentinized. If this is not actually the case, there may be some confusion in terminology between the bottom/top of the ophiolite and the sole serpentinites.

Corrected. Indeed, the serpentinization degree decreases from bottom to top...

Line 449-452 – If serpentinization of NC occurred prior to entering the subduction zone, is there a signature of this in the isotopes? It was stated earlier that the isotopes fall in the 'ophiolite serpentines' field vs. the oceanic serpentines field which seems to suggest that the processes that occurred in the subduction zone are not represented in the isotopic signature. Please clarify.

This paragraph has been clarified particularly due to the addition of a new model based on trace elements which confirms the results of the Monte-Carlo simulations, i.e., AOC-derived fluids are mainly responsible to the serpentinization of NC peridotites (see lines 520-574).

Figure 3. Why mention pyroxene in the caption if not shown in the figure?

Deleted

3B. Is S1 cut by 3 successive generations of serp veins as stated or by 4 as indicated by the range that is stated (S2 to S5 which would be S2, S3, S4, S5).

S1 is crosscut by 4 serpentine veins, thanks. This is now corrected.

3d. It's not apparent that (d) clarifies anything, the labels on d should be put on b and still be understood.

We do not agree with this comment. We would prefer to leave this figure without any annotations for a better appreciation of the readers.

Figure 5. This caption seems to include less observation/interpretation than captions for other figures and the reader would benefit if it included more observation/interpretation.

Figure 5 caption now includes more details.

Pg. 46 of the compiled pdf doesn't seem to belong in the manuscript.

It belongs to the Table 3 and the trouble is related to the automatic pdf conversion of the manuscript from the journal website.

Reviewer 2

General comments

This manuscript present details of serpentinization history of the New Caledonia ophiolite using petrological observations and a large geochemical dataset. The manuscript provides details on the formation of serpentinites in the ophiolite identifying multiple generation of serpentinization events based in petrography, geochemistry, stable isotopes and Monte Carlo simulations. They identify an early serpentinization event at high temperatures from AOC fluids during emplacement that is more developed towards the base of the ophiolite with 100% serpentinization and tapers upsection with lower degrees of serpentinization. Further serpentinization involved meteoric fluids result in the formation of chrysotile and polygonal serpentine with geochemical signatures similar to their precursors.

The manuscript would be suitable for publication in Contributions of Mineralogy and Petrology after moderate revisions.

Specific comments

Comments are arranged by section of the manuscript.

Geological settings

More details on the specific units described in the paper need a little description on this section. Describe the existence of the basal nappe and the upper serpentines. There is no clarity here on the existence of the serpentinite sole and the base of the peridotite nappe and its difference. This applies to Figure 1. If this is classification from the paper it should be more clearly stated in the results or in the discussion.

Following this comment, the existence of the basal serpentinite sole is clearly indicated in last paragraph of the introduction and the differences between the serpentinite sole and upper serpentines are now widely addressed in the different sections of the manuscript. Unfortunately, at Figure 1 scale, it is not possible to differentiate the serpentinite sole from the serpentinized peridotites in the ophiolitic massifs.

Line 91 add reference for age of ophiolite. Line 102 Space missing after references

Done

Line 106-107 I suggest authors remove asbestos connection. Stating that the serpentinites have not been extensively studied is enough.

Done

Lines 106-124 I recommend that this paragraph is reorganized and rewritten to clarify. For readers not familiar with the New Caledonia ophiolite is really difficult to follow. For example in line 114 it is no clear to which group of co-workers is referring and how MAR samples are related to the New Caledonia serpentinites or the important of this combined dataset.

[This paragraph has been reorganized and rewritten as suggested \(lines 120-127\)](#)

Materials and methods

Line 131 If available it will be good to add sample coordinates either in Table 3 or in a supplementary table. Currently table 3 only list the massif for each sample. Considering that Massif du Sud extends for tens of kilometers having precise locations would be useful.

[Sample coordinates are now available in supplementary table 1.](#)

Line 148 Minor suggestion remove thick.

Done

Line 148 It is not clear how they make take the average and how it relates to figure 4. Is the average for each point measured, for points in the same vein or each serpentine type?

[It is for each point measured. This is now specified.](#)

Line 160 Change french orthose to English orthoclase.

Done

Results

Line 206-209 This needs some reorganizing. It is confusing as written. If 10% is rare it should be treated as such and state first that moving up section from the base peridotites have moderate to high degrees of serpentinization with some occurrences in the top massifs where it is limited ~10%.

[The paragraph has been rephrased as suggested \(lines 227-232\).](#)

Line 210-213 Again this needs some reorganization the paragraph jumps back and forward from the base of the ophiolite and the upper sections making hard to follow. I suggest each unit is described consecutively instead of jumping between them.

Done

Line 214-216 This appears out of place. In the previous paragraph you mention the base and then come back to describe it here. Is this a new observation or was it previously describe by others? If the latter is true the difference between the base and the upper sections needs to be incorporated to the Geologic setting.

We do not fully agree with this comment. The serpentinite sole has never been extensively studied until recently by our group. In addition, this work is the first one identifying several serpentine generations in the serpentinite sole and providing a comprehensive dataset for each generation. Therefore, we would prefer to keep this paragraph at this place.

Lines 271 Try to be consistent on how numbers in this section are reported. For example, for NiO they report a range and for MnO they report average and confidence interval. This should be consistent across the manuscript. If reporting confidence interval include if it is one or two sigma. This should be done for all sections in the results.

We agree with this comment. Numbers are now given with a better consistency in all sections in the results.

Line 275 is there any variation in opx and olivine Mg#? If so add variability. Line 276 Remove) towards the end of the line.

There is no variation in opx and olivine Mg# (now specified in the text)

Line 331 Correct typo on displays

Line 332 remove display or show.

Done

Line 334 It is not clear when they refer to varieties if it is the same as the generations. If they are the six generations described in the petrography section this needs to be more clearly stated.

The term varieties has been replaced by species in the manuscript. Species is used to distinguish e.g., lizardite from chrysotile, while generations is used to characterize the chronology of each serpentinization event.

Line 338 This sentence just repeat what was said in line 333 to 334 and can be removed. Please just confirm which is the correct range for d180 as it differs between the two sentences.

Not really the same but we agree that it was a bit confusing as it was written. The sentence has been rephrased to be clearer.

Lines 341-344 How much silica is present in the samples? Is it enough to truly shift the d180 and discard the heavy d180 samples? If silica had d180=30‰ to get to d180=13‰ in the mixture it will require ~30% silica which should be identifiable prior to analysis. In figure 7a they show that all discarded samples except one plot in the ophiolite serpentinite field. This might not affect the results as their Montecarlo simulations have values up to d180=12‰.

The presence of silica was identified by XRD (not shown in the manuscript) but was not quantified. However, the predicted amount of ~30% you made is consistent with our previous study on the carbonation and silicification processes of the serpentinite sole (Ulrich et al., CTMP, 2014), where we show on the basis of chemical mapping that discrete silicification may easily represent 30% of the rock without significantly modifying its texture. Although it is true that only one of our samples plot off of the ophiolite serpentinite field, these 4 samples are really different from the others in terms of oxygen isotope composition. Thus we find more consistent to discard these samples which likely reflect a later, shallower process than serpentinization.

Line 343 Global makes this sentence confusing. I recommend it to be removed.

Done

Discussion

Lines 374-377 talk about of the serpentine-magnetite geothermometer. The next sentence implies multiple approaches for estimating temperature however in this paragraph it only has one (serpentine-magnetite).

This paragraph has been coupled to the previous one in order to be more clear.

Line 381 add "fluids derived from....."

Done

Line 385-392 This section needs to be rewritten. It is confusing what fractionation factors were used for d_{18O} and dD . In line 389 remove "quite". Line 391 it is not clear what authors mean with "is more consistent". If it is a preference based on experimental temperatures it should be said that.

This section has been deeply rewritten, and we now provide new details on how the Monte-Carlo simulations were calculated.

Line 392-393 I would add at the beginning of the sentence something like: Neither of this previous work describe.....

This sentence has been deleted from the manuscript.

Line 419 Change "et" for "and"

Done

Line 438 Change "such materials" for sediments.

Done

Line 439 Change "with regards" for "compared"

Done

Line 439 Unreadable should be changed to unresolvable

Done

Line 473 Missing reference to support idea that sole was formed under more oxidizing conditions. This ties up with the following sentence that attribute high Fe^{3+} in polygonal serpentine to meteoric fluids and incorporating more than the precursors. This creates a conundrum as in Figure 5 the highest Fe^{3+} is for antigorite and lizardite that seems to be from S2-S4. This suggest that the late polygonal serpentine has less Fe^{3+} than the precursor lizardite/antigorite and needs to be clarified.

We agree with this comment. In the present version of the manuscript, Fe^{3+} is calculated using an alternative approach (Beard and Frost, 2017) which is clearly more consistent than the approach of Droop (1987) initially used. A direct consequence is that polygonal serpentine has now the highest Fe^{3+} . The more appropriate

reference that support the idea that sole was formed under oxidizing conditions is already cited (Muñoz et al., JGE, 2019).

Figures

Figure 3 Add sample numbers to panels or caption. For panel C the caption is not clear. When you mean same as B is it the same thin section (insert) or same textures and serpentine generations in different sample?

The sample numbers have been added to the caption, and the caption for C panel has been corrected.

Figure 4 I suggest that in the top of the panel is S1 and goes down to S6 instead of the way is presented now.

Done

Figure 5 Add letters to panels. It would be good to add some transparency to the symbols. As presented is hard to match description in text with figure. For example line 299 Mg# in bastites range from 88 to 98 is impossible to see in figure.

Done

Figure 6 Add letters to panels or caption. Figure 7 Typo in AOC fluids in panels b,c,d

Done

We hope that you will now find this revised manuscript suitable for publication in Contributions to Petrology and Mineralogy. If you have any question, please, let me know at your convenience.

Sincerely yours,

Marc ULRICH



Click here to access/download
Electronic supplementary material
Supplementary tables.xlsx





Click here to access/download
Electronic supplementary material
Supplementary Figure.pdf

